THE TRANSACTIONS OF

The Royal Institution of Naval Architects

Vol 159 Part A3 2017

International Journal of Maritime Engineering

The Transactions of The Royal Institution of Naval Architects – Part A

International Journal of Maritime Engineering

The International Journal of Maritime Engineering (IJME) provides a forum for the reporting and discussion on technical and scientific issues associated with the design and construction of marine vessels and offshore structures. The IJME is published four times a year as Part A of the Transactions of The Royal Institution of Naval Architects. Contributions in the form of scientific and technical papers and notes on all aspects of maritime engineering, together with comment on published papers are welcomed.

PAPERS

Papers may introduce new theory or evaluate existing theory, or describe experimental or novel practical work, Papers presenting case histories will report on new or existing techniques, including design and production. Papers may also provide literary reviews which appraise and evaluate published work. All papers are refereed.

TECHNICAL NOTES

Technical notes will provide early announcement of new ideas, findings, procedures, applications, interim results, etc., which might later on form part of a full paper. Technical notes are refereed as for papers, but due allowance will be made for their immediate nature.

DISCUSSION

Comments on papers and technical notes will normally be published in the first available issue of the *IJME* following that in which the paper was published. Discussion may be continued in subsequent issues, at the discretion of the Editor. Authors will be invited to respond to published comment.

ISSN 1479-8751

The Transactions of The Royal Institution of Naval Architects

Vol 159 Part A3 2017 **ISSN 1479-8751**

International Journal of Maritime Engineering

CONTENTS

PAPERS

TECHNICAL NOTES

There are no Technical Notes published in this issue of IJME

DISCUSSION

RISK ANALYSIS OF OFFSHORE TRANSPORTATION ACCIDENT IN ARCTIC WATERS

(DOI No: 10.3940.rina.ijme.2017.a3.351)

R Abbassi, Australian Maritime College (AMC), University of Tasmania, Australia, **F Khan**, Centre for Risk, Integrity and Safety Engineering (C-RISE), Faculty of Engineering and Applied Science, Memorial University of Newfoundland, Canada; and AMC, University of Tasmania, Australia, **N Khakzad**, Safety and Security Science Group, TU Delft, Netherlands, **B Veitch**, Faculty of Engineering and Applied Science, Memorial University of Newfoundland, Canada, and **S Ehlers**, Institute for Ship Structural Design and Analysis, TU Hamburg-Harburg

SUMMARY

A methodology for risk analysis applicable to shipping in arctic waters is introduced. This methodology uses the Bowtie relationship to represent an accident causes and consequences. It is further used to quantify the probability of a ship accident and also the related accident consequences during navigation in arctic waters. Detailed fault trees for three possible ship accident scenarios in arctic transits are developed and represented as bowties. Factors related to cold and harsh conditions and their effects on grounding, foundering, and collision are considered as part of this study. To illustrate the application of the methodology, it is applied to a case of an oil-tanker navigating on the Northern Sea Route (NSR). The methodology is implemented in a Markov Chain Monte Carlo framework to assess the uncertainties arisen from historical data and expert judgments involved in the risk analysis.

1. INTRODUCTION

The size and number of ships has increased significantly over time (Toffoli et al., 2005). The quest for new energy sources in arctic regions has drawn attention to this area (Chance and Andreeva, 1995). The Northwest Passage and Northern Sea Route (NSR) are alternative trade routes with potential to shorten distances, reduce fuel consumption and lower emissions (Kitagawa, 2008). The environmental conditions of the region present challenges to mariners and the current ship technology and systems (Arctic Council, 2009). The cold temperatures, multi-year sea ice, ice ridges, pack ice, and severe climate are some of the features of this region (Kassens et al. 1994; Melling, 2002). For example, the thickness of ice varies seasonally in different areas. The central Arctic Ocean is almost permanently covered by ice, with a mean ice thickness of 3.4 m and standard deviation of 1.4 m (Bourke and Garrett, 1987). Although the effects of harsh and cold environmental conditions of arctic regions on human performance and control devices has been investigated (Noroozi et al., 2013), the work devoted to quantitative risk analysis of ship accidents in arctic transits is limited.

Accident statistics illustrates that number of serious ship accidents has decreased in the past few decades (Oltedal and Wadsworth, 2010). Regardless of this progress, about 500 serious accidents occur annually, 10% of which lead to fatalities (Fowler and Sorgard, 2000). The possibility of ship accident in this region is expected to increase as the number of arctic voyages increases (Borgerson, 2008).

Maritime traffic poses different risks to people, the environment, and assets (Youssef et al., 2014a). In the risk analysis of ship accidents, it is essential to obtain reasonable estimates for probabilities of accident scenarios and the associated consequences. The present study aims to develop a methodology based on Bow-tie (BT) diagram to represent different possible accident scenarios to quantify the risk of transit on arctic routes. The BT diagram, which is composed of a fault tree (FT) and an event tree (ET), represents the logical relationships between the causes and consequences of an accident. The probabilities of three possible accident scenarios on arctic routes are quantified using FTs. Then using the ET analysis, the possible consequences resulting from these accidents are determined and their probabilities are calculated. The methodology relies on expert judgments in the estimation of the probability distributions of primary events. Finally, to handle uncertainties arising from the distributions, the methodology is implemented in a Markov Chain Monte Carlo (MCMC) framework.

2. PROPOSED METHODOLOGY FOR SHIP ACCIDENT IN HARSH CONDITIONS

2.1 ACCIDENT PROBABILITY ANALYSIS: FAULT TREE MODELING

In risk analysis, it is necessary to have an estimation of an accident's probability to evaluate the risk of the accident (Youssef et al., 2014b). The basic probability may be obtained from historical data of previous reported accidents (Darbra and Casal, 2004), or from the application of probabilistic methods such as FT. FT presents a structured approach to investigate the probability of failure resulting from combinations of faults in a complex system (Tanaka et al. 1983). This logical and diagrammatic approach illustrates the minimum set of events that may cause the failure of a system. In FT technique, an undesired event (e.g., collision, foundering, and grounding) is defined and then decomposed to determine its environmental and operational basic events. The synthesis of the results is demonstrated with a graphical model presented by the logical AND-gates and OR-gates (Elliott, 1994).

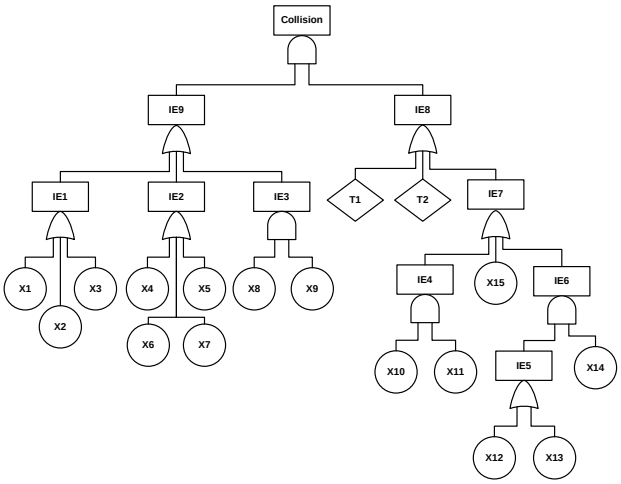

Figure 1. Fault tree of ship collision (events are explained in Table 1)

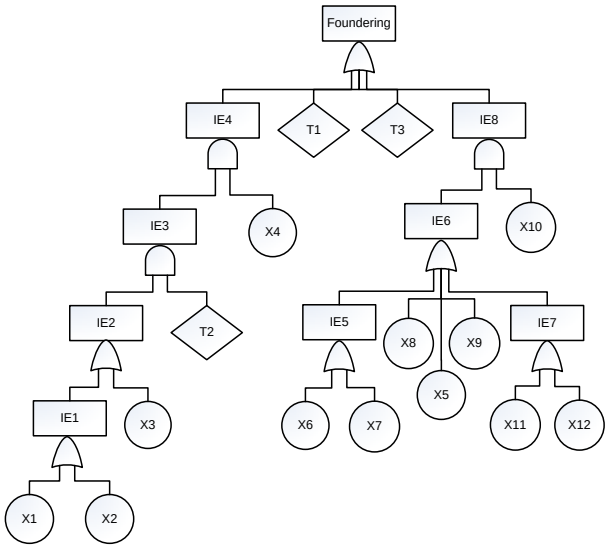

Figure 2. Fault tree of ship foundering (events are explained in Table 1)

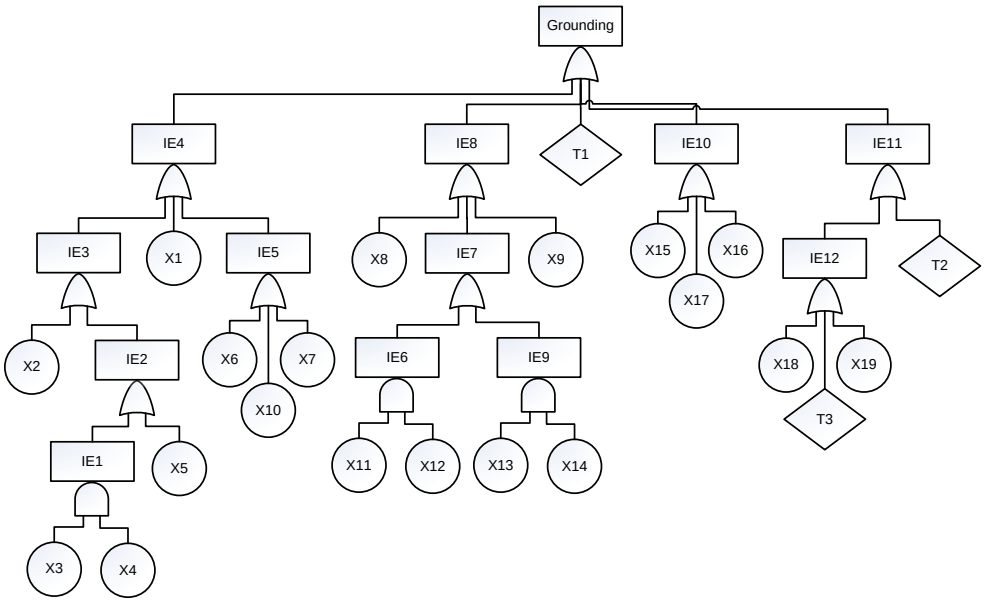

Figure 3. Fault tree of ship grounding (events are explained in Table 1)

Figures 1, 2, and 3 illustrate the relevant FTs for ship collision, foundering, and grounding accident scenarios, respectively. The FTs are developed according to previous literatures (e.g. Antao and Soares, 2006; Trucco et al. 2008) on ship accidents in normal environments and considering the particular characteristics of navigating in arctic environment using the expert opinions. Ship accidents are caused by a combination of accidental events and processes (Yang, Wang, and Li 2013). Human error and lack of visibility are recognized as main contributors to ship collisions (Macrae, 2009; Goerlandt and PenttiKujala, 2011). Fatigue, poor communication, faulty policies, practices and standards, poor knowledge of own ship systems and poor general technical knowledge are important human factor issues facing the marine industry (Talley, 2002; Dhillon, 2007).

In this study, the main focus is on the collision of a ship with arctic ice during arctic transits. One of the main reasons for ship collision with ice is detection failure, which, in turn, can be related to human error or failure of instrument used for detecting sea ice thickness and mass. In this study it is assumed that an icebreaker escorts a ship. The failure of the icebreaker to remove ice may lead to collision of a ship with ice. Finally, by increasing the arctic transit traffic in near

future, the fault of other vessels can be considered as a possibility for collision scenarios.

2.2 ACCIDENT CONSEQUENCES ANALYSIS: EVENT TREE MODELING

An ET demonstrates a logical combination of possible event outcomes following by an initiating event (Huang, Chen and Wang, 2001). The progress of an accident is divided into discrete events, starting from an initiating event, and enumerates all the possible outcomes based on failure/success of sequential top events. The probability of each outcome is calculated by multiplying the failure/success probabilities along each path.

In ship collision analysis, different consequences depending on the ship type are identified. Considering an oil tanker in this study, the first possible outcome after collision is a breach in the vessel hull. The breach can consequently give rise to large spill of hydrocarbons in the sea, causing significant damage to the environment, costly remediation techniques, and economic loss (Dave and Ghaly, 2011; Goerlandt, Stahlberg, and Kujala, 2012). The release of hydrocarbons can be followed by fire and explosion, threatening the vessel and the crew. If the fire cannot be controlled and extinguished in a timely manner, it may escalate to a catastrophic accident, which may cause many fatalities and the loss of entire vessel (Dave and Ghaly, 2011). The probability of the consequences considered in event tree is estimated considering the expert judgment for a particular accident scenario. It should be noted that emergency responses and evacuation procedures are challenging in marine environments particularly in arctic waters, due to the impacts of cold, ice, and a harsh and often remote operating environment on response personnel and equipments (Verny and Grigentin, 2009). This may lead to more severe consequences in case of a ship collision on arctic routes, which should be considered in the consequence analysis.

2.3 RISK ANALYSIS: BOW-TIE MODELING

A BT diagram is a constructive risk assessment and management tool that combines a FT and an ET to demonstrate the relation between hazards, threats, controls, and consequences (Cockshott, 2005; Nordgard, 2008). The application of BT to risk analysis of chemical process facilities and offshore oil and gas industry has previously been discussed by researchers (Mokhtari et al., 2011; Khakzad et al. 2012). One of the advantages of the BT model is that all connections between an undesired event, safety barriers, and outcomes are fully recognized (Markowski and Kotynia, 2011). Therefore, it can be adopted as a tool to consider possible controls and safety barriers to prevent the occurrence of an undesired event and/or to mitigate the ensuing possible outcomes. BT diagram is centered on an undesired event with a FT on the left-hand side, addressing potential primary causes leading to the undesired event (ship collision in this study), and with an ET on the right-hand side, exploring the possible consequences resulting from the undesired event. Combining the FT of collision shown in Figure 1 and the ET depicted in Figure 4, the BT diagram for the ship collision can be developed as illustrated in Figure 5.

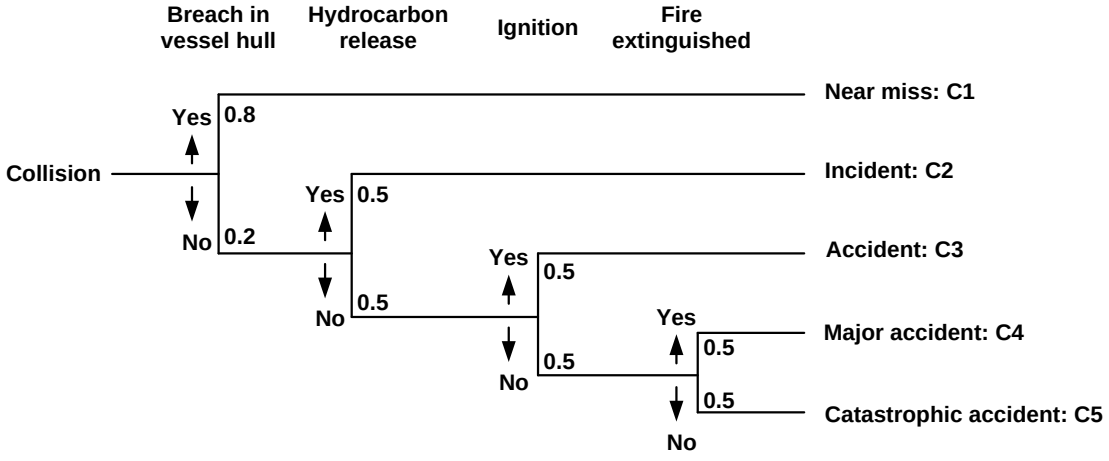

Figure 4. Event tree diagram for ship collision.

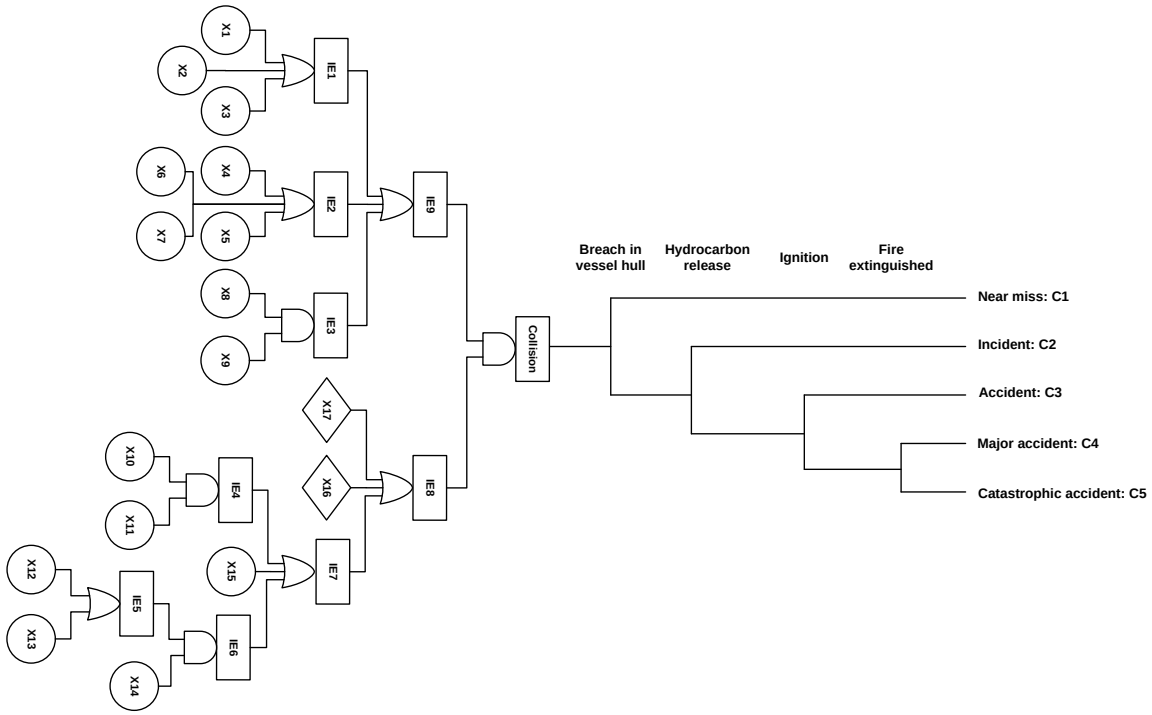

Figure 5**.** Bowtie diagram for ship collision.

2.4 HANDLING UNCERTAINTY IN RISK ANALYSIS

Information required for performing quantitative risk analysis can be achieved through historical data or expert judgment. The latter method is important, particularly, when the historical data to estimate the probabilities of events is missing or limited (Lindhe et al., 2009). However, expert knowledge is usually incomplete, inconsistent, vague, or imprecise, introducing sources of uncertainty to risk analysis (Goossens and Cooke, 1997; Mokhtari et al. 2011). Different approaches such as Monte Carlo simulation, evidence theory, and fuzzy sets have been adopted by researchers to model these uncertainties (Prassl, Peden, and Wong, 2005; Ferdous et al., 2009).

In this study, to model uncertainties in input data and propagate them through FT, a Markov Chain Monte Carlo (MCMC) simulation is used. MCMC methods (Geman and Geman, 1984) enable drawing samples from the joint posterior distribution of a set of parameters of interest. MCMC analysis has widely been used as a powerful tool for handling uncertainties (Rezaie et al., 2007; Smid et al., 2010; Khakzad et al., 2014).

To this end, the FT is implemented via OpenBUGS, a general-purpose software tool based on MCMC simulation (Lunn et al., 2009).

To apply the MCMC simulation, marginal probability distributions of the FT primary events can be determined using experts. In this study, a beta distribution is used for the natural events such as high wind, fog, and wave due to the flexibility of this distribution in modelling a wide variety of random events. Also, for events with unknown distributions such as radar failure or human error, a uniform distribution is applied. Finally, the normal distribution is adopted for two undeveloped events Chart error (T1) and Ice-breakers failure (T2) in the collision fault tree of Figure 1. For instance, the primary events High Speed (X2), Wave (X9), and Ice-breakers failure (T2) in Figure 1 can be modelled in OpenBUGS as:

```
Model {
X2 ~ dunif (0.001, 0.066)
X9 ~ dbeta (5.3, 1000)
T2 ~ dnorm (0.0073, 0.002)
}
```

where dunif, dbeta, and dnorm represent the uniform, beta, and normal distributions, respectively. After assigning the afore-mentioned probability distributions to the primary events, the probability distributions of the intermediate events and the top event can be derived based on logical gates of the FT. Furthermore, the mean value of each distribution along with the respective confidence interval can be calculated by the software. Having the probability distributions instead of single probability values facilitates the modelling of uncertainties more effectively.

3. APPLICATION OF THE METHODOLOGY

To illustrate the application of the proposed methodology, the probability of a ship collision navigating in the Northern Sea Route (NSR) is estimated. The NSR shortens the distance between a Northwest-European port

and the Far East by approximately 40% in comparison with the Suez Canal for the similar purposes. As a result, the emissions into the air are decreased and the cost of transportation is reduced (Schoyen and Brathen, 2011). The growth of the NSR will also assist in the extraction of natural resources such as petroleum, natural gas and minerals in the regions along the route (Granberg, 1998). There are many challenges in using the NSR as a navigation route, such as the building costs of ice-classed ships and their non-regularity and slower speeds (Liu and Kronbak, 2010), navigation difficulties, greater risks due to the harsh and cold conditions along the route, as well as the release of pollutants that may affect the ecological balance in the region (Ranger 2008). This subsequently necessitates a comprehensive methodology to investigate the risk of navigation through the NSR, considering the effects of harsh and cold environments. Application of the methodology to quantitative risk analysis of a ship collision navigating on the NSR is presented in the following sections.

3.1 ACCIDENT SCENARIO ANALYSIS

The NSR crosses the Bering Sea into the Barents Sea from the north of Russia (Kitagawa 2001). The NSR in arctic region includes the Chukchi Sea, East Siberian Sea, Laptev Sea, Kara Sea, and Barents Sea from east to west. To analyze the risk of collision of an oil tanker along the NSR, various parameters such as the effects of wind, current, temperature, and ice along the route are considered. These parameters affect the ship's navigation as well as human performance in emergency situations. Although, the bathymetry of the seas, ice conditions, and meteorological parameters along the route have been investigated in more details by researchers (Pavlov et al., 1996; Budikova, 2009; Shibata et al., 2013), the work devoted to the effect of harsh and cold conditions along the NSR is limited. The severe climate of arctic regions along the NSR justifies the reason for re-evaluating the ship accident scenarios using the data obtained from this environment. This is also considered by experts in this study when defining the probabilities of the events.

Along the NSR, currents and sea ice exhibit high spatial and temporal variability. The only route from the Pacific to Arctic is the Chukchi Sea with a surface area of 6.20 E 05 km^2. The average depth of the Chukchi Sea is 80 m, and approximately 50% of the area is less than 50 m deep (Hunt et al., 2013). It is almost ice-covered from early December to mid-May; however, it is losing about 80% of its maximum winter extent during the summer. Air temperature is between -30^{o}C to -20^{o}C during winter, varying from west to east, and reaching to 2^{o}C to 5^{o}C in the summer (Mulherin, Sodhi, and Smallidge, 1994). The East Siberian Sea has an area of 8.95 E 05 with a mean depth of 52 m (Anderson et al. 2011). It is almost ice-covered during the winter season, and 50% of ice remains during summer as well. The winter mean temperature is -30^{o}C (Mulherin, Sodhi, and Smallidge, 1994). Overall, the average depth of Chukchi Sea and East Siberian Sea makes the whole coastal region along the eastern NSR relatively shallow for all marine operations (Arctic Council, 2009). However, the average depth of Laptev Sea is much deeper at 519 m depth, and it has an area of 6.50 E 05 km^2. The average wind speed over the sea is 5 m/s, and storms occur in the sea, three to four times monthly. Fog is frequent over the sea and the total humidity is between 95-98% (Fofonova, 2012). The Kara Sea has an area of 8.80 E 05 km^2 with a mean depth of 110 m (Galimov, et al., 2006). It has an average humidity of 85-95% recorded in summer. Air temperature varies seasonally between -28^{o}C and 5^{o}C in winter and summer seasons, respectively (Pavlov et al. 1996). Finally, the Barents Sea has a surface area of 1.40E 06 km^2 and the mean depth of 230 m (Sakshaug, 1997; Smedsrud et al., 2010). The climate conditions of Barents Sea are mostly affected by warmer Atlantic water with a temperature of 3-6^{o}C (Sakshaug and Slagstad, 1992; Adlandsvik and Loeng, 2007). During the summer seasons, the entire Barents Sea is ice-free (Sakshaung, 1997). This provides an opportunity for marine transportation and exploration of natural resource deposits.

There are variations between the values of different parameters such as temperature, wind, current, ice, and humidity along the NSR. However, to our knowledge, there is no particular parameter that can be used to clearly divide the NSR to different regions. Therefore, we divided the NSR based on the different seas along the route and used the boundaries between the seas. The five different seas along the route provide five different regions considered in this study.

The collision probability of an oil tanker in each individual region is calculated based on the generic FT in Figure 1. The probabilities of primary causes are adopted from previous literatures on ship accident modeling in normal conditions. In case these probabilities could not be found or there are specific to arctic environments, expert judgment to find out the probabilities is used. Three different experts are used to define the probability distributions of primary events in each region. Each expert has more than 10 years of industrial and research experiences on ship transportation and accident modeling. They are also familiar with cold and harsh environmental conditions of arctic regions. The final value of the probabilities for each event is the mean value of the corresponding distribution function. Finally, using the BT diagram, consequence analysis is performed for the worst case scenario, i.e., the region with the highest collision probability.

3.2 RESULTS AND DISCUSSIONS

The input data for BT analysis in each particular region is received from the experts. The mean values of these data for each region are presented in Table 2.

One of the frequent contributing factors to ship collision, based on the probabilities assigned by the expert judgments, is the effect of human factors on the detection failure. This is in agreement with previous research on offshore and

maritime accidents, depicting that 80% or more of such accidents involve human error (Ruthblum et al., 2002). The cold temperature is another important factor that may affect the physical and cognitive performance of human activities. Cold temperature affects vigilance, reaction times, memory and recall, and strength (Enander, 1987; Hoffman, 2002; Noroozi et al., 2013). The collision of ship with pack ice and non-detected ice is another significant factor considered by the expert judgment to develop FTs. The existence of ice in arctic water is one of the main challenges for navigational purposes. The multiyear ice thickness can be greater than 3 m, and its presence on the NSR creates a dangerous environment for marine operations (Johannessen et al., 1997). Previous accidents such as the T/S 'Maxim Gorkiy' at in 1989, which, while navigating from Iceland to Spitsbergen, entered a field of drifting ice confirms the difference between the navigation in ice-covered waters and normal marine transportation (Jensen, 2007).

The results of the FT analysis illustrate the highest collision probability is in region 2 (the mean value of 4.61 E -03 with a 95% confidence interval as (1.01 E -03, 1.20 E -02)). The remote location, harsh environment, and the mostly unexplored physical oceanography (Munchow, Weingartner, and Cooper, 1999) are some of the characteristics of this region (East Siberian Sea) that create challenges for navigational purposes.

The final probability of the ship collision on the NSR is estimated by integrating the probabilities of collision in the all regions. The probability of collision on the NSR, according to the data received by expert judgments is calculated as 7.01 E -03. Having this probability value for the collision as the initiating event in the BT diagram, the probabilities of consequences are calculated as shown in Table 3. Likewise, the likelihood of catastrophic accident in NSR is 1.75 E -04. This confirms that the probability of a ship collision in NSR is higher than that of in temperate conditions (Fowler and Sorgard, 2000).

The possible safety measures to reduce the collision probability on the NSR and to mitigate the consequences are not considered in this study. However, the developed methodology can be used to investigate the possibility of preventing and mitigating ship collisions and the consequences.

4. CONCLUSION

A methodology was developed in this paper based on BT diagram, due to the need for reassessing ship accident scenarios in arctic transits. The methodology is aimed at helping decision makers and safety experts to estimate the probability of ship accidents and also to consider the factors that contribute the most to the overall accident probabilities. This provides a basis to decrease the risk of transportation in arctic routes.

Application of the proposed methodology to a ship accident scenario on the NSR confirms a higher probability for ship collision on this transit route. Due to significant variation of various parameters influencing a ship collision, the probability of accident is not similar within different regions along the route. It is demonstrated that the probability of an accident should be investigated in each individual region along the route to have an accurate estimation of the final accident probability. The total probability of ship collision on the NSR is calculated as 7.01 E -03, and the likelihood of a catastrophic accident is 1.75 E -04. This confirms a higher probability of collision on this transit route in comparison with that of temperate regions.

5. ACKNOWLEDGMENTS

The financial support of the Lloyd's Register Foundation is acknowledged with gratitude. The Lloyd's Register Foundation helps to protect life and property by supporting engineering-related education, public engagement and the application of research. Authors also thankfully acknowledge the support provided by Australia Maritime College, University of Tasmania as ongoing research collaboration with C-RISE, Memorial University.

6. REFERENCES

1. ADLANDSVIK, B., and LOENG, H. 2007. "*A study of the climatic system in the Barents Sea*." Polar Research 10(1): 45-49.
2. ANDERSON, L.G., BJORK, G., JUTTERSTROM, S., PIPKO, I., SHAKHOVA, N., SEMILETOV, I., and WAHLSTROM, I. 2011. "*East Siberian Sea, an Arctic region of very high biogeochemical activity*." Biogeosciences 8: 1745–1754.
3. ANTAO, P., and SOARES C.G. 2007. *Fault tree models of accident scenarios of RoPax vessels*. International Journal of Automation and computing 2: 107-116.
4. Arctic Council. 2009. *Arctic Marine Shipping Assessment*. Retrieved from: http://pame.is/images/stories/.
5. BORGERSON, S.G. 2008. "*Arctic meltdown: the economic and security implications of global warming*." Foreign Affairs 87(2): 63-77.
6. BOURKE, R.H., and GARRETT, R.P. 1987. *Sea ice thickness distribution in the Arctic Ocean*. Cold Regions Science and Technology 13: 259-280.
7. CHANCE, N.A., and ANDREEVA, E.N. 1995. "*Sustainability, equity, and natural resource development in Northwest Siberia and Arctic Alaska*." Human Ecology 23(2): 217-240.
8. COCKSHOTT, J.E. 2005. "*Probability Bowties: A Transparent Risk Management Tool*." Process Safety and Environmental Protection 83(4): 307-316.

9. DARBRA, R.M., and CASAL, J. 2004. "*Historical analysis of accidents in seaports*." Safety Science 42(2): 85-98.
10. DAVE, D., and GHALY, A.E. 2011. "*Remediation technologies for marine oil spills: a critical review and comparative analysis.*" American Journal of Environmental Sciences 7(5): 423-440.
11. DHILLON, B.S. 2007. "*Human Reliability and Error in Transportation Systems.*" Springer Series in Reliability Engineering XVI, 91-103.
12. ELLIOTT, M.S. 1994. "*Computer-assisted fault-tree construction using a knowledge-based approach.*" IEEE Transactions on Reliability 43(1): 112-120.
13. ENANDER, A. 1987. "*Effects of moderate cold on performance of psychomotor and cognitive tasks*." Ergonomics 30(10), 1431-1445.
14. FERDOUS, R., KHAN, F., SADIQ, R., AMYOTTE, P. and VEITCH B. 2009. "*Handling data uncertainties in event tree analysis*." Process Safety and Environmental Protection 87(5): 283-292.
15. FIRESTONE, M., CRISP, P.F., BARRY, T., BENNETT, D., CHANG, S., CALLAHAN, M., BURKE, A., MICHAUD, J., OLSEN, M., CIRONE, P., BARNES, D., WOOD, W.P. and KNOTT, S.M., 1997. *Guiding principles for Monte Carlo analysis.* USEPA, Washington, DC.
16. FOFONOVA, V. 2012. "*The Laptev Sea inshore zone modeling with focus on the Lena Delta region.*" Ph.D. Thesis Proposal, Alfred-Wegener-Institut, Jacobs University Bremen, Bremen, Germany.
17. FOWLER, T.G., and SORGARD, E. 2000. "*Modeling ship transportation risk*." Risk Analysis 20(2): 225-244.
18. GALIMOV, E.M., KODINA, L.A., STEPANETS, O.V. and KOROBEINIK, G.S. 2006. "*Biogeochemistry of the Russian Arctic. Kara Sea: Research Results under the SIRRO Project, 1995–2003*" Chemistry International 44(11): 1139-1191.
19. GEMAN, S., and GEMAN, D. 1984, "*Stochastic Relaxation, Gibbs Distributions, and the Bayesian Restoration of Images*." IEEE Transactions on Pattern Analysis and Machine Intelligence 6, 721–741.
20. GOERLANDT, F., and PENTTIKUJALA, P. 2011. "*Traffic simulation based ship collision probability modeling*." Reliability Engineering and System Safety 96: 91-107.
21. GOERLANDT, F., STAHLBERG, K., and KUJALA, P. 2012. "*Influence of impact scenario models on collision risk analysis*." Ocean Engineering 47: 74-87.
22. GOOSSENS, L.H.J., and COOKE, R.M. 1997. "*Application of some risk assessment techniques: formal expert judgment and accident sequence precursors*." Safety Science 26(1/2): 35-47.
23. GRANBERG, A.G., 1998. "*The northern sea route: trends and prospects of commercial use*." Ocean and Costal Management 41: 175-207.
24. HOFFMAN, R., 2002. *Human psychological performance in cold environments. Medical aspects of harsh environment*. Office of the Surgeon General United States Army, Falls Church, Virginia, USA.
25. HUANG, D., CHEN, T., and WANG, M.J.J. 2001. "*A fuzzy set approach for event tree analysis*", Fuzzy Sets and Systems 18: 153-165.
26. HUNT, G.L., BLANCHARD, A.L., BOVENG, P., DALPADADO, DRINKWATER, K.F., EISNER, L., HOPCROFT, R.R. et al. 2013. "*The Barents and Chukchi Seas: comparison of two Arctic shelf ecosystems*." Journal of Marine Systems 109-110: 43-68.
27. JENSEN, O., 2007. *The IMO guidelines for ships operating in arctic ice-covered waters*. Fridtj of Nansens Institutt, Lysaker, Norway.
28. JOHANNESSEN, O.M., SANDVEN, S., KLOSTER K, PETTERSSON, L.H., MELENTYEV, V.V., BOBYLEV, L.P., and KONDRATYEV, K.Y. 1997. "*Cover ERS-1/2 SAR monitoring of dangerous ice phenomena along the western part of Northern Sea Route*." International Journal of Remote Sensing 18:12: 2477-2481
29. KASSENS, H., HUBBERTEN, H.W., PRYAMIKOV, S.M., and STEIN, R. 1994. *Russian-German cooperation in the Siberian shelf seas: geo-system Laptev sea.* Ber. Polarforsch. 144, ISSN 01 76 – 5027.
30. KHAKZAD, N., KHAN, F., and AMYOTTE, P. 2012. *Dynamic risk analysis using bowtie approach*. Process Safety and Environmental Protection 104: 36-44.
31. KHAKZAD N., KHAN, F., and PALTRINIERI, N. 2014. *On the application of near accident data to risk analysis of major accidents*. Reliability Engineering & System Safety 126: 116-125.
32. KITAGAWA, H. 2001. *The Northern Sea Route: The shortest sea route linking East Asia and Europe*. Ship and Ocean Foundation, Tokyo, Japan.
33. KITAGAWA, H. 2008. "*Arctic routing: challenges and opportunities*." WMU Journal of Maritime Affairs 7(2): 485-503.
34. LINDHE, A., ROSEN, L., NORBERG, T., and BERGSTEDT, O. 2009. "*Fault tree analysis for integrated and probabilistic risk analysis of drinking water systems.*" Water Research 43: 1641-1653.
35. LIU, M., and KRONBAK, J. 2010. "*The potential economic viability of using the Northern Sea Route (NSR) as an alternative*

route between Asia and Europe." Journal of Transport Geography 18(3): 434-444.

36. MACRAE, C. 2009. "*Human factors at sea: common patterns of error in groundings and collisions.*" Maritime Policy and Management 36(1): 21-38.
37. MARKOWSKI, A.S., and KOTYNIA, A. 2011. "*Bowtie model in layer of protection analysis*." Process Safety and Environmental Protection 89: 205-213.
38. MELLING, H. 2002. "*Sea ice of the northern Canadian Arctic Archipelago*." Journal of Geophysical Research 107(C11): 2-1- 2-21.
39. METROPOLIS, N., ROSENBLUTH, A., ROSENBLUTH, M,. TELLER, A., and TELLER, E. 1953. "*Equations of State Calculations by Fast Computing Machines*." Journal of Chemical Physics 21 1087–1091.
40. MOKHTARI, K., REN, J., ROBERTS, C., and WANG, J. 2011. "*Application of a generic bowtie based risk analysis framework on risk management of sea ports and offshore terminals*." Journal of Hazardous Materials 192: 465-475.
41. MULHERIN, N., SODHI, D., and SMALLIDGE, E. 1994. *Northern Sea Route and icebreaking technology: an overview of current conditions.* US Army Corps of Engineer, Hanover, New Hampshire, US.
42. MUNCHOW, A., WEINGARTNER, T.J., and COOPER, L.W. 1999. "*The Summer hydrography and surface circulation of the East Siberian Shelf Sea.*" Journal of Physical Oceanography 29: 2167-2182.
43. NORDGARD, D.E. 2008. *Quantitative risk assessment in distribution system maintenance management using bowtie modeling*. 16th Power Systems Computation Conference (PSCC), Glasgow, Scotland.
44. NOROOZI, A., ABBASSI, R., MACKINNON, S., KHAN, F., KHAKZAD, N. 2014. "*Effects of cold environments on human reliability assessment in offshore oil and gas facilities*." Human Factors, 56(5): 825-839.
45. OLTEDAL, H., and WADSWORTH, E. 2010. "*Risk perception in the Norwegian shipping industry and identification of influencing factors*". Maritime Policy and Management 37(6): 601-623.
46. PAVLOV, V.K., TIMOKHOV, L.A., BASKAKOV, G.A., KULAKOV, M.Y., KURAZHOV, V.K., PAVLOV, P.V., PIVOVAROV, S.V., and STANOVOY, V.V., 1996. *Hydrometeorological regime of Kara, Laptev, and East Siberian seas.* Federal Service of Russia for Hydrometeorology and Monitoring of the Environment, The Arctic and Antarctic Research Institute, St. Petersburg, Russia.
47. PRASSL, W.F., PEDEN, J.M. and WONG, K.W. 2005. "*A process-knowledge management approach for assessment and mitigation of drilling risks*." Journal of Petroleum Science and Engineering 49: 142–161.
48. RAGNER, C.L., 'Den norrasjovagen'. In Hallberg, Torsten (ed), Barents– ettgränslandi Norden. Stockholm, Arena Norden, 2008, pp. 114-127.
49. REZAEI, K., AMALNIK, M.S., GEREIE, A., OSTADI, B. and SHAKHSENIAEE, M.. 2007. "*Using extended Monte Carlo simulation method for the improvement of risk management: Consideration of relationships between uncertainties.*" Applied Mathematics and Computation 190: 1492–1501.
50. ROTHBLUM, A., WHEAL, D., WITHINGTON, S., SHAPPELL, S.A., WIEGMANN, D.A., BOEHM, W., CHADERJIAN, M. 2002. *Improving Incident Investigation through Inclusion of Human Factors.* United States Department of Transportation - Publications & Papers. Paper 32.http://digitalcommons.unl.edu/usdot/32.
51. SAKSHAUG, E. 1997. "*Biomass and productivity distributions and their variability in the Barents Sea.*" ICES Journal of Marine Science 54: 341–350.
52. SAKSHAUG, E., and SLAGSTAD, D. 1992. "*Sea ice and wind: Effects on primary productivity in the Barents Sea*." Atmosphere Ocean 30(4): 579-591.
53. SCHOYEN, H., and BRATHEN, S. 2011. "*The Northern Sea Route versus the Suez Canal: cases from bulk shipping.*" Journal of Transport Geography 19(4): 977-983.
54. SHIBATA, H., IZUMIYAMA, K., TATEYAMA, K., ENOMOTO, H., and TAKAHASHI, S. 2013. "*Sea-ice coverage variability on the Northern Sea Routes, 1980-2011*." Annals of Glaciology 54(62): 139-148.
55. SMEDSRUD, L.H., INGVALDSEN, R., NILSEN, J.E.O., and SKAGSETH, O. 2010. "*Heat in the Barents Sea: transport, storage, and surface fluxes*." Ocean Science 6: 219-234.
56. SMID, J.H., VERLOO, D., BARKER, G.C., and HAVELAAR, A.H. 2010. "*Strengths and weaknesses of Monte Carlo simulation models and Bayesian belief networks in microbial risk assessment*." International Journal of Food Microbiology 139: S57-S63.
57. TALLEY, W.K. 2002. "*The safety of ferries: an accident injury perspective*". Maritime Policy and Management 29(3): 331-338.
58. TANAKA, H., FAN, L.T., LAI, F.S., and TOGUCHI, K. 1983. "*Fault-tree analysis by fuzzy probability*." IEEE Transactions on Reliability R-32(5): 453-457.
59. TOFFOLI, A., LEFEVRE, J.M., GREGERSEN, E.B., and MONBALIU, J. 2005. "*Towards the identification of warning criteria: Analysis of a ship accident database.*" Applied Ocean Research 27(6): 281-291.

60. TRUCCO, P., CAGNO, E., RUGGERI, F., and GRANDE, O. 2008. *A Bayesian belief network modeling of organizational factors in risk analysis: a case study in maritime transportation*. Reliability Engineering and System Safety 93: 823-834.
61. VERNY, J., and GRIGENTIN, C. 2009. "*Container shipping on the Northern Sea Route*." International Journal of Production Economics 122(1): 107-117.
62. YANG, Z.L., WANG, J., and LI, K.X. 2013. "*Maritime safety analysis in retrospect*". Maritime Policy and Management 40(3): 261-277.
63. YOUSSEF, S.A.M., INCE, S.T., KIM, Y.S., PAIK, J.K., CHENG, F., and KIM, M.S. 2014. *Quantitative risk assessment for collisions involving double hull oil tankers*. International Journal of Maritime Engineering, 156(A2): 156-174.
64. YOUSSEF, S.A.M., KIM, Y.S., PAIK, J.K., CHENG, F., and KIM, M.S. 2014b. *Hazard identification and probabilistic scenario selection for ship-ship collision accidents*. International Journal of Maritime Engineering, 156(A1): 61-80.

APPENDICIES

Table 1. Events used in the fault trees of Figures 1 – 3

Collision		**Foundering**		**Grounding**	
Index	*Event*	*Index*	*Event*	*Index*	*Event*
X1	Human error	X1	Human error	X1	Loss of power
X2	High Speed	X2	Not tight enough	X2	Basic failure of the propeller
X3	Equipment error	X3	Structural failure	X3	Contaminated fuel in banker tanks
X4	Radar failure	X4	Inadequate pumping	X4	On-board fuel clean-up system fails
X5	Human factor	X5	Faulty design/assembly	X5	Engine fails to operate
X6	Environmental obstacles	X6	Human error	X6	Mechanical failure
X7	Fog	X7	Leaking	X7	Environmental constraints
X8	High wind	X8	Metal failure	X8	Human error
X9	Wave	X9	Communication	X9	Equipment error
X10	High wind	X10	Heavy weather	X10	Operational failure
X11	Pack ice	X11	Excessive wear	X11	High wind
X12	Equipment error	X12	Faulty design	X12	Wave
X13	Human factor	T1	Cargo shift	X13	High wind
X14	Ridge ice and iceberg	T2	Water line reaches door	X14	Pack ice
X15	Non-detected multi-layer ice	T3	Harsh weather effect	X15	Radar failure
T1	Fault of other vessels	IE1	Doors open	X16	Human failure
T2	Ice-breakers failure	IE2	Operating above water	X17	Environmental constrain
IE1	Navigation	IE3	Flooding	X18	Assistance not requested
IE2	Visibility	IE4	Flooding effect	X19	Assistance does not arrive
IE3	Wave effect	IE5	Storage of water, duct, oil	T1	Chart error
IE4	Pack ice effect	IE6	Machinery failure	T2	Ice-breakers failure
IE5	Detection failure	IE7	Component failure	T3	Unable to put ship on safe track
IE6	Ridge ice and iceberg effect	IE8	Mechanical effect	IE1	Fuel supply to engine is contaminated
IE7	Dangerous ice condition	TE	Foundering	IE2	Engine stops
IE8	Potential obstacles			IE3	Vessel losses propulsion
IE9	Environmental/operational effects			IE4	Fault of the vessel
TE	Collision			IE5	Anchor failure
				IE6	Wave effect
				IE7	Environmental effect
				IE8	Navigation
				IE9	Dangerous ice conditions
				IE10	Visibility
				IE11	Assistance failure
				IE12	Failure of tug
				TE	Grounding

Table 2. Mean value of probabilities for primary events received by expert judgment

Input events	Region 1	Region 2	Region 3	Region 4	Region 5
X1	1.3E-03	4.0E-03	1.3E-03	7.0E-04	3.0E-04
X2	7.0E-04	5.0E-03	7.0E-04	3.0E-04	1.0E-04
X3	5.3E-05	5.0E-04	3.0E-04	5.0E-05	1.0E-05
X4	1.0E-03	7.0E-03	1.0E-03	5.3E-04	1.0E-04
X5	1.3E-03	4.0E-03	1.3E-03	7.0E-04	1.0E-04
X6	1.0E-02	2.0E-01	1.0E-01	7.0E-02	2.0E-02
X7	5.0E-03	1.0E-02	5.0E-03	1.0E-03	5.0E-04
X8	1.7E-03	5.3E-03	1.7E-03	5.0E-04	1.0E-04
X9	2.3E-03	5.3E-03	1.0E-03	8.3E-04	1.0E-04
X10	1.7E-03	5.3E-03	1.0E-03	7.0E-04	1.0E-04
X11	5.3E-03	1.0E-02	3.7E-03	1.0E-03	1.0E-04
X12	3.0E-04	1.0E-03	7.0E-04	1.0E-04	5.0E-05
X13	1.0E-01	2.0E-01	1.0E-01	1.0E-01	5.0E-02
X14	1.0E-03	1.0E-02	5.0E-03	1.0E-03	5.0E-04
X15	5.7E-03	1.0E-02	5.0E-03	5.0E-04	1.0E-04
T1	1.0E-03	5.0E-03	1.0E-03	5.0E-04	1.0E-04
T2	5.7E-04	7.3E-03	5.3E-04	2.0E-04	1.3 E-05
Collision Probability	**7.93E-04**	**5.33E-03**	**7.52E-04**	**1.3E-04**	**1.13E-05**
Final collision probability in NSR					**7.01E-03**

Table 3. Risk analysis of ship collision in NSR

Index	Probabilities
C1	5.61E-03
C2	7.01E-04
C3	3.50E-04
C4	1.75E-04
C5	1.75E-04

DEVELOPMENT OF AUTOMATIC MODE DETECTION SYSTEM BY IMPLEMENTING THE STATISTICAL ANALYSIS OF SHIP DATA TO MONITOR THE PERFORMANCE

(DOI No: 10.3940/rina.ijme.2017.a3.411)

I Zaman, **K Pazouki**, **R Norman**, School of Marine Science and Technology, Newcastle University, UK, **S Younessi**, Royston Ltd, UK, and **S Coleman**, Industrial Statistics Research Unit, Newcastle University, UK

SUMMARY

The shipping industry depends on a global regulatory framework to operate efficiently. The industry is currently facing various technical and regulatory challenges. Performance monitoring, vessel optimisation, reduction of emissions and maintenance have become high priorities for ship operators. The marine industry is also moving towards autonomous operation to reduce human error. The rate of sensor technology implementation has increased and also raised new technological challenges. The analysis of sensor data creates new challenges to achieve operational excellence. This paper presents the implementation of statistical analysis on ship data and develops a system to automatically detect the vessel operational modes based on sensor data.

NOMENCLATURE

IMO	International Maritime Organization
MARPOL	Marine Pollution
CO_2	Carbon dioxide
SO_X	Sulphur Oxides
NO_X	Nitrogen Oxides.
ECA	Emission Control Area
EEDI	Energy Efficiency Design Index
SEEMP	Ship Energy Efficiency Management Plan
EU	European Union
MRV	Monitoring Reporting and Verification
GT	Gross Tonnage
RV	Research Vessel
OSV	Offshore Supply Vessel
KPI	Key Performance Indicator
GPS	Global Positioning System
kn	Knots
NM	Nautical mile
hp	Horsepower
kW	Kilowatt
Lat	Latitude
Lon	Longitude
SPC	Statistical Process Control
I-MR	Individual-Moving Range
UCL	Upper Control Limit
LCL	Lower Control Limit
DP	Dynamic Positioning
t	Tonne
Con.	Consumption
GUI	Graphic user interface
AMD	Auto-Mode Detection

1. INTRODUCTION

The shipping industry currently operates under a complex set of national and international regulations. The industry will be required to adopt new technologies over the next decade to face upcoming regulations and market challenges. Key environmental regulations are coming into force to control the emissions of greenhouse gases, carbon dioxide (CO_2), sulphur oxides (SO_X) and nitrogen oxides (NO_X). According to the IMO MARPOL Annex VI, the industry must adhere to a sulphur limit of 0.1% of oil for ECA (Emission Controlled Areas) from 2015 and 0.5% globally from 2020. (DNV GL, 2012) NO_X emissions are regulated according to the MEPC 58 established in 2008 (revised MARPOL Annex VI) (DNV GL, 2012).

In parallel, the European Commission have introduced the MRV (Monitoring, Reporting and Verification) regulation to reduce CO_2 emissions from ships with GT more than 5000 moving in European waterways (European Commission, 2013). According to this regulation the ship operators will be required to monitor and report the verified annual amount of CO_2 emitted from their ships (European Commission, 2013).

One of the ways to reduce emissions of noxious and greenhouse gases is to improve energy efficiency in the shipping operation. Voyage optimisation and energy management are two principal options for increasing the energy efficiency (Buhaug *et al*, 2009). It is possible to reduce energy consumption on board a ship by working towards optimal operation for a given mission. However, this may require monitoring and hence benchmarking the performance of a ship in a specific activity. In light of this, performance monitoring is a key tool to increase a ship's operational efficiency and reduce harmful emissions.

Modern ships have various sensing and measuring devices providing values for parameters ranging from propulsion to navigational systems. Recording and analysis of data from these systems enables operators to monitor the energy consumed to perform an activity (Lloyd's Register, QinetiQ & University of Southampton, 2015). Robust and accurate knowledge of energy consumption of a ship for a given mission, without the need for the crew's input, will lead to optimal operational management. One of the key elements to achieve this goal is to distinguish different ship activities such as sailing, standby or cargo loading from each other, in other words, automatically detecting the mode of operation.

Automatic mode detection will first and foremost require a thorough understanding of the ship's activities coupled with the input of relevant data, which enables predictions to be made based on analysis and trends of the operational behaviour. These predictions, in turn, lead to the formulation of mode detection to identify the engine uses and fuel consumption based on the operational activities. This paper describes how the vessel operational modes are automatically detected and the impact of the mode detection on performance monitoring.

2. BIG DATA IN SHIPPING

'Big data' has become a buzzword in the shipping industry and has already changed the competitive landscape of many industries (Lloyd's Register, QinetiQ & University of Southampton, 2015). Big data refers to large amounts of data that are complex to analyse. Big data analytics defines the process of data analysis to uncover hidden patterns to identify correlations, ambiguities, trends and other useful information (DNV GL, 2014). The analysis and management of big data will become increasingly essential and is expected to have a great impact in the marine industry (Buhaug *et al*, 2009). Big data has four main dimensions: volume, velocity, variety and veracity (Lloyd's Register, QinetiQ & University of Southampton, 2015; DNV GL, 2014). The volume, which reflects the size of the data becomes larger day by day. There are technical challenges to sort and analyse high volumes of data. The data transmission rate (velocity) is getting faster, meaning more data is collected in a shorter time. In addition, the large volumes of data at high rates of transmission come from different types of sensors feeding the data into the system. The variation in big data is high. The industry will be faced with significant challenges in encountering and dealing with big, complex and fast data (DNV GL, 2014). However, by using statistical analysis to turn the data into value, there is great potential to improve ship operations.

3. SHIP OPERATIONAL MODES

The operational mode could be defined as the activity of a ship for a certain time to accomplish a mission, including waiting time at anchorage. The operational modes can be specific to the ship's type, or common. Specific operational modes vary from ship to ship. For instance, "Dynamic positioning" is a specific operational mode for an Offshore Supply Vessel (OSV) or "Towing" for a tug or "Loading" for a commercial vessel like a container ship. Examples of common modes are "Stand by" or "Sailing". The operational modes are influenced by weather conditions and vessel activities and affect the speed and fuel consumption.

Defining the modes helps the ship operators to know how economically a vessel was operated in performing activities during any specific time period. The operational modes also help the crew to track the fuel consumption and emissions and to determine performance of the ship for the given activity.

Royston Ltd has a fuel monitoring product focused on the marine industry called "engine*i*". It provides real time fuel consumption, speed over ground, estimated time of arrival and distance data. It also represents the data visually on the bridge and sends the data on-shore at regular intervals. "engine*i*" has an option for the manual logging of the operational mode by the crew. Manual entry of the operational mode has the following limitations:

- Manual mode operation is controlled by the crew. So there is an element of human error.
- The crew select vessel operational modes based on their experience, so entry could be subjective.
- The crew need to change the operational modes and this may conflict with their main duty at certain times.
- Unreliable data would be generated by selecting wrong modes or forgetting to change the mode.

Royston Ltd is aware of the limitations of manual mode logging and is therefore keen to develop an automatic mode detection method to improve performance monitoring.

4. AUTOMATIC MODE DETECTION METHOD

In this study, the Research Vessel (RV), "The Princess Royal", which belongs to Newcastle University was used as the basis ship. It has two Cummins QSM11 (600 hp) engines with fixed pitched propellers. The cruising speed is 15 knots and maximum speed is around 20 knots (Newcastle University, 2015). The Princess Royal was built and is used for scientific research and hence does not have any specific modes of operation. "engine*i*" had already been installed on the research vessel, so the data from The Princess Royal could be used to develop automatic mode detection. After developing the auto-mode detection system on the Princess Royal, it was applied to an OSV for further investigation as the OSV has different modes.

4.1 INITIAL DEVELOPMENT OF TOOLS

Auto-mode detection means that the vessel's operational modes would be automatically detected based on the operational activities. Ships function in different modes in various operational conditions. Using the auto-mode detection system, the crew would not be required to switch the mode every time the ship mode changed. It works based on statistical analysis of the vessel sensor data. The mode will be changed on a minute by minute basis according to the operational behaviour. A profile for an individual vessel will be made for the fuel consumption, distance travelled

and speed over the ground. The limits will be added based on the statistical analysis of these parameters for each minute. The mode will not be changed as long as the values are within limits.

The mode profiles would be different for different types of vessels and may vary even for vessels of the same type. For example, the same types of vessel with different engines would require different limits for fuel consumption and speed. The operational behaviour and activities need to be analysed to determine the mode limits in different conditions.

4.2 SYSTEM OVERVIEW

The auto-mode detection system will function without human intervention. The system has been developed based on a data-driven model with the sensor data (fuel flow meter and GPS) as input. Figure 1 shows the overall system diagram and demonstrates how the sensor data is used for developing the auto-mode detection.

Flow meters typically give the fuel consumption in litres and GPS sensors provide the position (latitude and longitude). This data forms the input to the "engine*i*" system on a minute-by-minute basis. The distance travelled is calculated from the latitude and longitude by using the haversine formula (Veness, 2007):

Distance (nautical mile) = acos[sin(Lat1) sin(Lat2)+ cos(Lat1) cos (Lat2) cos(Lon2 – Lon1)] 3440.065

The figure of 3440.065 is used to calculate the distance in nautical miles. The GPS sensor gives the latitude and longitude in degrees and this need to be converted to radians to calculate the distance. So the values need to be multiplied by $\pi/180$. Speed over ground in knots can be calculated by dividing the distance in nautical miles by the time in hours (Miller, 2013).

The "engine*i*" system outputs the values for fuel consumption, speed, distance and position to the data base and the parameters are statistically analysed for profiling and thresholds are created according to those profiles. Finally, the individual mode profile will be defined from the threshold limits.

A two-step process is used to generate the predicted mode based on the sensor data. Historical data needs to be statistically analysed to determine the operational behaviour of the vessel; this is done in Step-1 and the mode profile is created in Step-2 from the results from Step-1. Step-1 will be conducted only once in the auto-mode process. After creating the mode profile, all data will directly go through that profile from Step-2.

4.3 DATA ANALYSIS METHOD

Different data analysis methods, for example moving average or mean and standard deviation could be applied to data from on board monitoring as in this study. Simon and Litt (2012) used mean and standard deviation to determine the steady state in an aircraft's engine. Their study, however, showed that using standard deviation for a large scatter data could provide ambiguous results. Trodden *et al*. (2015) developed their own methods to sequentially filter data streamed from a tug boat to determine steady state operation. Other studies explore the use of multiple linear regression to develop prediction and control models for the ship fuel consumption (Bocchetti *et al*, 2015, Erto *et al*, 2015). In this study, statistical process control (SPC) and correlation analysis were used to identify the limits for the different operational activities. SPC is a group of tools and techniques used to achieve process stability and improve capability (Leavengood & Reeb, 1999, Khan, 2013). SPC involves defining the distribution of the process and continuously monitoring and comparing process performance (Leavengood & Reeb, 1999).

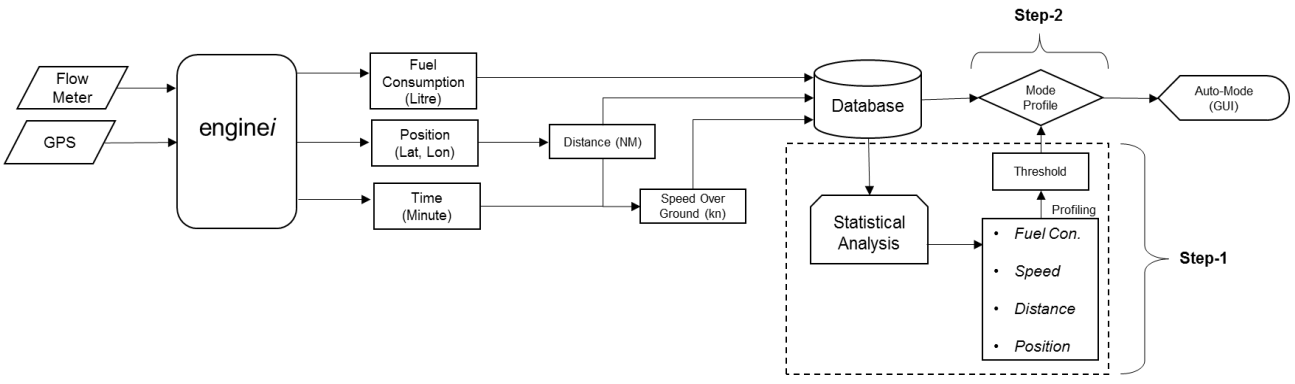

Figure 1: The overview of automatic mode detection.

Correlation analysis is a method of identifying the strength of linear relationships between multiple variables (Leavengood & Reeb, 1999). Correlation analysis is used to check the relationships between the parameters within each mode. Control charts are an effective tool for SPC. In control charts, samples are taken from the process and averages as well as ranges are calculated (Khan, 2013). These are plotted on a chart and interpreted with respect to the process limit or control limits. Control limits are the limits within which the process should be running under normal conditions (Leavengood & Reeb, 1999). I-MR chart is a method for displaying the process performance and was used as a control chart for auto-mode detection. It consists of two charts called Individual (I) and Moving Ranges (MR) charts. I-MR chart is used to detect changes in time ordered data to examine individual values and the control limits are calculated using the average moving range. This chart is used for comparing the performance of the process at different stages (Khan, 2013).

Figure 2 shows the I-MR chart for the distance travelled by The Princess Royal each minute for an hour. The changes of distance travelled and the moving ranges have been monitored. In Figure 2, the X-Axis is the minute of observation and Y-Axis is distance (NM). Similarly, separate I-MR charts have been created for fuel consumption and speed over the ground for each hour by considering 60-minute samples. Different upper (UCL) and lower (LCL) control limits have been obtained for individual hourly fuel consumption, distance travelled and speed. These can be used to identify the changes in the operational behaviour of the vessel.

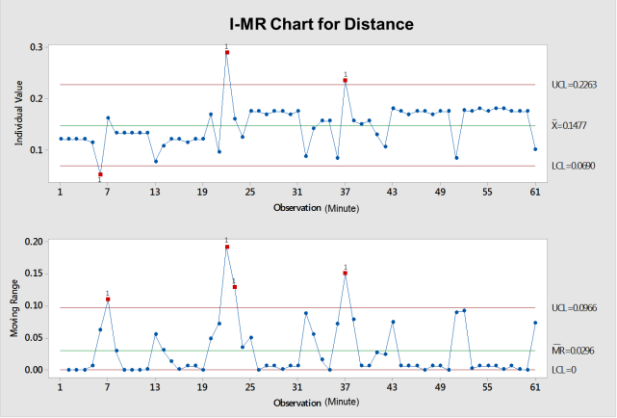

Figure 2: I-MR chart for distance (NM).

The thresholds were identified after analysing the limits and performing the correlation analysis. The mode profiles have been created based on the thresholds of fuel consumption, speed and distance travelled for the individual modes. The SPC method is given below.

UCL and LCL were calculated in Statistical Process Control (SPC) charts for the individual modes.

$$UCL = Mean + 3\,\hat{sd}$$

$$LCL = Mean - 3\,\hat{sd}$$

$$\hat{sd} = \frac{Average\ Moving\ Range}{d_2}, where\ d_2 = 1.128$$

(Bocchetti, *et al*, 2015)

d_2 is a coefficient based on the assumption that the values are normally distributed (Stephenson, 2015).

The mode profile will vary from vessel to vessel. After creating the mode profile, Step-1 will not run again and all data will go directly through the mode profile by following Step-2. "engine*i*" sends data recorded for each minute to the automatic mode detection system and will identify the corresponding mode. The vessel mode and information will be displayed on the bridge. All information would be accessible through a website for on-shore decision-making for optimum operations and, by applying trend analysis, decisions on maintenance scheduling can be taken.

5. TEST RESULT ANALYSIS

The auto-mode detection system has been experimentally implemented on the "The Princess Royal" (RV). The Princess Royal was run in three modes: *Mode-1* (Port), *Mode-2* (Sailing) and *Mode-3* (Stand By). The test results compare the crew pressed mode and the automatically predicted mode during a journey.

In this experiment, an additional mode has been used which is called *Mode-0*. Sometimes a vessel's operational activities are affected by various external factors like wind, wave, tide etc. So *Mode-0* will appear if the data does not match with any of the mode profiles.

The Princess Royal was operated over a two hour trial journey. During the trial, some false entries of the mode were intentionally made. After analysis of the auto-mode data and crew-pressed data, it was found that on two occasions, the auto-mode detection system correctly identified the modes, which were intentionally pressed wrongly by the crew. Firstly, the crew used the standby mode from the 12th minute until the 18th minute but during that period, the vessel speed over ground was 10 to 20 knots so the vessel was really in Sailing Mode. The auto-mode detection system identified the correct mode during that period.

After 91 minutes, the crew again pressed the standby mode but by using the GPS data, the auto-mode system identified that the vessel was in port. *Mode-0* (Undefined) was used in only 3 samples from the total of 120. Around 2.5% of modes were *Mode-0*. That amount did not match with any mode profile. The auto-mode system detected that 62% of the modes matched with the

crew pressed mode- whilst 35.5% of the modes were corrected by the auto-mode system. Those modes were entered intentionally incorrectly by the crew.

6. AUTOMATIC MODE DETECTION SYSTEM

Fuel consumption, speed over ground, distance and port position are the main input parameters for the Auto-Mode Detection system. Speed and Distance are highly correlated but not identical because speed is measured instantaneously and distance travelled is cumulative over time. Figure 3 shows the correlation between the speed over ground and the distance.

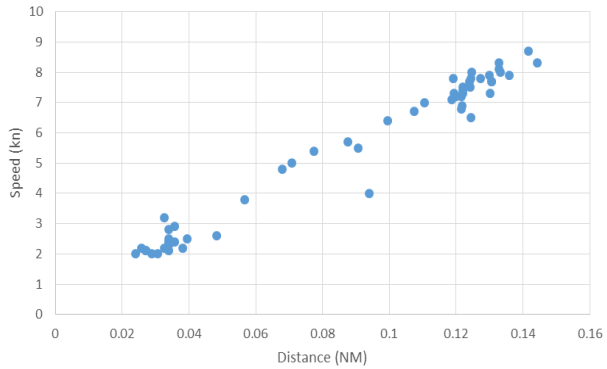

Figure 3: Speed and Distance correlation for Sailing data.

Fuel consumption is the key input parameter required for the Auto Mode Detection system. In addition, either distance or speed can be used to develop a robust system. There is a possibility of a conflict in the mode detection due to the narrow tolerance of the dataset especially during transition from one mode to another. Therefore, all sensor data was considered for the mode profile to reduce the areas of uncertainty.

The auto-mode detection system has also been developed for an OSV. The OSV has four modes: Port, Sailing, Stand By and DP (Dynamic Positioning). The auto-mode detection is a data-oriented system. To identify the mode profile, it is necessary to analyse several days' worth of data from the vessel using basic statistics, correlation analysis and statistical process control. The mode profile will be created for an individual mode by using the thresholds. The sensor data will go through the mode profile to compare with the threshold points. It will identify the vessel's mode when it gets a match with the thresholds. The threshold calculation process is discussed in Section 7. Five days' worth of data was analysed to monitor the OSV activities, speed and fuel consumption in different modes. The sampling rate was one sample per minute and therefore 1440 per day. However, the vessel does not necessarily operate in all modes on any given day. To overcome this, five random days were selected, following consultation with the operator to ensure the vessel had operated in all modes. Figure 4 shows how the OSV data was analysed to get the mode profile.

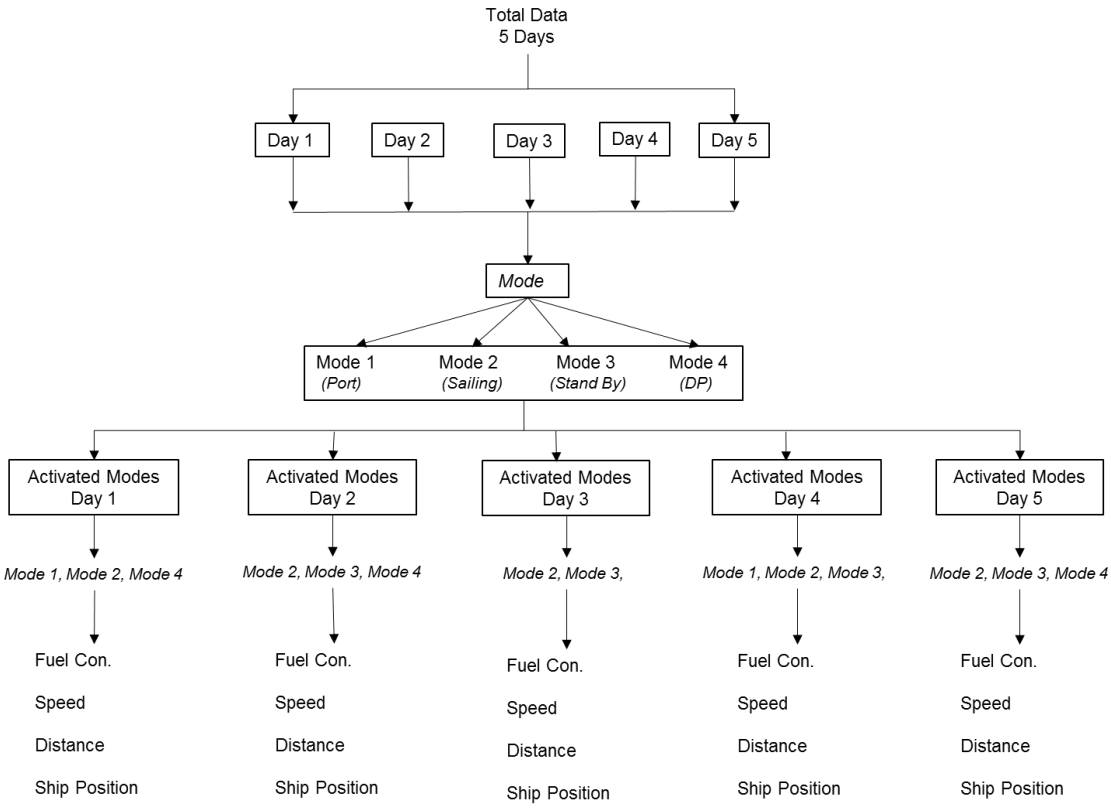

Figure 4: The OSV data structure for analysis to create the mode profile.

Port Mode is detected by using the latitude and longitude of the home port and the vessel's current position. The system will detect Port Mode automatically as soon as the vessel comes within one nautical mile of the port location. The auto-mode detection system could be used for multiple port operations as well. All other modes will not be activated in Port Mode, even if the vessel remains in stand-by or has significant speed in the Port area. Figure 5 illustrates this Port mode concept.

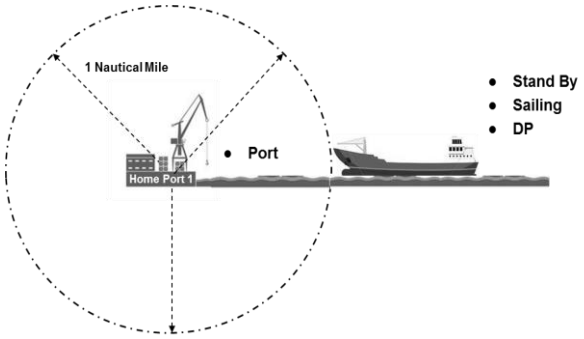

Figure 5: The OSV operations mode detection.

The relationship between the modes of the OSV has been analysed based on the ship's data. Table 1 shows the interrelationship of the fuel consumption, speed over ground and distance for all modes.

Table 1: Characteristics of different modes of the OSV

	Speed Over Ground (kn)			
Mode	**Port**	**Sailing**	**Stand By**	**DP**
Port	-	L	L	L
Sailing	H	-	H	H
Stand By	H	L	-	H
DP	H	L	H	-
	Distance (NM)			
Port	-	L	L	L
Sailing	H	-	H	H
Stand By	H	L	-	H
DP	H	L	L	-
	Fuel Consumption (Litre)			
Port	-	L	L	L
Sailing	H	-	H	H
Stand By	H	L	-	L
DP	H	L	H	-

Note:
L= Characteristic for the mode in far left column lower than for mode in each column.
H= Characteristic for the mode in far left column higher than for mode in each column.

DP would have higher fuel consumption than Stand By. Sailing Mode is expected to have higher fuel consumption than all others modes. In the case of distance, the Sailing Mode covers comperatively higher distances than other modes. The mode selection sequence for the auto-mode detection system is shown in Figure 6.

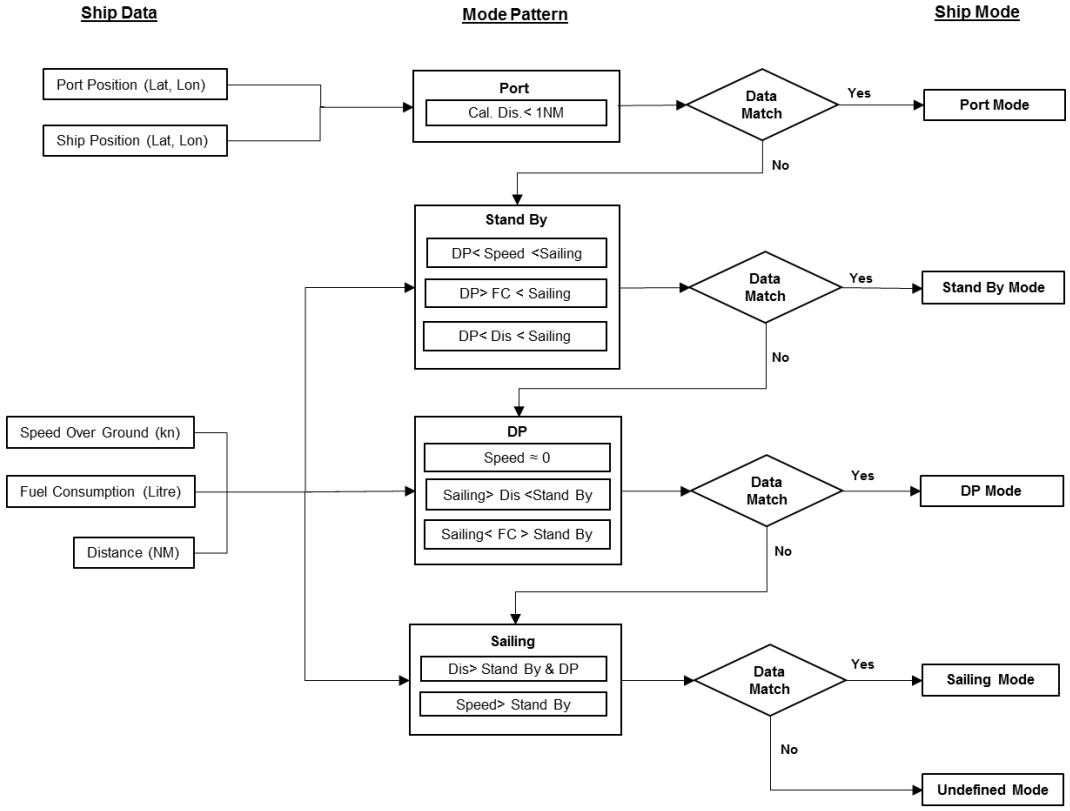

Figure 6: Mode identification process.

7. MODE PROFILE THRESHOLDS FOR THE OSV

Sailing Mode defines that the vessel is in running condition and covers a substantial distance from the previous point. The minimum speed at which the vessel would travel what would be considered to be a significant distance has been defined as the Sailing threshold.

Normally the OSV operates at a speed in the range of 8-10 knots in Sailing Mode. When the vessel is approaching a destination (rig or port) the speed reduces significantly. UCL and LCL contain 99.7% of measurements and data falling within the control limits indicates the expected mode of operation. However, to allow for the speed reduction, the average minimum speed and distance covered have been used for the thresholds of the Sailing Mode profile, rather than the average LCL, as detailed in Table 2.

Stand By and DP Modes are complex to distinguish in many cases. The Stand By Mode activates when the vessel stops outside of the port area. The vessel would be in this mode for different reasons like changing mode or if it has no operational activities while outside of the port area. In DP Mode, the vessel holds a fixed position and automatically compensates natural forces such as the wind, wave and current (Bjorneseth, Dunlop & Stand, 2008). Different types of thrusters are used in the DP Mode (Singh, 2016). The vessel speed is close to zero in both modes but the fuel consumption is expected to be higher in DP Mode. The expected distance travelled per minute will be very low for both modes although sometimes the OSV has non-zero but very low speed in the DP Mode due to the impact of weather conditions. For this project, the OSV was in calm weather conditions. Distance and fuel consumption data for the Stand By and the DP Mode is shown in Table 3 and Table 4.

The average UCL has been considered as the maximum limit for the fuel consumption. If both fuel consumption and speed go above the Stand By threshold limit, then the OSV is considered to be in Sailing Mode. If the fuel consumption is higher than the limit for the Stand By Mode but no speed has been gained, then the OSV would be in DP Mode.

8. MODE TRANSITION PERIOD AND ANALYSIS

Mode-0 will appear if the ship data does not match with any of the mode profiles. Further investigation has been made on *Mode-0* and any points where the auto-mode output did not match with the crew pressed mode.

Around 3.2% of the mode data was in *Mode-0* for Day-1 using the auto-mode system. Discrepancy analysis has been carried out on *Mode-0* for Day-1 considering 14 cases. Discrepancy analysis demonstrates disparity; a large difference between measurable parameters. Table 5 shows the discrepancy results for the day. Column-2 in Table 5 shows the number of times when the crew pressed mode and the auto-mode were not in agreement. Around 8.2% of the auto-mode data did not match with crew pressed mode. The auto-mode system runs on real-time data but it is not possible for the crew to change the mode every minute. In this case, the OSV has high conflict rates between the auto-mode and crew pressed mode because the crew left the system in Sailing Mode incorrectly when the OSV was in the port area on Day-1.

Column-3 in Table 5 represents *Mode-0* for other cases. The *Mode-0* rate is highest in DP Mode for the OSV. In DP Mode, the vessel is expected to consume higher fuel than Stand By Mode and also cover less distance than the Sailing Mode.

For the OSV, the fuel consumption matched with the DP Mode profile but the distance was over the limit many times. That is the main reason for the *Mode-0* in DP Mode. If the distance threshold is increased for the DP profile, the undefined mode (*Mode-0)* rate may be reduced by more than 50%.

It has been found that the unmatched mode with the crew operation mostly happened when the vessel changed from one mode to another (see the last 3 causes in Table 5). This Transition Period was defined to be associated with the next mode that the vessel operated in.

9. VERIFICATION AND VALIDATION

After working on the discrepancy analysis of the auto-mode detection system for the OSV, the mode profile was updated and implemented for the verification stage. Five other random days were selected and relevant operational data from the OSV collected to verify the developed Auto-Mode Detection system. The verification data was independent from data used for the development and testing of the system. The analysis of the results is shown below.

10 April 2016: Stand-By and DP
Matched with crew pressed mode- 1318 min (91.5%)
Not matched with crew pressed mode- 80 min (5.7%)
Transition Period- 40 min (2.7%)

14 April 2016: Stand-By and DP
Matched with crew pressed mode- 1216 min (84.4%)
Not matched with crew pressed mode- 208 min (14.4%)
Transition Period- 16 min (1.1%)

1 May 2016: Sailing and Stand-By
Matched with crew pressed mode- 1416 min (98.3%)
Not matched with crew pressed mode- 23 min (5.7%)
Transition Period- 1 min (0.07%)

3 May 2016: Stand-By and DP
Matched with crew pressed mode- 1282 min (89.02%)

Not matched with crew pressed mode- 117 min (8.12%)
Transition Period- 41 min (2.85%)

The results demonstrate that the use of the transition period is high when the vessel switches mode from DP to Stand By or vice versa. This increase may be due to a number of reasons such as the OSV getting closer to a rig or gaining some speed for a short excursion before mode changing which would not be considered as Sailing. So the transitional period is also essentially part of the operational activities.

10. DISCUSSION

The operational modes depend on the vessel's activities. Different types of mode could be used for the same types of vessel. If an additional mode needs to be added to the Auto-Mode Detection system, then the fuel consumption, speed and other related data during that mode would need to be analysed to allow the mode profile to be created. The new mode might conflict with the existing modes, so the threshold limits will need to be considered carefully to avoid mode conflict. The operational mode can be influenced by different external parameters like waves, wind or current. Therefore, the accuracy rate has been considered to be up to 5%. The fuel consumption in each mode can now be monitored and used to assess the ship's performance. It may be possible to calculate expected fuel consumption in each mode (Bocchetti *et al*, 2015; Erto *et al*, 2015) and this would provide a comparison that would monitor performance further.

The Auto-Mode Detection system is applicable for all types of vessel. Operational modes are different for different types of vessel and a particular vessel would need to run in all modes for a period of time to collect data. For example, "Towing" and "Manoeuvring" could be used as additional modes specifically for a tug.

The inherent added value of the Auto Mode Detection system is to include CO_2 emissions per unit time per ship's activity. The new European Union (EU) regulation on the monitoring, reporting and verification (MRV) of CO_2 emissions has already entered into force. This regulation covers on board CO_2 emissions and also includes a requirement for monitoring data on transportation work and cargo carried (Lloyd's Register Marine, 2015). It also requires annual reporting of the vessel's CO_2 emissions and the need to record each voyage data set in line with an approved monitoring plan (Lloyd's Register Marine, 2015; European Council, 2015). The CO_2 emissions monitoring will cover all emission sources on board such as the main engines, boiler, gas turbine and auxiliaries. The CO_2 emissions will be calculated based on fuel consumption using appropriate emission factors for the fuel type (IMO, 2009) or alternatively by using direct emission measurement (European Council, 2015).

The fuel consumption data per activity is one of the key uses of the auto-mode detection system. The auto-mode report will cover the different operational mode durations, mode fuel consumption, mode distance travelled and engine usage. Therefore, CO_2 emissions can be calculated for each mode of operation by using the carbon emission factor (IMO, 2009). The auto-mode detection system will support the ship operators in compliance with the EU regulation (MRV) by capturing the required data including data on CO_2 emissions, fuel consumption, distance travelled and time spent at sea and at berth.

11. CONCLUSION

A vessel's fuel consumption and profitability heavily depend on engine operating conditions. Monitoring a set of parameters relating to the condition of a system allows the operators to identify any significant changes leading to the development of faults.

This paper addresses how the statistical analysis of sensor data removes human intervention from the vessel operation and helps with decision support for engine maintenance. The auto-mode summary report will help to develop maintenance plans based on the use of the engines in different modes. The onboard and on-shore members of staff would be able to measure the vessel operational performance and emissions. This paper also demonstrates that the vessel operations contain human error and how those errors have been corrected by implementing statistical analysis of the vessel operation. It also addresses the mode transition period and validates the process by implementing it on data from different days.

12. ACKNOWLEDGEMENTS

The authors would like to acknowledge the support of Royston Ltd, Innovate UK and KTP Project 9738.

13. REFERENCES

1. DNV GL, *'Shipping 2020'*, DNV GL Final Report, 2012.
2. European Commission, '*Proposal for a regulation of the monitoring, reporting and verification of carbon dioxide emissions from maritime transport and amending Regulation (EU) No 525/2013*', European Commission Transportation, 2013.
3. BUHAUG Ø, CORBETT JJ, ENDRESEN Ø, EYRING V, FABER J, HANAYAMA S, et al. '*Second IMO GHG Study 2009*', International Maritime Organization (IMO), pp 240, 2009.
4. Lloyd's Register, QinetiQ and University of Southampton, '*Global Marine Technology Trends 2030*', LR Marine Project, 2015.
5. DNV GL, '*Big Data- the new data reality and industry impact*', Strategic Research & Innovation Position Paper-4, 2014.

6. Newcastle University, '*Blyth Marine Station and RV Princess Royal*', MAST Marine Station-RV Brochure, 2015.
7. VENESS, C., '*Calculating distance, bearing and more between two latitude/longitude points*', Institute of Geophysics Texas, 2007.
8. MILLER, S., '*Speed, Time & Distance*', School of sailing, 2013.
9. SIMON, D.L., LITT., J.S., '*A Data Filter for Identifying Steady-state Operating Points in Engine Flight Data for Condition Monitoring Applications*', National Aeronautics and Space Administration (Technical Report NASA /TM2010- 216359), 2010.
10. TRODDEN, D.G., MURPHY, A.J, PAZOUKI. K. and SARGEANT. J., '*Fuel usage data analysis for efficient shipping operations*', Ocean Engineering 110, pp 75–84, 2015.
11. BOCCHETTI, D., LEPORE, A., PALUMBO, B., and VITIELLO, L., '*A statistical approach to ship fuel consumption monitoring*', Journal of Ship Research, Volume 59, Number 3, pp 162-171(10), 2015.
12. ERTO, P., LEPORE, A,. PALUMBO, B., and VITIELLO, L., '*A Procedure for Predicting and Controlling the Ship Fuel Consumption: Its Implementation and Test*', Quality and Reliability Engineering International, Volume 31, Number 7, pp 1177-1184(8), 2015.
13. LEAVENGOOD, S. and REEB, J., '*Statistical Process Control: How and Why SPC Work*', Oregon State University (Extension forest product manufacturing catalogue), 1999.
14. KHAN, R., '*Statistical Process Control*', Problem Solving and Data Analysis using Minitab-ISBN 978-1-118-30757-1, 2013.
15. STEPHENSON, W.R. '*Control Chart Construction*', Iowa State University (Department of Statistics), 2015.
16. Lloyds's Register Marine, '*European Union Regulation on Monitoring, Reporting and Verification of Carbon Dioxide from Ships*', EU MRV Guidance (Version 4), 2015.
17. European Council, '*Regulation (Eu) 2015/757 of the European Parliament and of the Council on the monitoring, reporting and verification of carbon dioxide emissions from maritime transport, and amending Directive 2009/16/EC*', EUR-Lex: Access European Union Law, 2015.
18. IMO, '*Guidelines for voluntary use of the ship energy efficiency operational indicator (EEOI)*', MEPC.1/Circ.684, 2009.
19. BJORNESETH, F., DUNLOP, M.D., and STAND, J.P., '*Dynamic Positioning System-Usability and Interaction Styles*', NordiCHI, 2008.
20. SINGH, B., '*An Introduction to Dynamic Positioning System*', Marine Insight, 2016.

APPENDICIES

Table 2: Sailing mode data of the OSV.

Mode-2	**Sailing**					
Distance		Avg (NM)	Max (NM)	Min (NM)	UCL (NM)	LCL (NM)
	Day-1	0.19	0.54	0	0.203	0.175
	Day-2	0.191	0.391	0.042	0.203	0.177
	Day-3	0.144	2.62	0.024	0.156	0.126
	Day-4	0.139	0.202	0.03	0.16	0.12
	Day-5	0.148	0.182	0.038	0.161	0.135
	Avg.	0.1624	0.787	***0.0268***	0.1766	0.1466
	Max	0.191	2.62	0.042	0.203	0.177
	Min	0.139	0.182	0	0.156	0.12
Speed						
		Avg (kn)	Max (kn)	Min (kn)	UCL (kn)	LCL(kn)
	Day-1	11.36	12.7	2	11.63	11.09
	Day-2	11.44	12.8	2	11.72	11.13
	Day-3	8.49	11.5	2	9.38	7.59
	Day-4	8.34	12	2.1	9.39	7.33
	Day-5	8.88	10.8	2.2	9.71	8.04
	Avg.	9.702	11.96	***2.06***	10.366	9.036
	Max	11.44	12.8	2.2	11.72	11.13
	Min	8.34	10.8	2	9.38	7.33

Table 3: Stand By Mode data of the OSV.

Mode-3	**Stand By**					
Distance		Avg (NM)	Max (NM)	Min (NM)	UCL (NM)	LCL (NM)
	Day-1	0.01	0.66	0	0.0305	0
	Day-2	0.005	0.025	0	0.011	0
	Day-3	0.006	0.034	0	0.013	0
	Day-4	0.01	0.03	0.003	0.03	0.003
	Day-5	0.003	0.029	0	0.01	0
	Avg.	0.0068	0.1556	0.0006	0.0189	0.0006
	Max	0.01	0.66	0.003	***0.0305***	0.003
	Min	0.003	0.025	0	0.01	0
Fuel Con.						
		Avg (ltr)	Max (ltr)	Min (ltr)	UCL (ltr)	LCL(ltr)
	Day-1	2.41	5.41	1.61	2.64	2.18
	Day-2	2.71	5.02	2.07	3.3	2.12
	Day-3	3.83	6.09	2.6	4.88	2.78
	Day-4	3.91	7.07	3.07	5.2	2.63
	Day-5	3.05	5.35	2.4	3.59	2.5
	Avg.	3.182	5.788	2.35	***3.922***	2.442
	Max	3.91	7.07	3.07	5.2	2.78
	Min	2.41	5.02	1.61	2.64	2.12

Table 4: DP Mode data of the OSV.

Mode-4	**DP**					
Distance		Avg (NM)	Max (NM)	Min (NM)	UCL (NM)	LCL (NM)
	Day-1	0.003	0.066	0	0.01	0
	Day-2	0.004	0.033	0	0.012	0
	Day-3	-	-	-	-	-
	Day-4	-	-	-	-	-
	Day-5	0.002	0.048	0	0.006	0
	Avg.	0.003	0.049	0	0.009	0
	Max	0.004	0.066	0	0.012	0
	Min	0.002	0.033	0	0.006	0
Fuel Con.						
		Avg (ltr)	Max (ltr)	Min (ltr)	UCL (ltr)	LCL(ltr)
	Day-1	4.45	6.2	3.73	4.91	3.99
	Day-2	2.71	5.02	2.07	3.3	2.12
	Day-3	-	-	-	-	-
	Day-4	-	-	-	-	-
	Day-5	5	8.23	3.87	5.57	4.47
	Avg.	4.053	6.483	3.223	4.593	3.527
	Max	5	8.23	3.87	5.57	4.47
	Min	2.71	5.02	2.07	3.3	2.12

Table 5: Discrepancy analysis for Day-1.

Cause	**Number of occurrences Diff AMD/Crew**	**Mode-0**	**Total**
FC>4.1, Matched with DP Profile	17		
Dis>0.006, Speed=0, FC>4.1		42	
Dis<0.03*, dis low, speed>2		1	
Dis >0.03, FC>4.0, High FC and Dis for Stand By			
Dis>0.03, FC<4.0, Low FC for DP and High Distance for Stand By		3	
FC>4.0, Dis in range but high FC for Stand by			
FC>4.0 and FC<4.1, Speed=0, Dis=0		1	
FC<4.0, Matched with Stand by Profile	1		
FC<4.1, Stand by	1		
Vessel speed>2	2		
Port	30		
Stand by, Wrong mode continued	18		
DP, Wrong mode continued			
Sailing, Wrong mode continued	49		
Total	118	47	165
%	8.19	3.26	11.46

THE ECONOMICS OF A LONG TERM COATING

(DOI. No: 10.3940/rina.ijme.2017.a3.416)

R Willemen, **H Verstraelen**, **R Meskens**, **D Luyckx**, **K Vastmans**, Antwerp Maritime Academy, Belgium, **S Lenaerts**, Department of Bioscience Engineering, University of Antwerp, Belgium, **G Potters**, Antwerp Maritime Academy, Belgium and Department of Bioscience Engineering, University of Antwerp, Belgium, and **K De Baere,** Antwerp Maritime Academy, Belgium

SUMMARY

An important challenge during ship construction is the protection against corrosion of the ballast tanks. These tanks have many compartments, contain multiple structural elements and play a critical role in the seaworthiness. The majority of the ballast tanks are prepared and coated according to IMO Performance Standard for Protective Coating regulations (PSPC), using a light colored epoxy coating that, when maintenance is being performed by the crew, must remain in a "good" condition for 15 years. This method is set next to a protection system applied by a given owner who keeps its ships in an excellent condition for their complete lifetime using a long term coating. More attention is paid to the preparation and application of the coating and consequently it protects the ballast tanks for more than 25 years. These coating strategies are compared in an economic analysis, supplemented with a sensitivity analysis to evaluate the outcomes due to variable parameters. The results indicate that a long term coating only pays off for owners willing to keep the ballast tanks of their vessels in a good condition for the complete lifetime. The decisive factor is that a long term coating entails no recoating in dry dock. The latter results in less toxic components in the atmosphere.

1. INTRODUCTION

The corrosion rate on board of a merchant ship depends on many factors such as the ship's operational life, the quality of the steel, the methods of corrosion protection, the operation conditions, etc. The combination of all these factors may lead to substantial variation in the corrosion rate and thus differ considerable from case to case, calling for an increasing interest in building up phenomenological models for the probabilistic description of the corrosion, based on improved understanding of specific corrosion mechanisms (Lyuben, Ge & Ah Kuan, 2004).

Ship construction steel can only be protected in 2 ways: by making the steel cathodic, using sacrificial anodes or impressed current, and/or by applying a coating. Coating steel is by far the most practical way to protect it. The common protective coatings are paints, hot dip galvanizing, zinc or aluminum metal spray and any of the last three over coated with subsequently other layers of paints.

Several types of coatings have been developed providing long term protection by barrier mechanism (Thapar, 2013) (Popoola et al., 2014). Subsequent research has proven that oxygen and water, at a level sufficient to initiate the corrosion reaction, can indeed permeate through intact coatings. Current theories propose that water permeating through a coating to the steel surface can cause displacement of the coating from the steel allowing corrosion to occur. Low permeability and good 'wet adhesion' i.e. adhesion under immersion, are widely believed to be the single most important aspects of corrosion control by coatings (www.international-marine.com, 2014).

Within the context of this article only coated steel will be considered within ballast tanks. Today, ballast tanks are a critical area of weakness. The service life of many ships is not determined by the external battering of the ship's hull due to the waves but by the gradual internal corrosion of the ballast tanks (Thapar, 2013) (De Baere, 2011) (Lloyd's Register, 2006) (De Baere et al., 2013) (Sousa & Gorvatov, 2016).

The aim of this article is to economically assess the effect of the use of a long term coating. The latter implicates that the coating was well selected and applied in an appropriate manner; resulting in a good coating condition even after a life span of 25 years. On-site investigations identified a ship owner with a remarkable better coating performance when compared to the coating performance of an average ship (De Baere, Verstraelen, Willemen, Meskens & Potters, 2014).

Before determining the economic assessment of a long term coating, the corrosion rate and the corrosion wastage must be clearly identified as the economic assessment is based on the expected degradation of the ship's structure using actual corrosion rates. Additionally, a good coating condition is defined, as this is the target condition. This study is performed from an economic point of view; however, a long term coating is also beneficial for the environment. If less coating has to be applied there will be less toxic components and less volatile organic compounds will be expelled into the atmosphere. A ship with ballast tanks in a "good" condition is safer than a ship with her ballast tanks being classified "fair" or even "poor". 90% of ships failures can be attributed to corrosion (Melchers, 1999). Safer ships are better for crew, cargo and environment. Ships in better condition will last longer and so reduce the number of new ships to be built.

This paper will assess the economic impact of a long term coating compared to an average coating. In section

2, the assessment model is developed and presented. Section 3 presents the results, while section 4 concludes.

2. MATERIAL AND METHOD

2.1 INTRODUCTION

The objective is to compare the costs of two coating strategies that need to remain 'good' over a life span of 25 years. The first strategy (average coating) leads to an average coating performance and the second (long term coating) is a coating selected and applied so that it results in a longer service life. The approach is illustrated in Figure 1.

First, a 'good' coating condition is defined as the strategies imply to keep the coating 'good' over a life span of 25 years. Subsequently the resulting coating degradation or corrosion wastage over time is defined for both strategies. In order to be able to express this evolution, a corrosion index (CI) was used. With this corrosion index, the coating degradation is translated into one figure only. From this we obtain the degradation over time visualised in regression curves.

The comparison itself will be an economic assessment. Ship owners will only be interested in the use of a long term coating, with a higher application cost than the average coating, if it becomes financially beneficial over time. Therefore, the economic assessment will compare the coating costs of two vessels of which the ballast tanks have different coating strategies. For a proper comparison, an identical coating condition after a certain life span is put forward, namely "good" for a life span of 25 years.

2.2 CORROSION WASTAGE

Building models of physico-chemical processes has many purposes. They are of help to an engineer in the industry as much as to a researcher in a laboratory. Models are a tool to predict what may happen in the future (Nešić, 2007).

Corrosion models can be subdivided in different categories ranging from very simple to complex, such as linear models (Southwell, Bultman & Hummer, 1979), trilinear and power models (Melchers, 1998), the model of Guedes Soares & Gorbaotov (Soares & Garbatov, 1997), the Qin & Cui's model (Qin & Cui, 2003) and finally the most complete, the Melchers' physically based model (Melchers, 2003) for steel immersed in seawater (Luque, Hamann & Straub, 2014).

All the models above take into account a phased evolution of the corrosion process. Lyuben, Spencer & Ge (2003) stated that when considering reasonable simplified assumptions, the corrosion process of coated steel proceeds in 3 phases. The first phase (0 - T_1) is when the protective coating is intact and there is no corrosion wastage of the structure. The second phase (T_1 - T_2) is a gradual acceleration of the corrosion. Implicating that every year more surface will corrode than the amount of surface that corroded the year before. In the final phase (> T_2) the corrosion rate reaches its maximum. At this moment the corrosion rate is constant over the ship's lifetime, implicating that every year a same amount of surface will corrode.

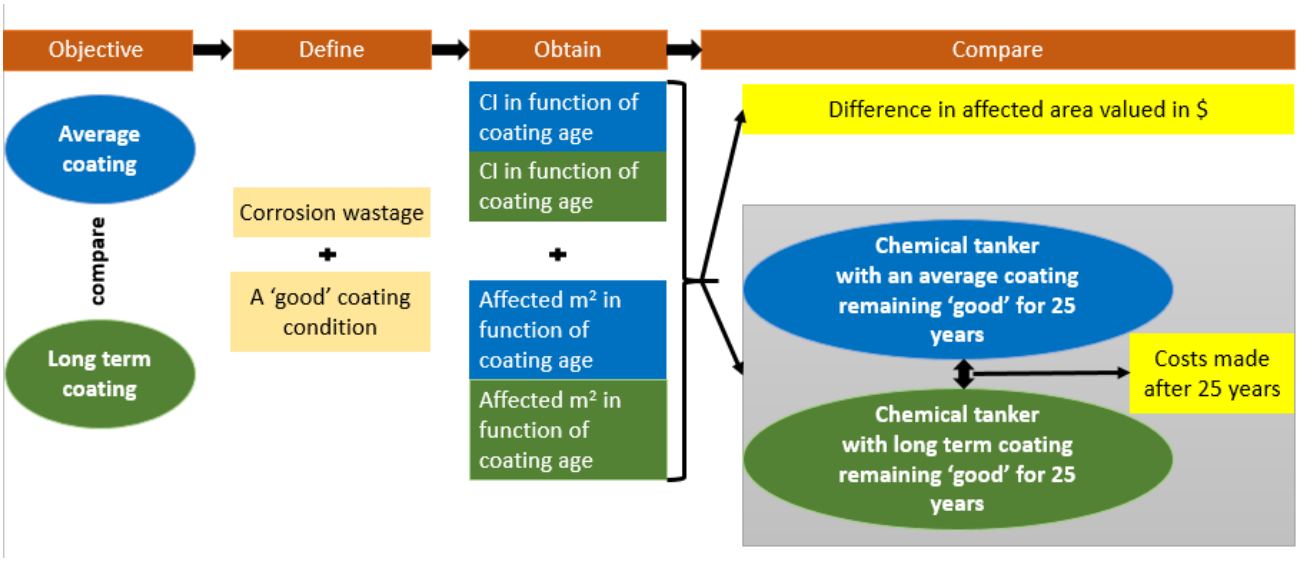

Figure 1: Schematic overview of the methodology used

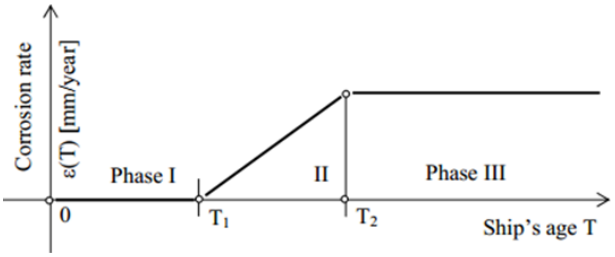

Figure 2: Corrosion rate versus ship's age, 3 distinctive phases. Phase I: no corrosion wastage, phase 2: gradual acceleration of corrosion, phase III constant corrosion rate (Lyuben et al., 2003)

The corrosion wastage or total corroded surface at any time, equals then the area under the curve of Figure 2.

$$\delta(T) = \int_0^T \varepsilon(T)\,dT$$

(Lyuben et al., 2003)

with: δ(T) = corrosion wastage at any time in mm

ε(T) = corrosion rate in mm/year

Corrosion is inevitably present on board of a ship and the amount of corrosion depends on the coating age. Limiting the corrosion wastage will extend the lifespan of a vessel.

The Performance Standard for Protective Coating (PSPC), adopted by the International Maritime Organization (IMO) Resolution MSC.215 (82), became mandatory on 1 July 2008 for dedicated seawater ballast tanks on all types of ships of not less than 500 gross tonnage and for double-side skin spaces arranged in bulk carriers of 150 m in length and upwards. The $PSPC_{15}$ standard set out a target useful coating life of 15 years, over which the coating is intended to remain in "good" condition from initial coating application.

The Tanker Structure Co-Operative Forum's (TSCF) guidelines for ballast tank coating systems and surface preparation is the conclusion of a study, based on experiences of coating lives and cross referencing these with the various application standards used. The design life specifications are designated as $TSCF_{10}$, $TSCF_{15}$ and $TSCF_{25}$. Following these specifications, it is intended to provide coating systems with life expectancies of not less than 10, 15 and 25 years respectively. Here the life of the coating is considered effective until the coating degrades, by normal wear and tear, to a "poor" condition as defined by IACS in the Enhanced Survey Program (ESP) (Shell, 2000).

In practice, comparing the difference between the 15 year system specification and a 25 year system specification is mainly surface preparation & edge grinding, more attention to application conditions with an increase in dry film thickness from 320 to 350µm and three full spray coats (+ three stripe coats) instead of two.

Table 1 stipulates the main differences between $PSPC_{15}$ and $TSCF_{25}$. For a complete overview please consult IMO resolution MSC.215 (82) and the TSCF guidelines for ballast tank coating systems and surface preparation (Shell, 2000).

Ballast tanks of 162 randomly chosen ships, including 21 ships owned by a company (further on designated as "X") with an excellent reputation in ballast tank performance, were investigated between 2007 and 2015 according to the protocol presented in Verstraelen et al., (2009) and De Baere et al., (2014). Except for the series of ships owned by company X, no selection criteria whatsoever were taken into account and the ships were visited as the opportunity arose. Owner "X" is able to obtain this good performance by using more demanding standards than $PSPC_{15}$. $TSCF_{25}$ is catalogued under more demanding standards.

The corrosion wastage of the water ballast tanks on board of the 162 ships has been assessed. The corrosion wastage was expressed as a corrosion index (CI) which was weighed based on ascertained local breakdown on edges and welds. The corrosion on the edges was used as a quantifier for the later defined distributive keys (Verstraelen et al., 2009).

Establishing the CI, every tank was divided into a maximum of three levels. For each level (1 [top], 2 [middle], or 3 [bottom]), the percentage breakdown of the coating was visually inspected and compared with a list of reference images. The reference images and values are based upon internationally used standards. (ABS, 2007), (IMO, 2009), (IACS, 2015).

Three separate values were noted for each level:
1. The percentage of corrosion on the flat surfaces (%)
2. The percentage of corrosion on edges and welds (%)
3. The percentage of the quantity of rust scale (%)

The percentages of corrosion on the flat surfaces, edges, and welds and the quantity of rust scale were each translated into a single figure or CI (Verstraelen et al., 2009) as follows:

1. The area of rust scale was included in the breakdown of coating on the flat surfaces and named "breakdown of coating or area rusted".
2. The percentages of "breakdown of coating or area rusted" (CP) and "local breakdown of coating or rust on edge or weld lines" (CE) were weighted using the following distributive keys based on the percentage of edge corrosion:
   - If CE < 20% then CI = (0.85 ×CP) + (0.15 ×CE)
   - If 20% ≤ CE ≤ 40% then CI = (0.725 ×CP) + (0.275 ×CE)
   - If CE > 40% then CI = (0.60 ×CP) + (0.40 ×CE)

Table 1: Differences $PSPC_{15}$ & $TSCF_{25}$ (TSCF, 2000)
* Most important difference between $TSCF_{25}$ & $PSPC_{15}$

	PSPC15	**TSCF25**
Primary surface Preparation:		
Blasting and profile	Sa 2 ½, 30-75 micron	Sa 2 ½, 30-75 micron
Blasting abrasive	No guidance	Some guidance
Soluble salt limit	50 mg/m²	30 mg/m²
Pre-construction primer:	Pre-qualified shop primer	Ethyl-zinc-silicate
Block holding primer:	No guidance	Not acceptable
Secondary surface preparation:		
Steel condition	Preparation grade P2, Three pass edge grinding.	Preparation grade P2, edge grinding to radius
Block joints*	Sa2.5	St3
Salt limit for secondary S.P.	50 mg/m²	30 mg/m²
Surface treatment	Sa 2 ½ on damaged preconstruction primer and welds, Sa2 on intact pre-construction primer removing 70% of primer.	Sa 2 ½ for full area
After erection	Butts St3 or better or Sa 2 ½ where practicable	Butts and damages Sa 2 ½
Profile requirements	30-75 micron or as per coating requirement	As per coating requirement
Dust	"1" for dust sizes class "3", "4" or "5"	"1"
Salts after blasting / grinding	50 mg/m²	30 mg/m²
Bellmouths	No guidance	Extra protection for the area under the bellmouth by reinforced coating or increased thickness

Painting Requirements:		
Minimum surface temp.	R.H.<85% & surface temp min 3° above dew point, only specified during coating, not while curing.	R.H. max. 60% Minimum +10°C, at all times.
Thickness requirement	320 mic dft minimum	350 mic dft minimum
Coating type	Light colour epoxy	Light colour epoxy
Number of coats	Minimum two full stripe coats followed by two full spray coats	Minimum three full stripe coats followed by three full spray coats.

Following the in-situ observations an average coating and a long term coating is identified by regressing the corrosion index (CI) on the coating age (in years). The impact of the regression curves is analysed by comparing the average CI (or affected area) for the general average coating, to the average CI (or affected area) for the coating of company X (long term coating) at any moment in time. The difference between the two coatings (average versus long term) is valued. This is referred to as the depreciation or the avoided costs of a long term coating.

For the translation of the CI into an affected area, a coated ballast tank area of 90,000m² (representing a chemical tanker with a summer deadweight of 37,000MT, a length over all of 170m and a breadth of 32m) is considered.

The value of the avoided costs is defined as the investment at any given moment in time equal to the cost necessary to recoat the extra corroded area of our traditional coating compared to the long term coating. The recoating cost is set at 60 USD/m² after consulting the pricelist of some major dry-docks, the principles brought forward in "Guide to ship repair estimates" (Butler, 2000), coating producers and experienced coating inspectors. The costs of staging, sandblasting, removal of grit, tank conditioning, coating application, removal of staging, time charter equivalent is taken into account as well as the cost for renting the dock.

2.3 COATING CONDITION

Ship owners are not only pushed by international legislation (IMO, 2009) but also by commercial needs in preserving a good reputation, to keep the ballast tanks of their vessels in a "good" condition to avoid extra inspections and costs.

A "good" coating condition is put forward by various institutions. IACS states that the recommended short, medium and long term maintenance (e.g. 5, 10 and 15 years' target lifetime respectively) is to either maintain or to restore "good" coating conditions (IACS, 2015). IMO PSPC

MSC.215 (82) states: "*This standard is based on specifications and requirements which intend to provide a target useful coating life of 15 years, which is considered to be the time period, from initial application, over which the coating system is intended to remain in "good" condition.*" Cargo owners reject ships because the coating in the ballast tanks does not meet IACS "good" requirements as interpreted by the class surveyor, even if the structure is entirely sound (Eliasson, 2003).

A coating is defined "good" when noticing spot rusting on less than 3% of the area under consideration without visible failure (breakdown) of the coating. Rusting edges or welds should be less than 20% of edges or weld lines in the area under consideration. This definition results from the IMO standard which is illustrated in Table 2.

Table 2 is not explicit and consequently open for discussion. Firstly, it is not clear if the three ratings/conditions have to be considered separately or in combination. Secondly, a straightforward definition of "the area under consideration" is missing. According IMO's Maritime Safety Committee, MSC.1/Circ.1330, 4.2, 11 June 2009, "areas under consideration" are areas small enough to be readily examined and evaluated by the surveyor. However, the areas subdivided should not be so small as to be structurally insignificant or too numerous to practically report on.

This unstable definition gives a class surveyor a lot of room for personal interpretation. At the same time this encumbers him with a big responsibility, seeing the consequence of ranking tanks as "fair" or "poor" instead of "good" has huge financial and practical implications. Coming into the "fair" region entails that the inspection program of the ballast tanks becomes more stringent, which can be understood from Table 3. The inspection regime will change from the dry-dock periods to a yearly regime.

Translating the IMO guideline coating conditions scale into the CI, the boundaries of the fair regions were taken as follows:

Minimum Fair condition: CP 3% + CE 20% thus CI = 8%
Maximum Fair condition: CP 20% + CE 50% thus CI = 32%

This results in Table 4.

Table 2: IMO guidelines "GOOD", "FAIR" and "POOR" coating conditions (IMO, 2009)

	GOOD [3]	**FAIR**	**POOR**
Breakdown of coating or area rusted [1]	< 3%	3 – 20%	> 20%
Area of hard rust scale [1]	-	< 10%	≥ 10%
Local breakdown of coating or rust on edges or weld line [2]	< 20%	20 – 50 %	> 50%

Notes:

1 *% is the percentage calculated on basis of the area under consideration or of the "critical structural area"*

2 *% is the percentage calculated on basis of edges or weld lines in the area under consideration or of the "critical structural area"*

3 *spot rusting, i.e. rusting in spot without visible failure of coating*

Table 3: Surveys prescribed according to IACS Rec. 87. S: special survey, I: intermediate survey, A: annual survey (IACS, 2015)

Coating condition	**Surveys (Internal inspection)**															
GOOD	S			I		S			I		S			I		S
FAIR or POOR	S	A	A	I	A	S	A	A	I	A	S	A	A	I	A	S
Vessel age	5	6	7	8	9	10	11	12	13	14	15	16	17	18	19	20

Table 4: CI % translated into the IMO guideline coating conditions scale. CI is corrosion index

	GOOD	**FAIR**	**POOR**
CI	< 8%	8 – 32%	> 32%

2.4 ECONOMIC ANALYSIS

The economic analysis compares the coating costs made to have two ships in a "good" coating condition during the lifespan of 25 years when each use a different strategy, namely the average coating performance and a more demanding standard in accordance with a long term coating strategy (i.e. $TSCF_{25}$).

The consequences of sailing with a ship with ballast tanks in an IACS "fair" condition are significant. Time and money consuming coating surveys come at a yearly interval instead of once every 5 years. Freight will be lost since certain cargoes will not be loaded because the ship did not pass vetting inspections even if the structure is entirely sound (Eliasson, 2003). Safety and environment are compromised.

Cost and benefits (avoided costs) of the long term coating are analysed over the life span of a vessel when compared to the average coating.

As basic premises, the model ship selected for this study is a chemical tanker with a summer deadweight of 37,000MT, a length over all of 170m, a breadth of 32m and 90,000m² of coated ballast tank. The same ballast tank surface is being considered as formerly used to define the depreciation between the regression curves.

The first cost to be taken into consideration is the initial application cost of the coating upon newbuilding of the vessel. Consulting owner "X", coating producers and experienced coating inspectors, the initial coating costs are rated as follows:

- average coating = "standard" coating ($PSPC_{15}$ was considered) 40 USD/m²
- long term coating = "excellent" coating (following the input of company X, $TSCF_{25}$ was considered) at 50 USD/m².

This leads to an initial average coating cost equal to 3,600,000 USD and the long term coating cost comes down to 4,500,000 USD.

Each coating system has a lifespan. The end of the "good" coating condition and thus the start of the "fair" coating condition is considered within this study as the end of the coating's service life. Consequently, in case a ship enters the "fair" condition prior to the age of 25, recoating in dry dock will be taken into account. The value of recoating is again set at 60 USD/m^2 (similar to part 2.2).

Finally ballast tank maintenance must be considered. The most unidentified factor is the "on-board" coating maintenance cost effected within the ballast tanks. The guidelines for maintenance and repair of protective coatings states that "*Maintenance means minor coating restoration work regularly performed by a ship's crew using normal shipboard means and tools to maintain "good" or "fair" coating conditions. Maintenance delays or slows down the coating deterioration and effects short term steel protection*." (IMO, 2009). Consequently, with onboard maintenance one can try to maintain its IACS classification "good" or "fair", but it will not upgrade your classification to a higher level. The fact that onboard maintenance may only be a very short term barrier to slow down coating deterioration is supported by ABS stating that "*Ship operators traditionally carry out maintenance of coatings while at sea by the crew. Studies have shown that this type of maintenance has limited efficacy. This has been attributed to a variety of practical reasons including dirty surfaces, non-performance of coatings, inability to provide even coatings and others. These reasons ignore the critical performance issue: the structure is in working mode (in stress cycles and corresponding deflections) and as such the coating cannot perform as it cannot properly cure due to the disturbances introduced by the vessel's motions"* (Contraros, 2003).

The quotes stress even more the importance of a good coating application in order to obtain an excellent coating performance. Written confirmations of relevant ship-owners suggest that on average shipboard coating maintenance in ballast tanks is minimal to non-existent. Our own observations of 162 ballast tanks surveys revealed very sporadic touch-ups and thus maintenance is not taken into consideration for the traditional coating.

On the contrary, company "X" puts maintenance as a top priority, sailing with crews far in excess of the minimum manning. This in order to keep the ship in showroom condition and thus passing vetting inspections with flying colors. This excellent coating performance can partly be attributed to an intensive on board maintenance program. By maintenance we mean touch-up of local damages, regular de-mudding, rinsing with fresh water and cleaning of the anodes if present. Traces of coating touch-ups were regularly observed. We assume that on board the "X" ship ballast tank coating maintenance is standard routine. Following discussions with former "X" employees, observations on board and own deductions using the International Labor Organization (ILO) salary wages, we concluded that on average 25,000 USD per year is a realistic cost for the on board ballast tanks coating maintenance for the long term coating strategy.

Within this study the inflation % is based on the Long Term U.S. Inflation since 1913 (McMahon, consulted 02/2015). The discount % is based on the average Weighted Average Cost of Capital (WACC) of some important shipping companies as shown in Table 5.

The economic assessment concludes a sensitivity analysis as some uncertainties were noticed. Discussion with tanker companies indicated that the ILO salary wages are not always representing the actual salaries. Literature study revealed a variety in figures as to the recoating/refurbishing cost in dry dock. These uncertainties were consequently incorporated in the model.

Table 5: WACC of some major shipping companies

	WACC	Year	Source
Teekay Cooperation	7.8%	2012	11th Annual German Ship Finance Forum
Golar LNG	8.9%	2012	11th Annual German Ship Finance Forum
Seaspan	6.7%	2012	11th Annual German Ship Finance Forum
Euronav	7.4%	2012	Annual report Euronav 2012
CMB	9.4%	2013	Annual report 2013
AP Moller Maersk	9.0%	2013	Credit Suisse
Overview	8.0%	2011	Audi Capital The shipping Industry – Navigate with the flow
Average	8.2%		

3. RESULTS

3.1 AVERAGE AND LONG TERM COATING PERFORMANCE

Figure 3 shows the CI as a function of the time after coating application of the surveyed ballast tanks. Only 157 ships, for which the date of application of the coating is known, were taken into consideration.

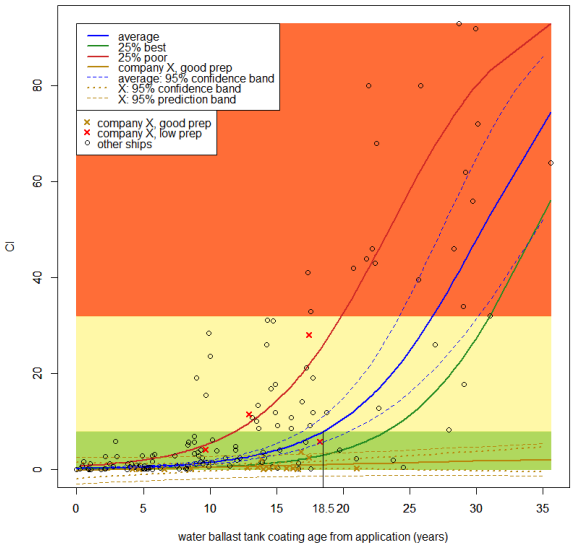

Figure 3: Corrosion % as a function of time after coating application. Blue, red and green using a logistic model. Yellow using a linear model. Blue curve gives average trend line for all 157 vessels (including those of company "X"), green curve shows the 25% best performing vessels and red line the 25% poorest performing vessels. The yellow and red x indicate ships owned by company "X"; the yellow curve is the (extrapolated) linear model for vessels with a long term coating. Definition of "good" using the CI and a visualizing the performance of long term coating within the "good" definition. The dotted lines give the 95% prediction band.

Inspecting the logistic corrosion wastage evolution of the average coating from our database (blue line in Figure 3), we notice that the coating starts to degrade slightly after 5 to 6 years, thus outlining the position T_1. The first 5 to 6 years the coating will age and might show minor rust, but no significant increase in the corrosion rate is identified. After T_1 a clear increase in corrosion rate is detected and around the age of 26 years this increase stabilizes, becomes constant, indicated by the linear continuation of the blue curve. This shows a clear similarity with the trend of the corrosion rate versus the ship's age as suggested in Figure 2. The parameters of the logistic models are statistically significant at the 95% level.

The average of the 25% poorest performing coatings is illustrated by the red line in Figure 3. In this case there is no significant phase 1 (period of intact coating condition). Using the assumption of a negligible CI below 0.5% and using the logistic trend, a CI below 0.5% is never obtained. The transition between phase II and phase III (phase III being the linear growth) occurs at the age of about 20 years.

The green line represents the average of the 25% best performing coatings. Here, the end of phase I can be set around 10 years after coating application; more specifically it is calculated to be 10.1 years when we assume a negligible CI below 0.5%. Phase III is reached after around 30 years.

Following the inspections performed on the 157 ships/coatings, 21 ships of a distinct ship owner "X" with a long term coating strategy could be identified, visualised by the yellow and red crosses in Figure 3. Company "X" has an outstanding reputation when it comes to the selection and application of coatings. The effect of his approach is obvious, seeing the position of the yellow crosses as indicated in Figure 3. The yellow crosses are clearly indicating a performance as good as or even better than the overall 25% best performing vessels from the database. The four red crosses are also vessels owned by "X". As these were either bought second hand or the stringent coating selection and application conditions could not be met, they deviate from the other vessels from the "X" fleet. Seeing that the coating for these off-cases was not controlled by company "X", these cannot be considered in this investigation to validate the importance of a good coating selection and application.

In order to be able to define the corrosion wastage and rate of the long term coating, a linear regression was used based on the observations of company "X". As the CI of those vessels hardly increases over time, a logistic model cannot describe the trend for vessels with a long term coating. The linear model for company "X" shows a slight increase of CI over time, at a rate of 0.07% per year.

For company "X", data on older ships are scarce: only one vessel has a coating aged more than 20 years (21 years). Hence all predictions for the long term coating after 25 years are based on an extrapolation of the regression curve. For this reason the 95% prediction band for the linear regression of company "X" was included on Figure 3 (dashed yellow line). This prediction band stays entirely below a CI of 8, even after 35 years. If we adopt the linear model, we may assume that vessels with a long term coating will remain in "good" condition for more than 25 years.

Comparing the linear regression line for company "X" with the logistic model for all vessels, we notice that the long term coating strategy promises an important reduction of the corrosion rate. This means that the coating is more sustainable and thus more resistant to corrosion. A long term coating can consequently be defined as a well selected coating applied with care and according to high standards. As this definition of a long term coating is established based on in-situ expertise, it is hereby proven that maintaining a long term (lifetime lasting) coating is possible for ballast tanks. It is a matter of selecting a good coating and above all applying it with the necessary care when it comes to application parameters.

In general coatings are applied according to $PSPC_{15}$ which targets a coating useful life of 15 years, over which the coating is intended to remain in a "good" condition from initial coating application (Wei et al., 2011). Figure 3 shows that the average ship transfers from "good" to "fair" condition after approximately 18.5 years (95% confidence interval for CI after 18.5 years is [5.67 ; 10.98]). This implicates that the average vessel meets the objectives of $PSPC_{15}$. It should be noted that the latter also implicates that a lot of ships do not meet with the $PSPC_{15}$ requirements. For the logistic model on all 157 ships, the mean CI at 15 years is 4.02 with a one-sided 65% prediction interval of [0 ; 7.7]. This implies that more than 65% of all vessels are expected to remain in "good" condition (CI < 8) for at least 15 years. Ships are built with an economic life expectancy of typically 25 years and consequently $PSPC_{15}$ may not suffice. Therefore, a "good" $PSPC_{15}$ coating will only be maintained during the entire lifetime when the entire ballast tanks are recoated upon dry docking prior to reaching the fair status, implicating around 15 years. Figure 3 illustrates that owner "X**"** is able to maintain a "good" coating condition throughout a life span of 25 years and longer. The linear trend (yellow line) is the best possible model for the data at hand, but exact values for the age of 25 years must be used with caution. Nevertheless the extrapolated linear regression line gives a good impression of the evolution to be expected and predicted values for the age of 25 years stay well below a CI of 8, with a probability of 95% Hence we may assume that owner "X" will be able to keep his vessels in "good" condition even after 25 years, thanks to the use of more demanding standards. An example of such a standard is for instance $TSCF_{25}$**.** The coating performance of company "X", will be referred to as the long term coating performance.

Figure 4 shows the regression curves, namely the logistic trend (blue line) of the traditional coating and the linear trend (orange line) of the long term coating. When considering a coated ballast tank area of 90,000m² the regression curves can also be expressed in affected area in m^2 (left axis), in addition to being expressed in % CI (right axis). This is depicted in Figure 4.

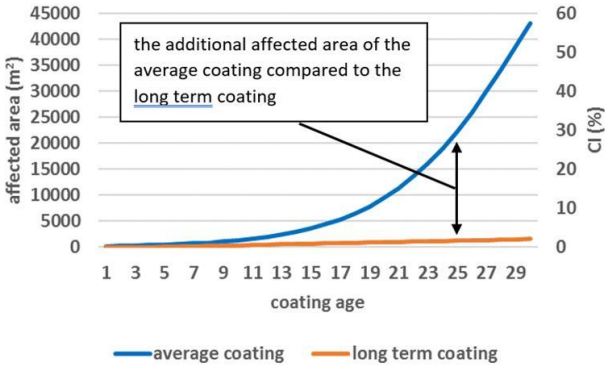

Figure 4: Regression curves of the average coating degradation versus the long term coating degradation expressed in affected area (considering 90,000m² ballast tank area) and expressed in CI.

Without taking into account inflation and discount the avoided costs or benefit of a long term coating is 1,261,261 USD at the age of 25, measured as the difference between the blue and orange line in affected area multiplied with 60 USD per m^2.

It should be noted that it is impossible to only recoat the affected spots. The affected area, resulting from the corresponding CI, represents the sum of all locally corroded spots/areas. In order to recoat a corroded spot one should treat an area which is much larger than the rusted spot itself. Only performing refurbishments of the affected areas will locally ameliorate the condition but the surrounding coating is still aged and will rapidly deteriorate. Only full blasting and recoating is able to place the timer of the coating lifespan back to zero.

3.2 ECONOMIC ASSESSMENT

An average ship with an average ballast tank coating slips into a "fair" condition at the age of 18.5 years. In order to obtain a 'good' coating life of 25 years, the average coating will be recoated in dry dock at the age of 15. Each classed vessel is subjected to a specified programme of surveys based on a five-year cycle. At the end of this cycle a class renewal/special survey is held, which coincides with a dry dock inspection. Following this general survey regime recoating at the age of 15 was put forward and not at the age of 18.5. This can be compared to a ship coated according to $PCPC_{15}$. Following IMO $PSPC_{15}$ a useful coating life of 15 years

is put forward. This demands that the ballast tanks will be recoated at 15 years, when in dry dock. As explained previously, maintenance is not included for the average coating strategy.

Company "X" demonstrates (see Figures 3 & 5) that a lifetime protection of ballast tanks is possible by using a well selected coating and an application without compromises. The company is able to maintain a "good" coating condition of his ballast tanks up to the age of 25 and beyond and thus may be considered as a "good" reference standard. This long term coating strategy can be compared to a ship with ballast tanks coated accruing to $TSCF_{25}$. Here dry-docking is not necessary, however maintenance is considered.

In this economic assessment of the long term coating, the avoided costs (=benefits) are compared with the initial additional coating costs and the additional maintenance costs of long term coating.

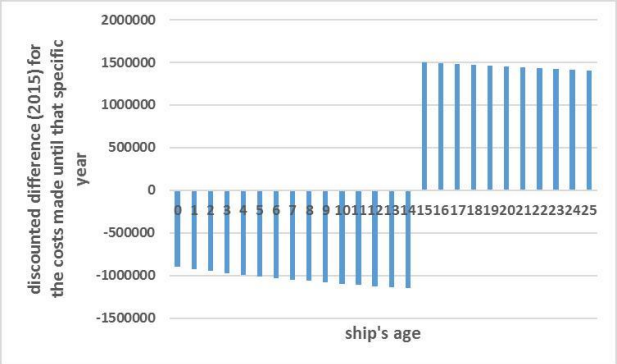

Figure 5: Difference of the costs between long term coating and average coating, expressed in USD, spent to have both ships in the "good" condition during its lifetime. (inflation 3.2% and discount rate 8.17%; 100% of the coating replaced during the 15 year dry-dock at a cost of 60 USD/m^2, 25,000 USD/year on ballast tanks maintenance spent by "X").

Figure 5 shows that coating repairs during dry-dock are an overwhelming factor. The blue bars with negative values implicate a more expensive long term coating, whilst the blue bars with positive values implicate a more expensive average coating. Knowing that a 100% recoating replacement is necessary to guarantee a "good" condition, a long term coating is clearly the best solution with a difference in cost of 1,407,834 USD (3,875,000 USD in case of non-discounted values), when envisaging a lifetime of 25 years.

Following discussions with tanker companies we learned that the ILO salary wages are not always representing the actual salaries, which brings our calculation to a possible maintenance cost of about 35,000 USD/year. On the other hand, from literature study (OceanSaver, 2011) we conclude that touch-ups/maintenance can also be much cheaper. Therefore, a sensitivity analysis with maintenance costs of 15,000; 25,000 and 35,000 USD was applied as illustrated in Table 6. As to the recoating/refurbishing cost in dry dock, we notice a variety in figures ranging from 40 USD/m^2 (OceanSaver, 2011) to 60 USD/m^2 (Safinah, 2007) and even up to 100 USD/m^2 (Kattan, 2010); again a sensitivity analysis was used, ranging from 40 to 80 USD/m^2.

Table 6: Difference in costs with discounted and non-discounted values for ships aged 25 years with a variation in the recoating cost in dry dock of the average coating strategy and the maintenance costs of a long term coating strategy

Recoating cost for the average coating strategy	Maintenance cost for the long term coating strategy	Difference: average coating cost minus long term coating cost USD/year	
USD/m^2	USD/year	index = 0% discount = 0%	index = 3.2% discount = 8.17%
40	15,000	2,325,000	662,486
40	25,000	2,075,000	518,908
40	35,000	1,825,000	375,331
60	15,000	4,125,000	1,551,411
60	25,000	3,875,000	1,407,834
60	35,000	3,625,000	1,264,257
80	15,000	5,925,000	2,440,337
80	25,000	5,675,000	2,296,760
80	35,000	5,425,000	2,153,183

4. CONCLUSION

$PSPC_{15}$ is developed to guarantee a coating in IACS "good" condition for at least 15 years. In-situ investigations learned that on average, a ship with an average traditional ballast tank coating slips only into a "fair" condition at the age of 18.5.

The ballast tank condition is a crucial element during vetting inspections. If the tanks are in a "good" condition the ship-owner will have access to better paying cargoes.

However, the advantages of a ballast tank coating well applied, maintained and repaired go beyond economic considerations. If less coating has to be applied less toxic components will find their way to the marine environment and less volatile organic compounds will be expelled into the atmosphere.

When a traditional ship owner envisages to sail with "good" ballast tanks for more than 18.5 years, a full recoat is necessary. Following a general survey regime this will take place at 15 years of age.

Figure 5 demonstrates clearly that if a ship-owner sails 15 years or less with his ship, $PSPC_{15}$ will always be the cheapest solution. Expensive coating application and maintenance are only making sense if the ship-

owner sails for extended periods with his ships (cradle to grave policy).

If ballast tank coatings become more sustainable there will be less need for coating repair and ship building improving the impact of shipping on the environment.

5. ACKNOWLEDGEMENT

The authors gratefully acknowledge support of the Research Fund of the University of Antwerp (PS ID (Antigoon): 34052). O. Schalm is thanked for his assistance in the discussions.

6. REFERENCES

1. ABS. (2007). *The Inspection, Maintenance and Application of Marine Coating Systems*. Houston: ABS.
2. BUTLER, D. (2000). *Guide to ship repair estimates*. Oxford: Butterworth Heinemann.
3. CONTRAROS, PD. (2003). *"The Domino Effect" Coating Breakdown – Corrosion – Structural Failures Leading to Possible Design Ramifications*. London: Proceedings of Lloyd's Register Conference on the prevention and management of Marine Corrosion.
4. DE BAERE, K. (2011). *Corrosion in ballast tanks of merchant vessels.* Antwerp: p.184.
5. DE BAERE, K., VERSTRAELEN, H., RIGO, P., VAN PASSEL, S., LENAERTS, S. and POTTERS, G. (2013). *Study on alternative approaches to corrosion protection of ballast tanks using an economic model*: Marine Structures 32, 1-17.
6. DE BAERE, K., VERSTRAELEN, H., WILLEMEN, R., MESKENS, R. and POTTERS, G. (2014). *Taking care of Ballast Tank Coatings =Green Ballast Tanks Coatings*. Alexandria: SNAME, p. 1-14.
7. ELIASSON, J. (2003) *Prevention and Management of Marine Corrosion.* London: Lloyd's List events Conference, p. 23.
8. IACS. (2015). *Recommendation 87, Guidelines for coating maintenance & repairs for ballast tanks and combined cargo/ballast tanks on oil tankers*. London: IACS.
9. INTERNATIONAL MARINE COATINGS. (2014). *What is corrosion?* www.internationalmarine.com; [accessed 26.12.2014].
10. IMO. (2009). *MSC.1/Circ.1330, 4.2 Guidelines for maintenance and repair of protective coatings.* London: IMO.
11. IMO. (2006). *Resolution MSC.215 (82) Performance Standard for Protective Coatings for Dedicated Seawater Ballast Tanks in all Types of Ships and Double-Side Skin Spaces of Bulk Carriers*. London: IMO; adopted on 8 December.
12. KATTAN, R. (2010). *Corrosion in ballast tanks*: RINA conference.
13. LLOYD'S REGISTER. (2006). *Tanker Focus*, London: Lloyds Register. Issue 1.
14. LUQUE, J., HAMANN, R. and STRAUB, D. (2014). *Spatial model for corrosion in ships and FPSOS*. USA, California, san Francisco: ASME: Proceedings of the 15. ASME 2014 33rd International Conference on Ocean, Offshore and Arctic Engineering, p. 1-11.
16. LYUBEN, I., GE, W., AH KUAN, S. (2004). *Evaluating Corrosion Wastage and Structural Safety*. Houston: ABS.
17. LYUBEN, I., SPENCER, J. and GE, W. (2003). *Probabilistic evaluation of hull structure renewals.* Houston: ABS.
18. MCMAHON, T. *Long Term Inflation*. http://inflationdata.com/Inflation/Inflation_Rate/Long_Term_Inflation.asp. [accessed 02.2015].
19. MELCHERS, R. (1998). *Probabilistic modelling of immersion marine corrosion*. Structural safety and reliability, vol. 3: p. 1143-1149.
20. MELCHERS, R. (1999). *Corrosion uncertainty modelling for steel structures*. J Constr Steel, 52:p 3–19.
21. MELCHERS, R. (2003). *Modeling of marine immersion corrosion for mild and low-alloy steels—Part 1: Phenomenological model.* Corrosion Vol. 59, No. 4.
22. NEŠIĆ, S. (2007). *Key issues related to modelling of internal corrosion of oil and gas pipelines – A review*. Corrosion Science - Vol. 49, Issue 12: p. 4308–4338.
23. OCEANSAVER. (2011). *About Corrosion and Ballast Water Treatment Systems*. Napels: Industry conference Atenanazionale.
24. POPOOLA, A., OLORUNNIWO, O., IGE, O. (2014). *Corrosion Resistance Through the Application of Anti-Corrosion Coatings*. South Africa: Intech, In M. Aliofkhazraei, Developments in corrosion protection, p. 241- 265.
25. QIN, S. and CUI, W. (2003). *Effect of corrosion models on the time dependent reliability of steel plated elements*. Marine Structures vol. 16, 15-34.
26. SAFINAH. (2007). *Coating Performance Standard, a review.* Amsterdam: PCE-PSPC workshop.
27. SHELL IT. (2000). *Ballast Tanks an overview of the TSCF Guidelines for ballast tank coating systems and surface preparation.* Tokyo: Tanker Structures Co-Operative Forum Shipbuilders Meeting.
28. SOARES, C. G. and GARBATOV, Y. (1997). *Reliability assessment of maintained ship hulls with corroded elements*. Marine Structures - vol.10: p. 629-653.

29. SOUSA, S. and GORVATOV, Y. (2016). *Coating breakdown assessment of steel plates in marine structures subjected to compressive load*. Lisbon: CRC Press. Maritime Technology & Engineering, p. 557.
30. SOUTHWELL, C., BULTMAN, J. and HUMMER, C.J. (1979). *Estimating of service life of steel in seawater*. In M. Schumacher, New Jersey: Noyes Data Corporation. Estimating, p. 374-387.
31. TSCF. (2002). *Guidelines for Ballast Tank Coatings and Surface Preparation*, Livingston: Witherbys publishing.
32. THAPAR, LV. (2013). *Corrosion Prevention in Ballast Tanks*. New Delhi.
33. VERSTRAELEN, H., DE BAERE, K., SCHILLEMANS, W., DEWIL, R., LENAERTS, S. and POTTERS, G. (2009). *In situ study of ballast tank corrosion on ships.* Materials Performance; 48(10): p. 48-51.
34. WEI, C., ELIASSON, J., JANSEN, E., WANG, G. and BASU, RI. (2011). *IMO PSPC implementation and 15 years of target useful coating life*. Houston: Ship Structure Committee ABS, p.15.

AN OPTIMIZATION MODEL FOR PRELIMINARY STABILITY AND CONFIGURATION ANALYSES OF SEMI-SUBMERSIBLES

(DOI No: 10.3940/rina.ijme.2017.a3.421)

G D Gosain, Oceaneering Subsea Distribution Solutions, India, **R Sharma**, Design and Simulation Laboratory, Department of Ocean Engineering, IIT Madras, India and **Tae-wan Kim**, Department of Naval Architecture and Ocean Engineering, SNU, Republic of Korea

SUMMARY

In the modern era of design governed by economics and efficiency, the preliminary design of a semi-submersible is critically important because in an evolutionary design environment new designs evolve from the basic preliminary designs and the basic dimensions and configurations affect almost all the parameters related to the economics and efficiency (e.g. hydrodynamic response, stability, deck load and structural steel weight of the structure, etc.). The present paper is focused on exploring an optimum design method that aims not only at optimum motion characteristics but also optimum stability, manufacturing and operational efficiency. Our proposed method determines the most preferable optimum principal dimensions of a semi-submersible that satisfies the desired requirements for motion performance and stability at the preliminary stage of design. Our proposed design approach interlinks the mathematical design model with the global optimization techniques and this paper presents the preliminary design approach, the mathematical model of optimization. Finally, a real world design example of a semi-submersible is presented to show the applicability and efficiency of the proposed design optimization model at the preliminary stage of design.

1. INTRODUCTION

In the design of engineering structures, a normal design approach is to maximize the safety and operational performance and minimize the cost. It is well known that from the design point of view some of these functional parameters (i.e. parameters that are minimized or maximized in the design process) are often either antagonistic or conflicting in nature or both. These can be treated with the application of 'Multiple Criteria Decision Making (MCDM)' optimization methods, for more details see Deb (2009), Papanikolaou *et al*. (2010), Coello *et al*. (2014). A simple and illustrative example relates the objectives like cost and safety, e.g. in general if cost (e.g. through less freeboard, less plate thickness, less coatings of paint, and lower size of stiffeners, etc.) is reduced then the safety is compromised and vice versa. There exists a critical demand from the industry to have a preliminary design model that is based on the advanced empirical techniques, is computationally efficient and allows the designer to compute optimal design solutions satisfying the requirements of the owner/order placing agency. This demand has motivated the present research.

Our primary aim is to investigate a preliminary design approach that interlinks the mathematical design model with global optimization techniques. We investigate the design and development of an optimization model for semi-submersibles and focus on exploring an optimum design method which aims not only at optimum motion characteristics but also optimum stability, weight and operational efficiency. The stability parameters are accounted through the GM in different 'Degrees of Freedoms (dofs)', the manufacturing cost is accounted through the steel weight and operational efficiency is accounted through motion characteristics. The manufacturing efficiency is related to cost which is directly related to steel weight, and high motion responses adversely affect the comfort levels and operational requirements (of station keeping through dynamic positioning system, and mooring lines, etc.). However, these parameters are indirect parameters and that is a limitation in our current research. In the future, we shall be interested in incorporating more direct functional parameters related to manufacturing and operational efficiency. Through optimization studies the aim is to determine the most preferable principal dimensions of a semi-submersible that satisfies the desired requirements for motion performance and stability at the preliminary stage of design. We present a preliminary design approach, the mathematical model of optimization and a semi-submersible design example to show the application of the proposed design optimization model.

In the present paper, the use of 'Genetic Algorithm (GA)' to solve the MCDM optimization problem has been inspired from Deb (2009) and Papanikolaou *et al*. (2010). Papanikolaou *et al*. (2010) compared the 'Non-linear Goal Programming (NLGP)' and the GA methods to solve MCDM optimization problems and reported that although the NGLP is faster as compared to the GA, it does not efficiently compute the desired broader spectrum of the feasible design solutions. As in the design, it is highly desired that the design agency offers maximum range of possible feasible design solutions to the owner/order placing agency, the application of GA is preferable in our opinion. Our application of the GA allows us a complete investigation of the possible feasible design solutions at a higher computational cost and it is justified in our opinion. Furthermore, the GA based method is applicable for ill-defined problems also where computation of derivatives is difficult or derivatives do not exist. The GA based methods search primarily randomly, though can be in some pre-defined manner, and are likely to miss local minima/maxima. Even with these limitations, the GA based methods are

attractive for optimization because of their inherent strength in working with ill-defined problems that do not admit a continuous solution, e.g. semi-submersible dimensions cannot vary continuously because requirements of stability, safety, and motion are conflicting and admit only discrete solutions.

We use an empirical approach for the estimation of responses of semi-submersible and the approach is derived from the earlier works. Possibly, starting with Burke (1970), Ochi and Vuolo (1971), and Hooft (1970 and 1971) have developed simple empirical approaches for the computation of hydrodynamic motion responses and validated their results against model scale experimental data. Oo and Miller (1977) discussed a method to compute the wave induced heave motion response of a variety of semi-submersible hull configurations. Natvig and Pendered (1977) presented a sophisticated approach to compute the hydrodynamic motion responses. Santen (1985) presented some approximate methods to be used in the determination of heave motions of semi-submersibles. Later, the approximate method of Santen (1985) was found to be in good agreement with more sophisticated and detailed computations reported by other researchers, e.g. Barltrop (1998).

There are three emerging directions in the field of design and analysis of offshore structures: 1) design for complete life cycle - from conception to design to manufacture to decommissioning; 2) modularization of design - to reduce the design cycle lead time and unit cost of design; and 3) optimization covering the entire life cycle and at each of the stages in lifecycle in the environment of integration, e.g. for more details see Goldan (1985), Sharma and Kim (2010), Gallala (2013), and Misra (2015). In this regard, we present a 'Multiple Criteria Decision Making (MCDM)' driven optimization method for the semi-submersible design applicable at the early stage of design. The unique feature of proposed optimization method is that it deals with conflicting requirements and offers the designer a wider spectrum of design selections (based upon the chosen function/s and level of compromise). Also, the presented method is simple and is useful for small and medium scale shipyards that do not have financial resources to buy costly software solutions. Our presented method is simple, efficient and implementable with a general purpose computing software, Matlab*TM. Also, the present method is integrable in the complete life cycle and other advanced stages of design.

As we focus on the application of optimization method for developing a design method to be applicable at the preliminary stage of design, we prefer to use simple, efficient and fairly accurate empirical methods for the estimation of hydrodynamic characteristics, e.g. Hooft (1970 and 1971).

The remaining of this paper is organized: Section 2 describes the basics of semi-submersible optimization problem, Section 3 presents the semi-submersible optimization design process, Section 4 discusses the proposed semi-submersible optimization model with a design example and Section 5 presents the conclusions and future scope of research. A more detailed treatment of the results of this paper can be found in the thesis of first author (Gosain, 2013).

2. SEMI-SUBMERSIBLE OPTIMIZATION PROBLEM

2.1. THEORETICAL DETAILS

In the proposed empirical model, we use Morison equations (Morison *et al*., 1950) and Hooft's approach (Hooft, 1971) for the computation of motion analysis and forces acting on the structure with the added mass coefficient C_m that is selected from the DNV codes, i.e. DNV (1987 and 2011) recommendations.

Following Lewandowski (2003), the equation of heave motion of semi-submersible platform in regular waves can be written as:

$$m\ddot{z} + C_z\dot{z} + (\rho g A_w) z = F_o \cos(\omega t + \sigma) \qquad (1)$$

where,

$$m = m_s + m_a \qquad (2)$$

and

m = total mass of the platform,
m_s = structural mass of the platform,
m_a = added mass of entrained water of the platform,
C_z = equivalent damping coefficient assuming damping proportional to velocity,
$(\rho g A_w)$ = restoring coefficient or spring constant for A_w being the water plane area,
z = linear vertical displacement of the platform from its calm-water position,
$\dot{z} = \frac{dz}{dt}$ = heaving velocity of the platform,
$\ddot{z} = \frac{d^2 z}{dt^2}$ = heaving acceleration of the platform,
F_o = amplitude of wave exciting force,
ω = circular frequency of wave
t = time, and
σ = phase angle by which exciting force leads wave elevation when its value is positive.

The solution to equation of heaving motion is:

$$z = z_a \cos(\omega t - \epsilon) \qquad (3)$$

where, $z_a = \dfrac{F_o}{\sqrt{\left(\rho g A_w - m\omega^2\right)^2 + \left(C_z\omega\right)^2}}$, and (4)

ϵ = phase angle by which heaving motion lags wave elevation when its value is positive.

Since the natural frequency of heaving motion of the platform is:

$$\omega_n = \sqrt{\frac{\rho g A_w}{m}}, \quad (5)$$

the amplitude of heaving motion of the platform can be re-written:

$$z_a = \frac{F_o / \rho g A_w}{\sqrt{\left\{1-\left(\frac{\omega}{\omega_n}\right)^2\right\}^2 + (2\gamma)^2\left(\frac{\omega}{\omega_n}\right)^2}}, \quad (6)$$

where,

$$\gamma = \frac{actual\ damping}{critical\ damping} = \frac{C_z}{2m\omega_n}. \quad (7)$$

We can observe from Equation (6) that the heave amplitude is directly proportional to the amplitude of exciting force F_o and to the magnification factor that is:

$$\frac{1}{\sqrt{\left\{1-\left(\frac{\omega}{\omega_n}\right)^2\right\}^2 + (2\gamma)^2\left(\frac{\omega}{\omega_n}\right)^2}}, \quad (8)$$

and it is inversely proportional to the water plane area A_w. The responses of semi-submersible towards the motions of surge, heave and pitch are computed by multiplication of the wave energy spectrum with the square of the 'Response Amplitude Operator (RAO)' function to evaluate the response spectrum value at particular frequency. The expression of motion-response spectrum is written in the following forms:

$$S_z(\omega) = \left[RAO(\omega)\right]^2 S_\zeta(\omega), \quad (9)$$

and

$$S_z(\omega) = \left[\frac{F_0 / \zeta_a}{[\left(K - m\omega^2\right)^2 + \left(C_z\omega\right)^2]^2}\right](\omega). \quad (10)$$

where the RAO is amplitude of response per unit of the wave amplitude, F_0 is the force, K is the stiffness of the structure associated with different type of motion, m is the summation of mass and added mass of the structure associated with different type of motion, C_z is the structural damping ratio, ζ_a is the wave amplitude corresponding to particular frequency, ω is the natural frequency corresponding to particular frequency, and $S_\zeta(\omega)$ is the wave spectrum.

We use the 'Bretschneider (B-S)' wave spectrum model to define $S_\zeta(\omega)$ for the motion response analysis using Equations (9-10) in our semi-submersible optimization model. The B-S spectrum replaced the Pierson-Moskowitz spectrum as a standard in the 'International Towing Tank Conference (ITTC)' recommendations. It is usually employed to describe tropical storm waves, such as those generated by hurricanes in the Gulf of Mexico or typhoons in South China Sea. Also, the B-S allows the user to specify the modal frequency and significant wave height and that means that the B-S can be used for sea states of varying severity from developing to decaying. In general, the B-S spectrum has a greater frequency bandwidth than the JONSWAP spectrum.

There exists different forms of definition for B-S wave spectrum and they are:

- Following Chakrabarti (2003), the B-S wave spectrum in terms of significant wave height H_s and significant wave frequency ω_s is:

$$S_\zeta(\omega) = 0.1687\left(\frac{\omega_s^4}{\omega^5}\right)H_s^2 exp\left(-0.675*\left[\frac{\omega_s^4}{\omega^4}\right]\right).$$

in m^2/(rad/s), (11a)

where,

ω_s = significant wave frequency defined as the average frequency corresponding to the significant waves in the short-term record, in rad/s, and ω_s = (1/0.946)* ω_m ;

H_s = significant wave height defined as the average height of the highest one third waves in a short-term record, in meters; and

ω = frequency of the wave, in rad/s.

- Following Michel (1999 and 1968), Tucker and Pitt (2001), Techet (2005), ABS (2010) and OBS (2017), the B-S wave spectrum in terms of significant wave height H_s and modal frequency ω_m is:

$$S_\zeta(\omega) = \frac{5}{16}\left(\frac{\omega_m^4}{\omega^5}\right)H_s^2 exp\left(-1.25*\frac{\omega_m^4}{\omega^4}\right)$$ in

m^2/(rad/s), (11b)

where,

ω_m = modal (peak) frequency corresponding to the highest peak of the spectrum, in rad/s,

H_s = significant wave height, in meters, and
ω = circular frequency of the wave or encountering wave, in rad/s.

We use Equation (11b) and for the B-S, relationship between the peak frequency and the significant height for the wave is:

$$\omega_m = 0.161g / H_s . \tag{12}$$

Following Hooft (1970 and 1971), the wave excited hydrodynamic forces on a semi-submersible platform are approximated by the sum of the following three forces:

- The undisturbed pressure force F_P arising from the pressure change over the hull in a wave that is not disturbed by the presence of the hull, i.e. Froude-Krylov force.
- The inertia force F_I arising from the acceleration of the water particles in a wave, which is not disturbed by the presence of the hull.
- The damping force F_C arising from the damping due to hull, of the velocity of the water particles in a wave that is not disturbed by the presence of the hull.

Now, the total wave excited force on the semi-submersible platform is:

$$F_z = \sqrt{\left(F_P + F_I\right)^2 + \left(F_C\right)^2} . \tag{13}$$

The F_C is most important in the evaluation of motion amplitudes near the resonance. However, outside the region of resonance the F_C shows a little effect on the amplitude. Since, the F_C on a semi-submersible platform is much less than the undisturbed pressure force and the inertia force, it can be treated as small except near the resonance. Also, since the semi-submersible platforms have very low natural frequencies (i.e. of the order of 0.314 radian per second or a natural period of 20 seconds and higher), the frequencies of most of the encountering waves will be much greater than the natural frequencies and will be outside the region of resonance.

Utilizing this and simplifying Equation (13) results into neglecting the damping force and the total wave excited force is:

$$F_z = F_P + F_I \tag{14}$$

where the F_P and F_I are computed for a hull cross-section as given by Faltinsen (1993):

$$F_I = \left(1 + C_a\right)\rho BH\zeta_a \left(\frac{\omega^2}{k}\right) e^{-k\left(h_1 + \frac{H}{2}\right)} \left(2sin\left(k\frac{L}{2}\right)sin\left(\omega t\right)\right) \tag{15}$$

$$F_P = -A_w\zeta_a \rho g e^{-kh_1}\left(2cos\left(k\frac{3L}{8}\right)sin\left(\omega t\right)\right), \tag{16}$$

and

$$\zeta_a = \sqrt{2 * S_\zeta(\omega) * \Delta\omega} . \tag{17}$$

The F_0 in Equation (10) is a force and this is replaced with the F_z for computing heave response spectrum. The area under heave response spectrum is one of the objective functions that are minimized. Following, Penny (1984) the structural steel weight distribution for semi-submersible is:

$$W_{col} = 0.286 d_1^{1.612} h_{tcol} , \tag{18}$$

$$W_{pont} = 9.4\times10^{-3}\left(S_p T_{op}\right)^{1.05}, \tag{19}$$

$$S_p = 2L\left(B + H\right), \tag{20}$$

$$W_{deck} = 0.218\times d\times A - 0.082\times10^{-4}\left(d\cdot A\right), \tag{21}$$

and

$$\text{Total structural steel weight} = W_{col} + W_{pont} + W_{deck} . \tag{22}$$

In Equations (18-22), the parameters are:

L, B, H = Pontoon section length, width and height,
d = Deck height,
A = Deck area,
d_1 = Column diameter,
h_{tcol} = Column height,
S_p = Pontoon area, and
T_{op} = Operational draft.

Following Moore (2010), the stability parameters for roll and pitch are defined:

$$GMr = KB + BMr - KG , \tag{23}$$

$$BMr = \frac{I_{xx}}{\nabla} , \tag{24}$$

$$GMp = KB + BMp - KG , \text{ and} \tag{25}$$

$$BMp = \frac{I_{yy}}{\nabla} \tag{26}$$

where,

GMr = Metacentric height in roll,
GMp = Metacentric height in pitch,
BMr = Distance from the center of buoyancy to the meta-center in roll,
BMp = Distance from the center of buoyancy to the meta-center in pitch,
KB = Distance from keel to the center of buoyancy,
KG = Distance from keel to the center of gravity,
I_{xx} = Moment of inertia about the length wise longitudinal x-axis,
I_{yy} = Moment of inertia about the breadth/width wise y-axis, and
∇ = Displaced volume.

3. SEMI-SUBMERSIBLE OPTIMIZATION DESIGN PROCESS

As mentioned previously, we consider the semi-submersible design problem as a multi-objective optimization problem. A multi-objective optimization problem (i.e. multi-objective programming, vector optimization, multi-criteria optimization, multi-attribute optimization or Pareto optimization) is primarily an area of multiple criteria decision making and it concerns with mathematical optimization problems involving more than one objective function to be optimized simultaneously. In the multi-objective optimization, optimal decisions need to be taken in the presence of trade-offs between two or more conflicting objective functions, e.g. minimizing structural steel weight while minimizing the motion response and maximizing stability for a semi-submersible in roll and pitch.

From Deb (2009) and Coello *et al*. (2014), it is well known that for a non-trivial multi-objective optimization problem a single solution does not exist which simultaneously optimizes each of the defined objective functions. Furthermore, since the objective functions are conflicting in nature, there exists (possibly infinite number of) Pareto optimal solutions. A solution is called non-dominated (i.e. Pareto optimal, Pareto efficient or non-inferior), if none of the objective functions can be improved in value without impairment in some of the other objective values. In the absence of any other additional preferential information, all Pareto optimal solutions are considered mathematically equally good because the vectors cannot be ordered completely. In the present paper, our aim is to find a representative set of Pareto optimal solutions and quantifying the trade-offs in satisfying the different objectives.

Again from Deb (2009) and Coello *et al*. (2014), the evolutionary algorithms (under the class of a posteriori methods) are popular approaches to generating Pareto optimal solutions to the multi-objective optimization problems. At present, the 'Evolutionary Multi-objective Optimization (EMO)' algorithms apply Pareto-based ranking schemes, and the evolutionary algorithms (e.g. 'Non-dominated Sorting Genetic Algorithm (NSGA)' and strength Pareto evolutionary algorithm) are considered standard approaches now. The important advantage of evolutionary algorithms, for the efficient solution of multi-objective optimization problems, is that they ideally generate sets of solutions and allow computation of an approximation of the entire Pareto front. However, they also have limitations, e.g. low computational efficiency, higher computational time and the Pareto optimality of the solutions cannot be guaranteed. In the EMO, it is known that none of the generated solutions dominates the others even though optimality of the solutions cannot be guaranteed.

In our opinion, in the real world design practices, even with their limitations the EMO are useful because they generate sets of solutions that are essential at the preliminary design stage of a semi-submersible design. And, because of this reason, in the present work the evolutionary algorithm (i.e. NSGA) is used. We use NSGA-II as proposed by Deb *et al*. (2002) and our proposed design optimization model for the semi-submersibles is shown in Figure. 1. The optimization model is implemented in a general purpose computing software (i.e. Matlab^{*TM}) and various interfaces have been written in the C++ computing language utilizing its object oriented features, Quarteroni *et al*. (2010) and Prata (2011).

Our main objective is to obtain optimized principal dimensions of a semi-submersible at the preliminary stage of design while satisfying the desired requirements for motion performance, structural steel weight and stability. Our scope is to give the designer a set of optimal solutions (Pareto front-best design alternatives) without costly and time-consuming model experiments and these optimal solutions will offer the designer and owner/order placing agency a well informed choice of selection.

In an optimization problem, it is important that the parameters and variables affecting the objective function are accounted accurately and efficiently, and for this first we conduct a sensitivity analysis to account for each of the variables affecting motion response or forces acting on the semi-submersible in beam and head sea conditions. For the sake of completeness and full and complete reproducibility, we show all the results. Figures. 2 to 13 show the effect of various dimensional parameters on motion response of semi-submersible in two different wave conditions i.e. beam sea and head sea conditions.

We observe from Figures. 2 (a) and 2 (b) that the forces become zero at three sets of wave frequency and the heave response become zero at the frequencies of zero forces for both the beam-sea and head-sea conditions (in the range of frequencies considered). The reason for this is that at very low frequencies (long waves) the forces on the columns predominate and are in-phase with the

waves. As the frequency increases the forces on the hulls predominate so that for all the designs there is a frequency when the force on the columns is exactly equal and opposite to the forces on the hulls and above this frequency the force on the hulls predominates and is anti-phase to the wave. At much higher frequencies there are some numbers of zero or near zero force positions which are primarily due to the dimensions of the platform relative to the wave lengths.

We note that for the beam seas, the zero force at around $\omega_n = 0.4 rad/sec$ is due to the pressure and inertia forces cancelling one another while the zeros at $\omega = 0.717$ and 1.242 rad/sec are due to the cos $(\mathrm{k}\frac{b}{2})$ term which appears in F_z. We observe from Figures. 3 (a) and 3 (b) that the vertical forces and the heave response of the platform in the head seas are greater than those of the beam seas. In general, theese observations apply to all the other cases too. Furthermore, we note that for the beam sea, the variation of the number of columns has very little effect on the vertical forces and on the heave response. And, for the head sea, the maximum force and the maximum heave response of the platform decrease as the number of columns increases. The maximum response is reduced by around 15 % when the number of columns is increased from 2 to 6.

We observe from Figures. 4 (a), 4 (b), 5 (a) and 5 (b) that for both the beam and head sea conditions as the volume ratio increases the froces and heave responses of the platform reduce. This effect is mainly due to the increased draught with increasing volume ratios since the pressure and water particle acceleration in waves decrease exponentially with increasing depth from the mean sea level. Also, the results show that the maximum heave response is reduced by around 55 % in the head seas and by around 54 % in the beam seas as the volume ratio is increased from 0.2 to 0.4. Thus, the change in volume ratio does lead to a reduced response apart from the draught effect.

We observe from Figures. 6 (a), 6 (b), 7 (a) and 7 (b) that for both the beam and head sea conditions the vertical forces on the platform increase as the displaced volume increases but the heave response of the platform decreases. The reduction in response is mainly due to the increase in waterplane area, i.e. spring stifffness effect increases with increasing displacement. For the head sea condition, the maximum heave response is reduced by around 15% and for the beam sea condition the maximum response is reduced by around 14 % when the displacement volume is increased from 20, 000 m^3 to 40, 000 m^3.

We observe from Figures. 8 (a), 8 (b), 9 (a) and 9 (b) that for the beam sea condition the maximum heave response of the platform is reduced by around 10 % as the pontoon spacing is incresased from 40 meters to 60 meters; and for the head sea condition the maximum force decreases slightly but the maximum heave response is increased by 14 %. In the beam sea condition the heave response reduces as the pontoon spacing increases, but in the head sea condition the response increases.

We observe from Figures. 10 (a), 10 (b), 11 (a) and 11 (b) that for both the beam and head sea conditions as the natural heave frequency increases while keeping the draft as constant; the maximum wave excited heave force and heave response reduce. For the head sea condition, the maximum response is reduced by 45% and for the beam sea condition it reduces by 31%. Furthermore, the frequency of maximum response moves toward a higher frequency as the natural frequency is increased from 0.258 to 0.314 rad/sec. Although, the response can be reduced by increasing the natural frequency, it can be noted that at a higher frequency there is a risk of synchronism or resonance with high wave frequencies commonly encountered at sea and there can be extremely severe response due to the synchronism. Because of this the option of high natural frequency is not implementable in the design practices.

From Figures. 2 to 11, we can observe that the heave response reduces with: Higher number of vertical columns; larger volume ratio or deeper draught; larger displacement volume; smaller pontoon spacing or length; and larger natural heave frequency at a constant draught.

We observe from Figure. 12 (a) that the vertical elliptical cross-section results into low heave and the difference between the circular and square cross-sections is negligibly small. Figure. 12 (b) shows that the vertical wave-excited force is considerably low for the vertical elliptical section because of its lower added mass at wave frequencies higher than 0.5 rad/sec. The horizontal elliptical section experiences the highest wave forces due to its high added mass. However, for the wave frequencies smaller than 0.35 rad/sec, it experiences a low wave force. Thus, for the waves with frequencies larger than 0.5 rad/sec, the heave force is highest for the horizontal elliptical section and smallest for the vertical elliptical section. And, for the wave frequencies lower than 0.35 rad/sec, the heave response is highest for the vertical elliptical section and is lowest for the horizontal elliptical section.

The number of columns that we use in our formulation is the number per pontoon, e.g. 2 columns per pontoon and two pontoons (minimum number of the pontoons). As we report in Figures. 2 and 3, a detailed study is done to study the effect of number of columns (per pontoon) in both the head and beam sea conditions. Although, our results of Figures 2 and 3 show that the number of columns (per pontoon) affects the response, in practice the manufacturing cost associated with it actually rules the application, e.g. higher number means higher cost. Because of this, in our application too, the number is fixed to 2 considering cost and manufacturing impacts.

After, the sensitivity analysis, now we focus on the objective functions. As mentioned previously, in order to use the design objectives indicative of desired platform behavior in waves, we consider the following objective functions:

- Minimizing the heave motion: This is implemented through the area under heave response curve as has been implemented by other researchers, e.g. Birk and Clauss (2008). We first compute the RAOs to check the effect of different design parameters on response of the structure and then these are incorporated in the optimization model. They also help in understanding whether the particular parameter is worth considering in the optimization model or not? In the final optimization model the B-S wave spectrum is used the heave response spectrum and the area of response spectrum are used to compare the structural responses for different designs.

- Minimizing the structural steel weight of structure: This is implemented through the structural steel structural steel weight as computed by the empirical approach.

- Maximize stability in roll: This is implemented through the GM_r (meta-centric height in roll).

- Maximize stability in pitch: This is implemented through the GM_p (meta-centric height in pitch).

Our model emphasizes on maximizing the GM in roll and pitch degrees of freedom. However an upper constraint can be placed on the roll and pitch accelerations as per the operational requirements put up by the client. Also, the optimized solution sets obtained from the use of GA in our model are in the form of pareto-front and they give us different options to choose the rolling and pitching parameters from the optimized solution sets, as per the preferences of client.

The minimization of heave motion and structural steel weight of structure and the maximization of stability in roll and pitch are subjected to the constraints. We use three constraints: Geometric inequality constraint (i.e. pontoon length, pontoon width, pontoon height, column diameter, column height, pontoon spacing, B/H, deck_area, $D \leq B$, L-2*B, and displacement); equality constraints (i.e. air gap and deck height); and stability parameters (i.e. GMr, GMp, and heave natural period). The detailed listing is reported in Table 1. These constraints are specified either by the shipbuilding yards (i.e. as per availability or limitations or both of the manufacturing facilities) or the owner/order placing agency or the classification societies or all. The basic geometry of semi-submersible platform is shown in Fig. 13. The design characteristics associated with the platform geometric properties are listed in Table 2.

The specification of deck area is one of the design characteristics selected early in the preliminary stage of design of semi-submersible. In the proposed formulation, minimum deck area is assumed to be 6000 m^2 and the reference system for vertical measurement is the base line (keel). The computed results show that the deck area is higher than the minimum required and the displacement or total structural steel weight of the structure achieves the required feasible range and gives broad optimal design choices.

4. SEMI-SUBMERSIBLE OPTIMIZATION MODEL WITH A DESIGN EXAMPLE

The feasible solution space sets searched by the proposed optimization algorithm model are shown in Figure. 14. The optimum results obtained from semi-submersible optimization model in the form of 'Pareto Optimal Front (POF)' are shown in Figures. 15 to 17. In Figures 15 - 17, the blue color shows the '*feasible space*' and the red color shows the '*Pareto frontier*'.

The dimensions of offshore platform have impact on the stability and response. A too high GM value results into a large righting moment and thus into the increased accelerations in the pitch and roll degrees of freedom. In this regard, a stiff platform tends to respond to the wave profile more quickly and tends to assume the slope of the passing wave. This increases the responses in pitch and rolls degrees of freedom and creates shorter pitching and rolling periods that are uncomfortable for the crew.

On the reverse side, a lower GM value results into platform becoming vulnerable to large heeling moments. Hence, in a balanced design, there needs to be a compromise between the stability and motion response of the platform. This is reflected in the results reported in Figures. 15 (a) and 15 (b). In our opinion, a higher emphasis on stability is expected to compromise adversely on the response of platform and vice-versa also. This emphasis on stability can be quantified through the use of weights. The use of weights as preferences is important and can be implemented also in our model. However, we have not implemented this because of: Quantification of weights is as per the client's preferences, specifications and requirements and clients do not allow that to be reported; and current implementation emphasizes on equal weights to all design parameters as we focus on a preliminary detailed study.

Since, the area under the heave response curve and total structural steel weight are objectives that are conflicting in nature, Figure. 15a indicates the feasible designs and the POF between the area under heave response curve and structural steel weight. Figure. 15 (b) shows the feasible designs and the POF between the area under heave response curve and meta-centric height in pitch. Since, the total structural steel weight and pitch meta-centric height are the objectives that are conflicting in nature, Figure. 16 (a) shows feasible designs and the

Pareto frontier between total structural steel weight and meta-centric height in pitch. Figure. 16 (b) shows feasible designs and the Pareto frontier between area under heave response curve and meta-centric height in roll. Since, the total structural steel weight and roll meta-centric height are the objectives that are conflicting in nature, Figure. 17 (a) shows feasible designs and the Pareto frontier between structural steel weight and meta-centric height in roll.

Now, from Figures. 15-17, we select the optimized results in the form of Pareto-optimal solution sets and list them in Table 3. In our results the units are in SI system unless stated otherwise. An offshore platform like semi-submersible is a moored structure and the mooring system on semi-submersible usually offers restoring forces predominantly in the horizontal plane and very little in the vertical plane. Although, the motions in pitch and roll degrees of freedom have an adverse effect on the drilling operation, they are not as significant as the heave motions. From the analysis of available field data it has been found that the operations are halted by excessive heave motion rather than excessive roll or pitch motions. Hence, our focus is on the stability in horizontal plane and because of this we report heave time periods in Table 3.

In Table 3, there are 9 designs, and they are chosen taking into consideration the objective of minimum structural steel weight, maximum KM (in roll and pitch degrees of freedom) and minimum response area in each of the graphs. The minimum and maximum objectives are colored in red and underlined to indicate the best in each of the stated goals.

As we mentioned previously, the primary motivation of the present research is to offer the designer a wider spectrum of possible design solutions and in this regard from Table 3, a designer can select the best design from the options available depending upon the specific choice/s of selection. Additionally, a designer can use structural steel weight to each of the objectives to select the best compromised choice.

From the design point of view, we observe the following key designs from Table 3:

- Design 1 is best in context of its minimum total structural steel weight of the structure.
- Design 2 is best for its minimum response area.
- Designs 3 and 4 have the advantage of having maximum meta-centric height in roll and pitch respectively.

However, the ‘Designs 1 to 4’ pay some penalty to achieve these minimum or maximum objectives. ‘Designs 5 to 9’ show a compromised solution with paying minimum penalty to achieve the objectives mentioned to arrive at the optimum design of semi-submersible. Since the objective functions are conflicting one can assign systematically structural steel weight attributes to each of the objective functions to choose the best design according to the requirements. In the field of offshore and ship structures, although the material cost is much less than the system and machinery costs, the material cost is ‘only’ the cost that is reducible through the design directly. Other costs can be reduced through design indirectly, e.g. design for less motion will reduce power consumption by the position control systems and thereby reducing cost. This material cost is related to the structural steel weight and we think that a correlation can be found between each of the objective functions and structural steel weight. Furthermore, there are ongoing investigations focusing on the exploration of lighter structural configurations other than steel plate and sections that can be applied to the offshore platforms, e.g. corrugated shell plating, Ringsberg *et al*. (2014). Once, a suitable structural steel weight is assigned to each of the objectives then it will be easy to select the best compromised choice in terms of less material cost. However, these ideas are at the nascent stage only and we do not have any results in these directions. In future, we shall focus on detailed exploration of these ideas.

A closer analysis of the results show that the ‘Design 1’ weighs 25% lesser and costs 6.34 million Euros lesser when compared to the ‘Design 2’, i.e. one ton of steel costs 800 Euros, adapted from Ringsberg (2011). Also, for the ‘Design 1’ maximum heave response is 21% greater than the ‘Design 2’ for the same sea conditions. So a compromise solution, i.e. ‘Design 5’ between structural steel weight/cost and response can be selected from the Pareto optimal front which weighs 3% more than the ‘Design 1’ and 23% lesser than the ‘Design 2’ with cost of 5.89 million Euros lesser than the ‘Design 2’ with maximum heave response of 7% greater than the ‘Design 1’. This is shown in Figure. 17b. Similarly, the ‘Designs 6 to 9’ represent compromise design solutions for different design requirements.

Based upon the above analysis, we state that essentially, the proposed optimization model offers a broad spectrum of the design choices at the preliminary stage of design, where the design can be selected according to the requirements placed by either the owner/order placing agency or the classification societies or all.

5. CONCLUSIONS

This paper has presented a critical parameter (from sensitivity analysis) driven optimum design model for semi-submersible platform. The design has been carried to optimize the parameters of structural steel weight, stability and motion performance. The presented optimization model for design of semi-submersible takes all design variables into considerations, reveals compromised solution set with broad design choices where minimum penalty is paid in terms of cost (manufacturing and operational); with an emphasis on

increasing motion performance and stability. The optimized design obtained in terms of Pareto optimal front can be investigated further for detailed analysis accounting for the non-linearities followed by model experiments.

Since the proposed design model is based upon a highly iterative process, the dimensions are refined in step wise manner, and the proposed model can be efficiently used in practice. The proposed model meets applicable operational requirements while minimizing costs/structural steel weight. The model is based upon some chosen parameters which can be used by the user depending upon variable set of requirements placed by either the owner/order placing agency or the classification societies or all.

However, the proposed design model is based upon simple empirical models and that is useful only at the preliminary stage of design. For a detailed motion analysis one needs to consider the moments of the response spectrum along with a probability distribution (e.g. Raleigh distribution), and then these moments of the response spectrum can be used to compute probabilities of exceedance. The moments of response spectrum and probabilities of exceedance are useful in the advance stage of design. Furthermore, in the later advanced stages of design with more detailed design available an integration with the 'Computational Fluid Dynamics (CFD', 'Finite Element Analysis (FEA)', 'Computer Aided Design/Engineering (CAD/E)' software solutions will be highly desired to arrive at design solution set that can be used for the selection of 'Final Design' at the contract signing and production stages. Our future work shall go in this direction and currently this is under investigation.

Trademark and copyrights

*Trademark and copyright with MathWorks, Inc., USA.

6. ACKNOWLEDGEMENTS

This research was supported by the internal research grants of IIT Madras, India via a scheme - OE10S014 and a scholarship scheme of the MHRD, GoI, India.

7. REFERENCES

1. ABS (2010), *Guide for spectral-based fatigue analysis for floating production, storage and offloading (FPSO) installations*, American Bureau of Shipping, USA, pp. 10-11.
2. BARLTROP, N. D. P. (1998), *Floating Structures: A Guide for Design and Analysis*, Oilfield Publications, Inc., USA.
3. BIRK, L. and G.F. CLAUSS (2008) *Optimization of offshore structures based on linear analysis of wave-body interaction*. Proceedings ASME Offshore Mechanics and Arctic Engineering Estoril, Portugal, June 15-20.
4. BURKE, B. G. (1970), *The analysis of motions of semisubmersible drilling vessels in waves*, Society of Petroleum Engineers Journal, 10 (3), DOI http://dx.doi.org/10.2118/2725-PA.
5. CHAKRABARTI, S. K. (2003), *Hydrodynamics of Offshore Structures*, WIT Press, USA.
6. COELLO, C. C., LAMONT, G. B. AND VELDHUIZEN, D. A. VAN (2014), *Evolutionary Algorithms for Solving Multi-Objective Problems*, Genetic and Evolutionary Computation Series, 2nd edition, Springer.
7. DEB, K. (2009), *Multi-Objective Optimization Using Evolutionary Algorithms*, John Wiley and Sons, USA.
8. DEB, K., A. PRATAP, S. AGARWAL and T. MEYARIVAN (2012), *A Fast and Elitist Multiobjective Genetic Algorithm*: NSGA-II. IEEE Transactions on Evolutionary Computation, 6 (2), April 2002, pp. 182 – 197.
9. DNV (1987), CN 31.4 - *Strength analysis of main structures of column stabilized units (semisubmersible platforms)*, Det Norske Veritas, pp. 1-94.
10. DNV (2011), RP H103 - *Modelling and analysis of marine operations*, Det Norske Veritas, pp. 1-150.
11. FALTINSEN, O.M. (1990), *Sea Loads on Ships and Offshore Structures*. Cambridge University Press, UK.
12. GALLALA, J. R. (2013), *Hull dimensions of a semi-submersible rig a parametric optimization approach*, Master's Thesis in Marine Technology, NTNU Trondheim, Norway.
13. GOLDAN, M. (1985), *The application of modular elements in the design and construction of semi-submersible platforms*, PhD Thesis, Technische Universiteit Delft, The Netherlands.
14. GOSAIN, G. D. (2013), *Optimization Model for Design of Semi-Submersibles*, Master of Science (By Research) Thesis, Department of Ocean Engineering, IIT Madras, India.
15. HOOFT, J. P. (1970), *Oscillatory Wave Force on Small Bodies*, International Shipbuilding Progress, 17, pp. 127-135.
16. HOOFT, J. P. (1971), *A mathematical method for determining hydro-dynamically induced forces on a semisubmersible*, SNAME Transactions, 79, pp-28-70.
17. ISHERWOOD, R. M. (1983) *Some aspects of semi-submersible design*, RINA Offshore Group Symposium on Semi-submersibles, London, March 17-18.
18. LEWANDOWSKI, E. M. (2003), *The Dynamics of Marine Craft: Maneuvering and Seakeeping*, World Scientific Publication Company Inc., Singapore.
19. MICHEL, W. H. (1999), *Sea Spectra Revisited*, Marine Technology, 36 (4), pp. 211-227.

20. MICHEL, W. H. (1968), *Sea Spectra Simplified*, Marine Technology, Jan. 1968, pp. 17-30.
21. MISRA, S. C. (2015), *Design Principles of Ships and Marine Structures*, 1st edition, CRC Press, USA.
22. MOORE, C. S. (2010), *Principles of Naval Architecture Series: Intact Stability*, Editor: Paulling, J. R., SNAME, USA.
23. MORISON, J. R., O'BRIEN, M. P., JOHNSON, J. W., and SCHAAF S. A. (1950), *The forces exerted by surface waves on piles*, Petroleum Transactions, AIME, 189, pp. 149-157.
24. NATVIG, B. J. and PENDERED, J. W. (1977), *Non-linear motion response of floating structures to wave excitation*, Offshore Technology Conference, pp. 2796 - 2806.
25. NATVIG, B. J. and PENDERED, J. W. (1980), *Motion response of floating structures to regular waves*, Applied Ocean Research, 2 (3), pp. 99-106.
26. OBS (2017), *'OrcaFlex - Waves: Wave Spectra'*, Orcina Limited, UK, website address: www.orcina.com/SoftwareProducts/OrcaFlex/Documentation/Help/Content/html/Waves,WaveSpectra.htm
27. OCHI, M. K. and VUOLO, R. M. (1971), *Sea-keeping characteristics of a multi-unit ocean platform*, SNAME Spring Meeting, Honolulu, Hawaii, USA.
28. OO, K.M. and N.S. MILLER (1977), *Semi-submersible design: the effect of differing geometries on heaving response and stability*, Transactions of the RINA, 119, pp. 97-119.
29. PAPANIKOLAOU A., ZARAPHONITIS, G., BOULOUGOURIS, E., LANGBECKER, U., U. MATHO, S., SAMES, P. 2010, *Multi-objective optimization of oil tanker design*, Journal of Marine Science and Technology, 15, pp. 359-373.
30. QUARTERONI, A., SALERI, F. and GERVASIO, P. (2010), *Scientific Computing with MATLAB and Octave*, Texts in Computational Science and Engineering, 3rd edition, Springer.
31. PENNY, P.W. and RIISER, R.M. (1984), *Preliminary design of semisubmersibles*, RINA Offshore Group Symposium on Semi-Submersibles, London, UK.
32. PRATA, S. (2011), *C++ Primer Plus*, 6th edition, Addison-Wesley Professional, USA.
33. RINGSBERG, J. W., SAĞLAM, H., SARDER, M. A. and ULFVARSON, A. (2014), *Lightweight design of offshore platform marine structures - Optimisation of weight to strength utilisation of corrugated shell plating*, Ships and Offshore Structures, 9 (1), pp. 38-53, DOI: 10.1080/17445302.2012.712005.
34. SANTEN, J. A. VAN (1985), *Approximative formulae for calculating the motions of semi-submersibles*, Ocean Engineering, 12 (3), pp. 235-252.
35. SHARMA R. and KIM, T-W (2010), *Development of a logic-based product life-cycle management (lbplm) system for shipbuilding industry - conceptual development*, Journal of Ship Production and Design, 26 (4), pp. 231 - 251.
36. TECHET, A. H. (2005), *Design Principles for Ocean Vehicles*, Lecture notes - 13.42, Department of Mechanical Engineering, MIT, USA.

APPENDICES

Table 1: Constraints for semi-submersible optimization problem

Geometric inequality constraints	(i) 90 < Pontoon Length (L in m) < 110, (ii) 10 < Pontoon Width (B in m) < 15, (iii) 5 < Pontoon Height (H in m) < 15, (iv) 5 < Column Diameter (d_1 in m) < 15, (v) 9 < Column Height (ht_{col} in m) < 31, (vi) 60 < Pontoon Spacing (in m) < 75, (vii) B/H > 1 and B/H < 2, (viii) deck_area (A=L**b*, in m^2) > 6000 m^2, (ix) D ≤ B, both in m, (x) L-2*B > 10, both in m, and (xi) Displacement (in tons)* < 50000.
Equality constraints	(i) Air gap (in m) = 9, and (ii) Deck height (*d* in m) = 7.
Stability parameters	(i) GMr (in m) > 0, (ii) GMp (in m) > 0, and (iii) Heave natural period** (in s) > 18.

*Note that the displacement as given in Equation (22) is dependent upon the d_1, ht_{col}, L, B and H, etc. These values have the upper and lower bounds associate with them. Using the lower bounds of parameters will result into lower bound for the displacement. Hence, because of this, the displacement is given in terms of upper bound with constraints on dimensions.

**The natural period in heave degree of freedom less than 18 seconds is of serious concern for the semi-submersibles. Furthermore, the downtime of semi-submersibles is mainly governed by the heave motions. Because of this our focus is on the heave motion.

Table 2: Basic dimensions related properties/characteristics of the semi-submersible platform

S. no.	Design parameters	Governing equation
1	Water line area (in m^2)	$A_{wl} = \sum_{i=1}^{ncol} \frac{\pi d_1^2}{4}$
2	Equivalent diameter (in m)	$D_{equi} = \sqrt{\frac{4BH}{\pi}}$
3	Transversal moment of inertia (in m^4)	$I_{xx} = \sum_{i=1}^{ncol} I_{xx}(i) + y^2(i) \cdot A_{wl}(i)$
4	Longitudinal moment of inertia (in m^4)	$I_{yy} = \sum_{i=1}^{ncol} I_{yy}(i) + x^2(i) \cdot A_{wl}(i)$
5	Volume of the columns (in m^3)	$V_c = \sum_{i=1}^{ncol} A_{wl} h_{tcol}$
6	Submerged volume of the columns (in m^3)	$V_{mc} = \sum_{i=1}^{ncol} A_{wl} h_1$
7	Volume of the pontoons (in m^3)	$V_p = \sum_{i=1}^{npont} \frac{\pi D_{equi}^2}{4} l_i$ or $V_p = \sum_{i=1}^{npont} LBH$
8	Displacement (in tons)	$\triangle = (V_{mc} + V_p) \cdot \gamma$

Nomenclature: γ = Water specific density; B, H = Width and height of the cross section, in m; d_1 = Column diameter, in m; x, y = Column distances from the length wise and breadth/width wise axes respectively, in m; h_1 = Submerged columns height, in m; L = Pontoon length, in m; $ncol$ = Number of columns; $npont$ = Number of pontoons; and h_{tcol} = Total column height in m.

Table 3: List of the optimized results in the form of Pareto-optimal solution sets.

Design parameter	**Design 1**	**Design 2**	**Design 3**	**Design 4**	**Design 5**	**Design 6**	**Design 7**	**Design 8**	**Design 9**
Pontoon length - L (in m)	90.51721	109.474	90.1065	108.8142	90.0957	91.60072	94.08344	106.5726	107.6659
Pontoon breadth - B (in m)	12.72714	11.9236	11.9236	14.75612	12.12217	11.9003	11.72224	13.78383	13.70918
Pontoon height - H (in m)	6.434266	7.40971	6.2204	7.849512	6.847735	5.953942	6.150722	7.310521	6.966525
Column diameter - d_1 (in m)	12.54891	11.747	11.747	14.73967	11.7413	11.77601	11.69111	13.78308	13.67346
Height of column - ht_{col} (in m)	24.9767	35.0487	35.2332	9.74136	28.20123	35.65414	37.37359	14.50501	18.09055
Pontoon spacing - pont_spc (in m)	66.39504	74.8975	74.8975	60.816	67.1399	73.45316	74.93374	60.56642	64.4107
Total structural weight - total_wt (in tons)	***22710.79***	30636.1	24741	25683.96	***23264.47***	***24602.11***	25752.73	***24772.12***	25897.01
Deck area - deck_area (A in m^2)	6009.894	8199.36	6748.76	6617.645	6049.017	6728.363	7050.023	6454.719	6934.834
Submerged height of column - h_1 (in m)	15.94008	26.0475	26.2386	0.698022	19.18033	26.67594	28.37886	5.519492	9.077317
Metacentric height in roll - GMr (in m)	4.266614	0.01875	4.20019	5.871289	2.013876	3.665777	3.150674	3.655063	4.093915
Metacentric height in pitch - GMp (in m)	13.67998	9.83783	6.83426	36.02517	9.176403	7.787396	7.249893	28.95267	26.49012
KMr (in m)	23.00161	24.0219	***28.0947***	18.45936	22.31862	***27.61035***	***28.04324***	17.97657	19.97586
KMp (in m)	32.41497	33.841	30.7288	***48.61325***	29.48115	31.73197	32.14246	***43.27418***	***42.37207***
KG (in m)	18.73499	24.0031	23.8945	12.58807	20.30475	23.94457	24.89256	14.32151	15.88194
KB (in m)	4.530233	5.83523	5.95731	3.944855	5.010462	5.960839	6.241283	3.892149	3.971547
Heave time period - heave_tim_pd (in s)	18.02623	22.2024	19.3123	18.05805	19.43407	19.12065	19.69884	18.35079	18.49834
Area under heave response spectrum curve - Aera_und_curv (in $unit^2$)	3.927717	***3.15544***	3.5999	4.428898	***3.676167***	3.613926	***3.501146***	4.086634	***3.91233***
Area moment of inertia about the X axis - Ixx (in m^4)	1.97E+10	3.80E+10	3.02E+10	1.50E+10	2.19E+10	2.93E+10	3.25E+10	1.55E+10	1.90E+10
Area moment of inertia about the Y axis -Iyy (in m^4)	2.30E+10	4.70E+10	2.89E+10	3.03E+10	2.46E+10	2.95E+10	3.29E+10	2.93E+10	3.21E+10
Area moment of inertia about the Z axis -Izz (in m^4)	3.11E+10	5.83E+10	3.85E+10	3.97E+10	3.23E+10	3.81E+10	4.19E+10	3.77E+10	4.18E+10
Radius of gyration in roll - Rr (in m)	29.431	35.2162	34.9456	24.188	30.6726	34.5023	35.5384	25.0374	27.0642
Radius of gyration in pitch - Rp (in m)	31.8484	39.1657	34.1797	34.3353	32.4969	34.6301	35.7294	34.3801	35.2195
Radius of gyration in yaw - Ry (in m)	36.9949	43.6161	39.4551	39.3268	37.2395	39.3719	40.3534	38.9901	40.1727
Parametric choice of selection	**Min weight**	**Min area**	**Max KM_r**	**Max KM_p**	**Com Awt**	**Com WKM_r**	**Com AKM_r**	**Com WKM_p**	**Com AKM_p**

Nomenclature: Min weight - Minimum weight; Min area - Minimum area under the response curve; Max KM_r - Maximum KM_r; Max KM_p - Maximum KM_p; Com Awt - Compromise between area under the response curve and weight; Com WKM_r - Compromise between the weight and KM_r; Com AKM_r - Compromise between area under the response curve and KM_r; Com WKM_p - Compromise between the weight and KM_p; and Com AKM_p - Compromise between area under the response curve and KM_p.

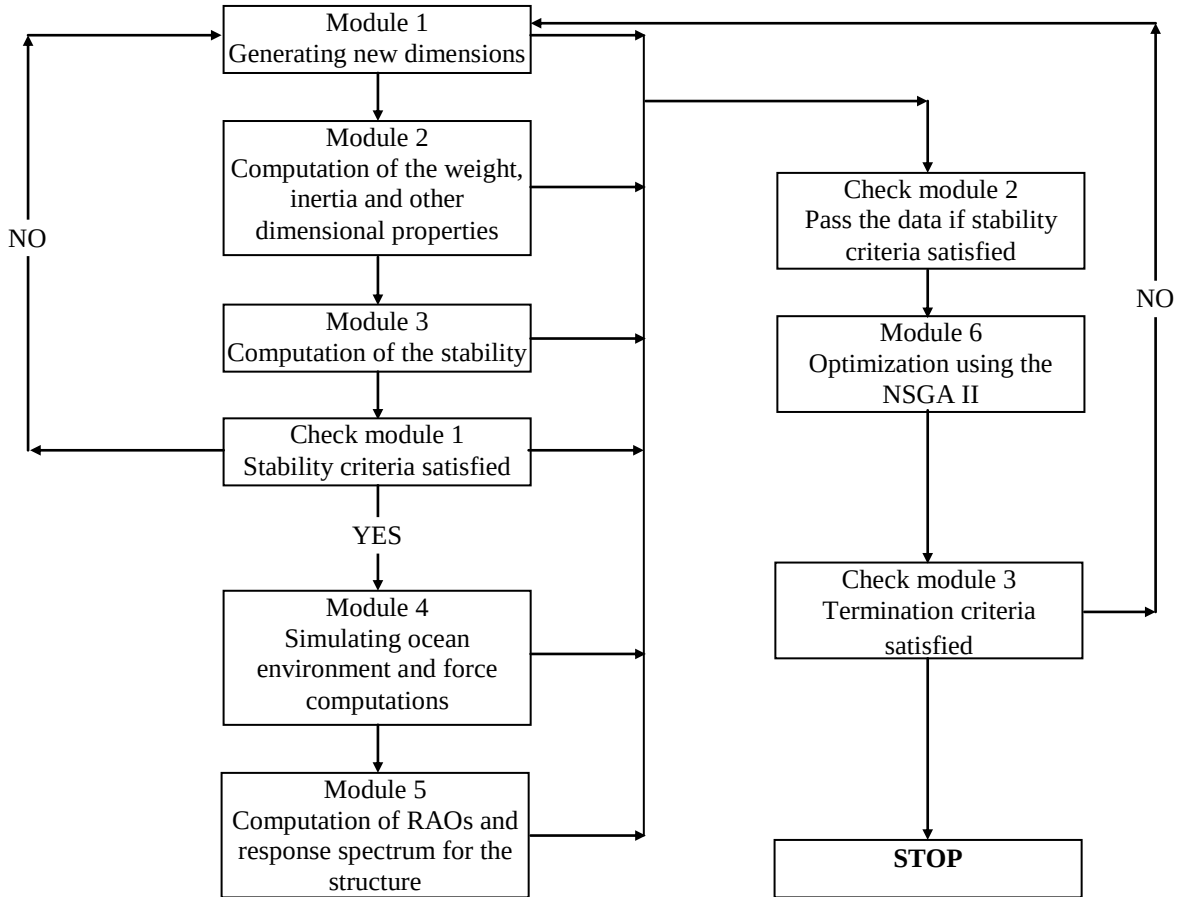

Figure 1: Optimization design model for the semi-submersibles.

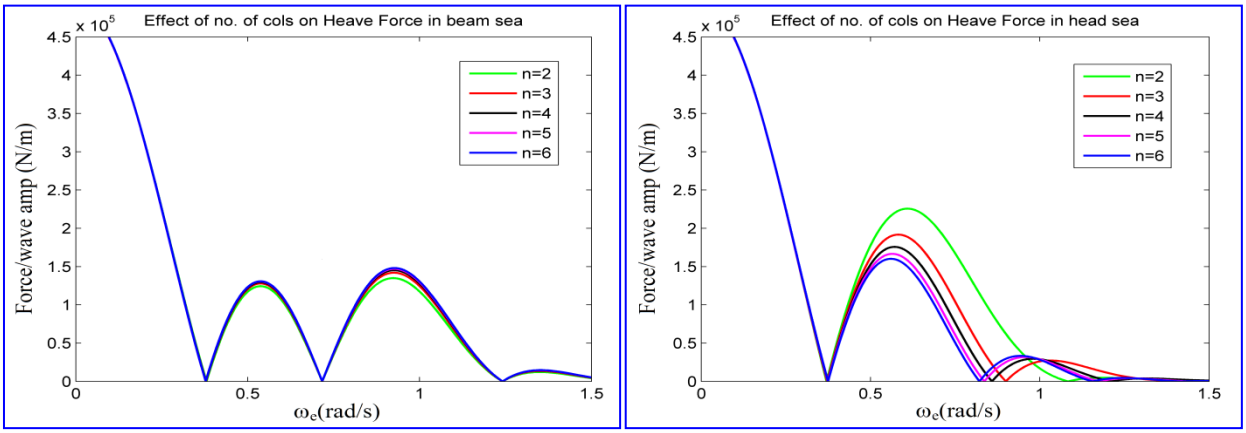

(a) Beam sea condition (b) Head sea condition

Figure 2: Effect of the number of columns on heave force in beam and head sea conditions.

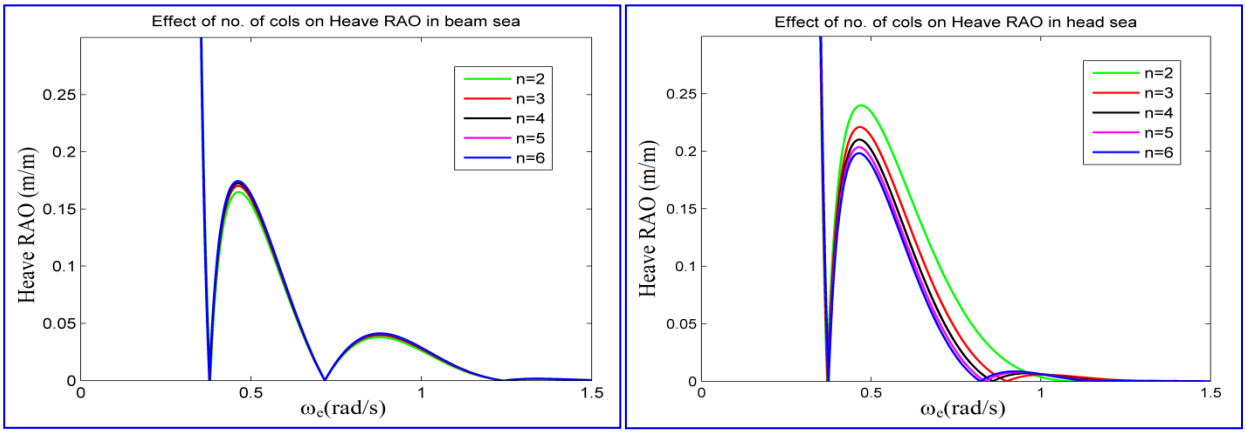

(a) Beam sea condition (b) Head sea condition

Figure 3: Effect of the number of columns on heave RAO in beam and head sea conditions.

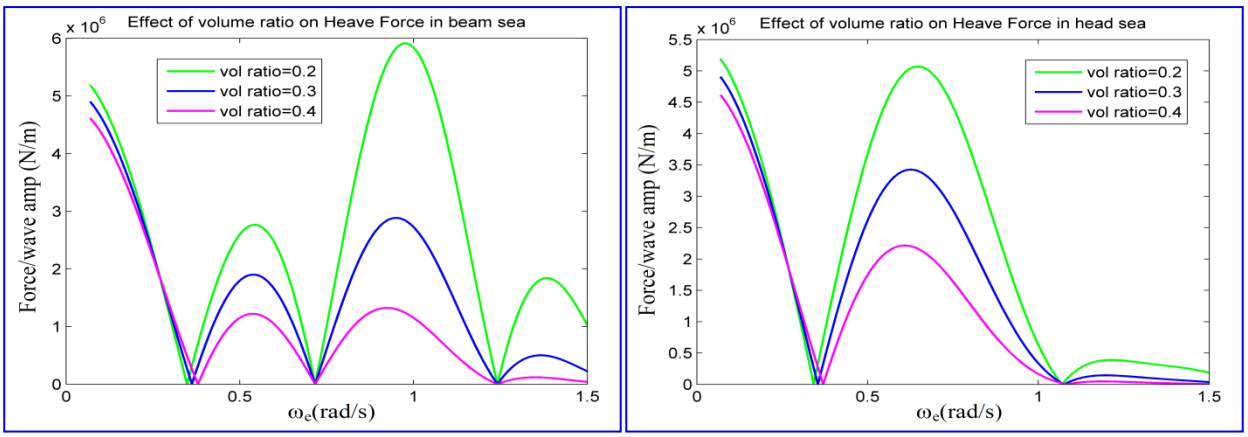

(a) Beam sea condition (b) Head sea condition

Figure 4: Effect of the volume ratio on heave force in beam and head sea conditions.

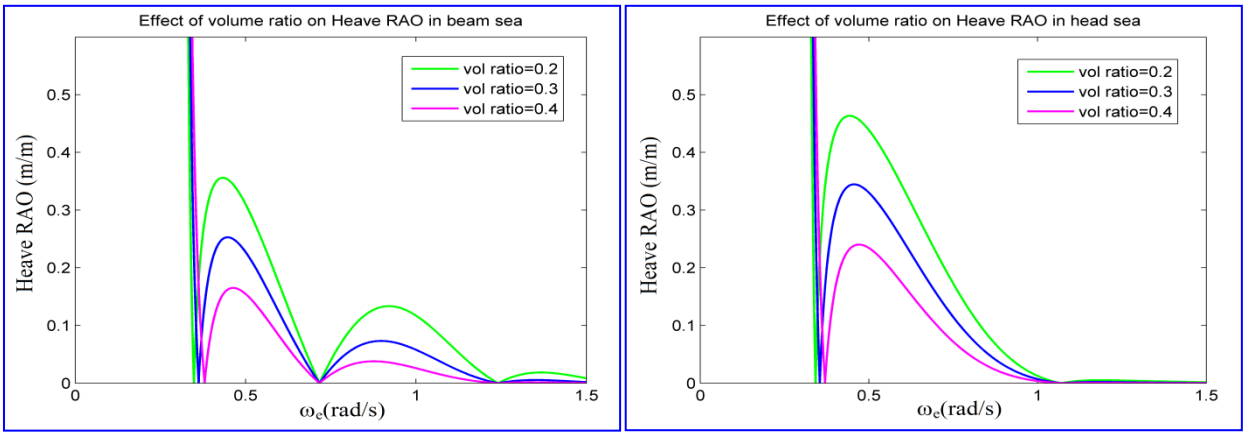

(a) Beam sea condition (b) Head sea condition

Figure 5: Effect of the volume ratio on heave RAO in beam and head sea conditions.

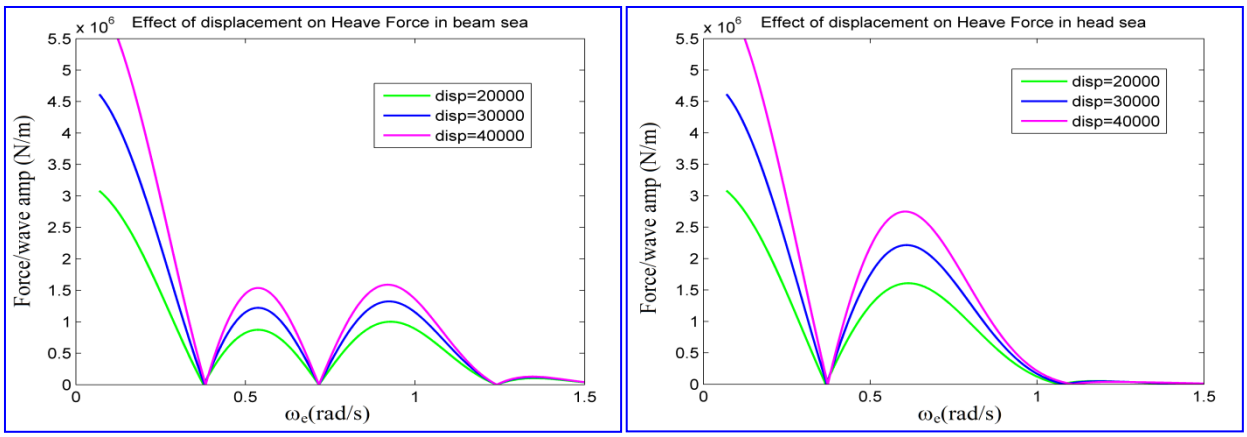

(a) Beam sea condition (b) Head sea condition

Figure 6: Effect of the displacement on heave force in beam and head sea conditions.

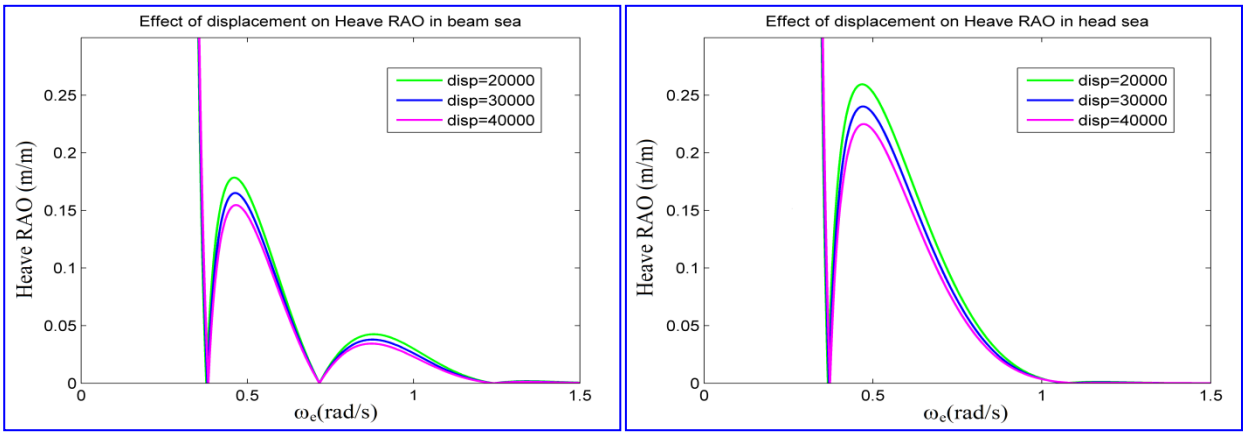

(a) Beam sea condition (b) Head sea condition

Figure 7: Effect of the displacement on heave RAO in beam and head sea condition.

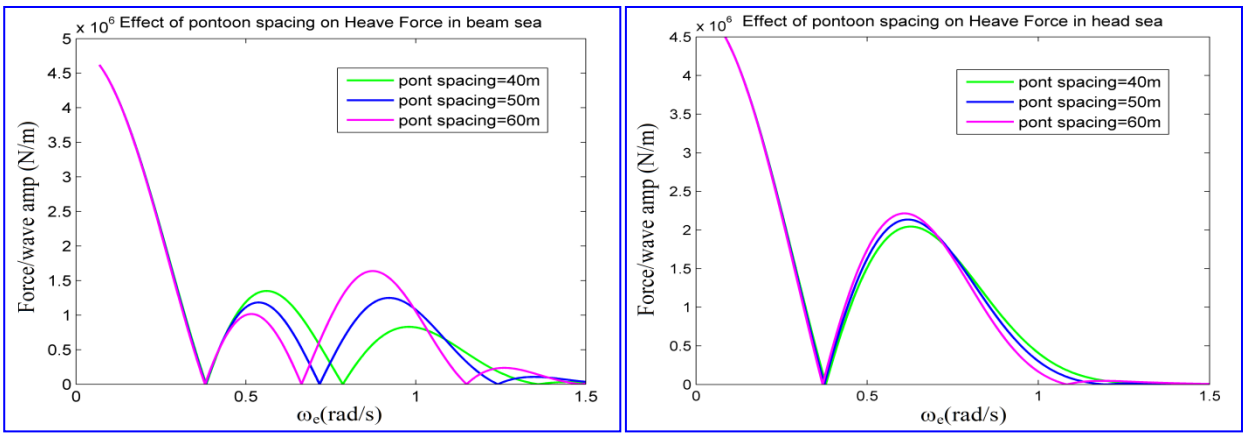

(a) Beam sea condition (b) Head sea condition

Figure 8: Effect of the pontoon spacing on heave force in beam and head sea conditions.

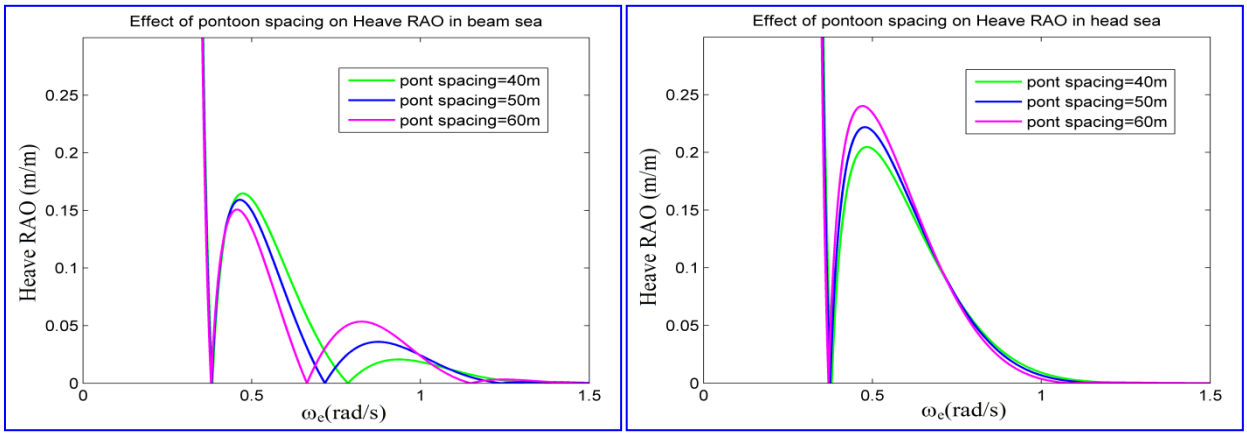

(a) Beam sea condition (b) Head sea condition

Figure 9: Effect of the pontoon spacing on heave RAO in beam and head sea conditions.

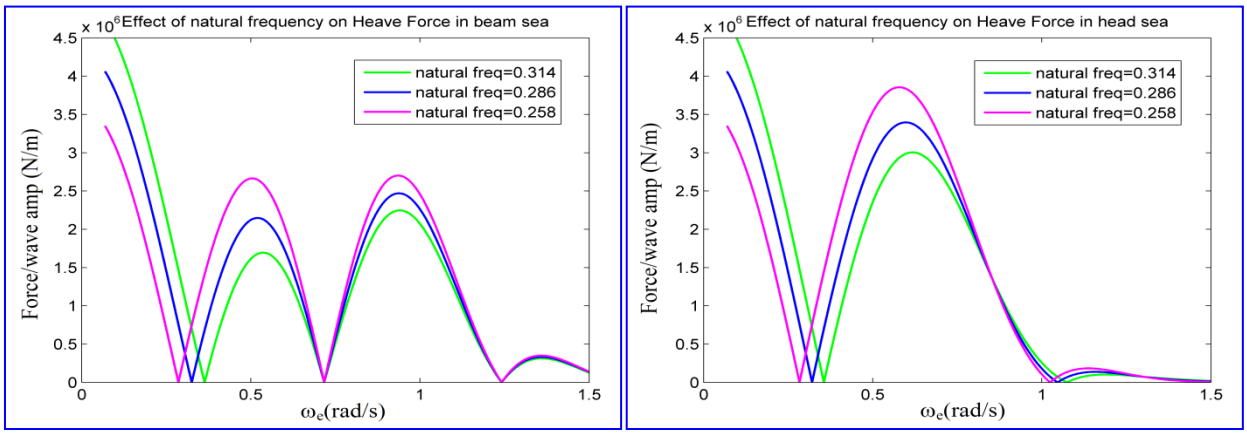

(a) Beam sea condition (b) Head sea condition

Figure 10: Effect of the natural frequency on heave force in beam and head sea conditions.

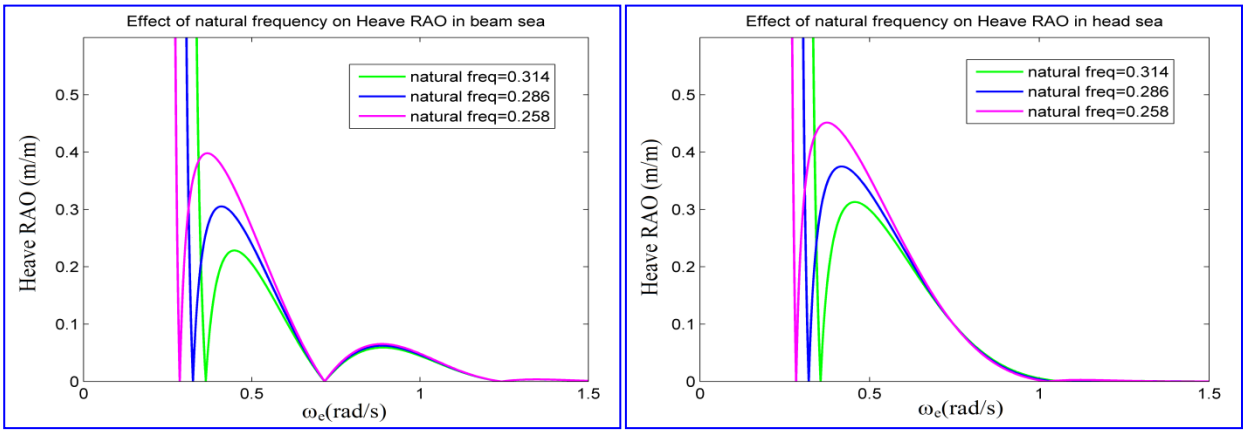

(a) Beam sea condition (b) Head sea condition

Figure 11: Effect of the natural frequency on heave RAO in beam and head sea conditions.

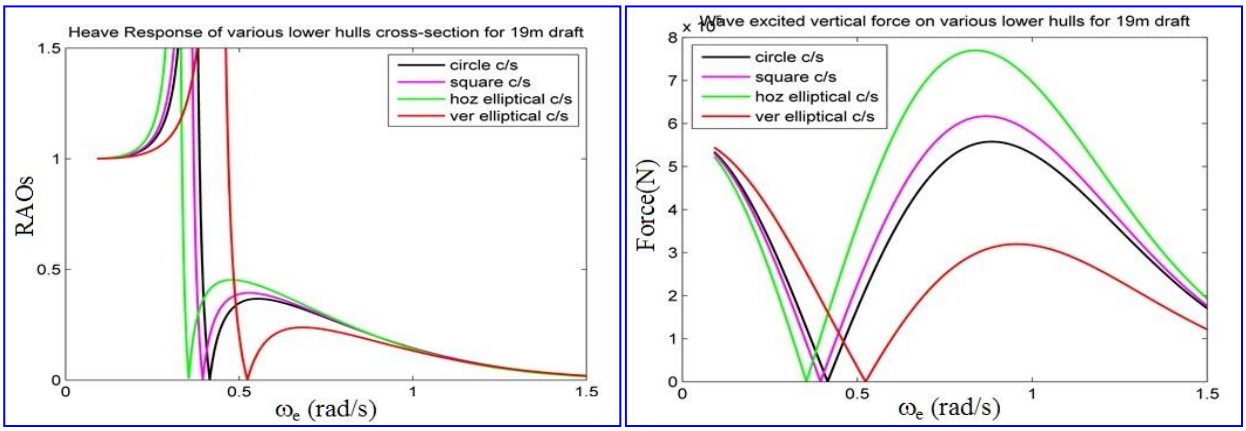

(a) Heave response of various pontoon cross-sections. (b) Force acting on lower hull of semi-submersible.

Figure 12: Heave response and force acting on lower hull of semi-submersible for different types of the pontoon cross-sections.

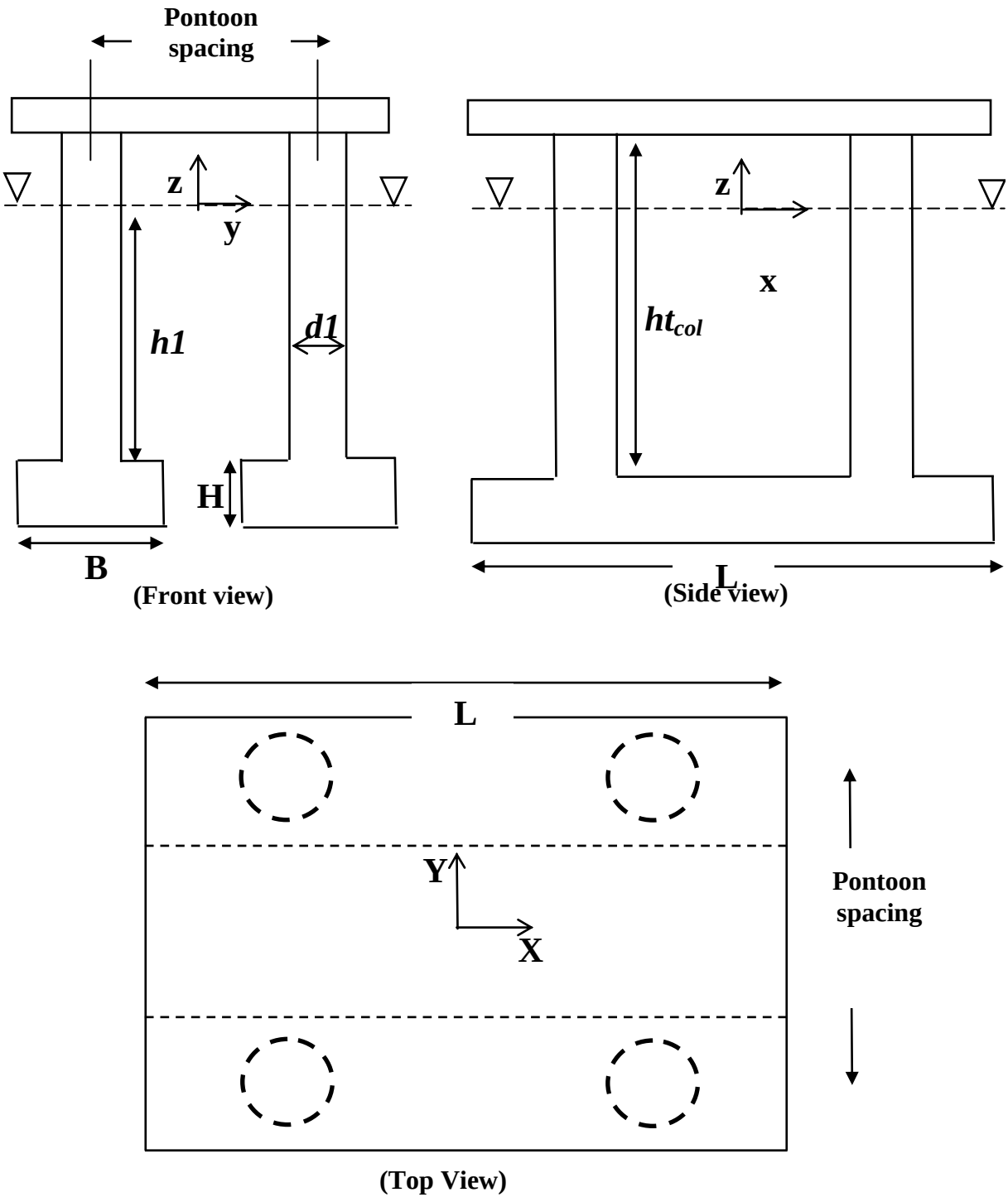

Figure 13: Description of the semi-submersible model for optimization.

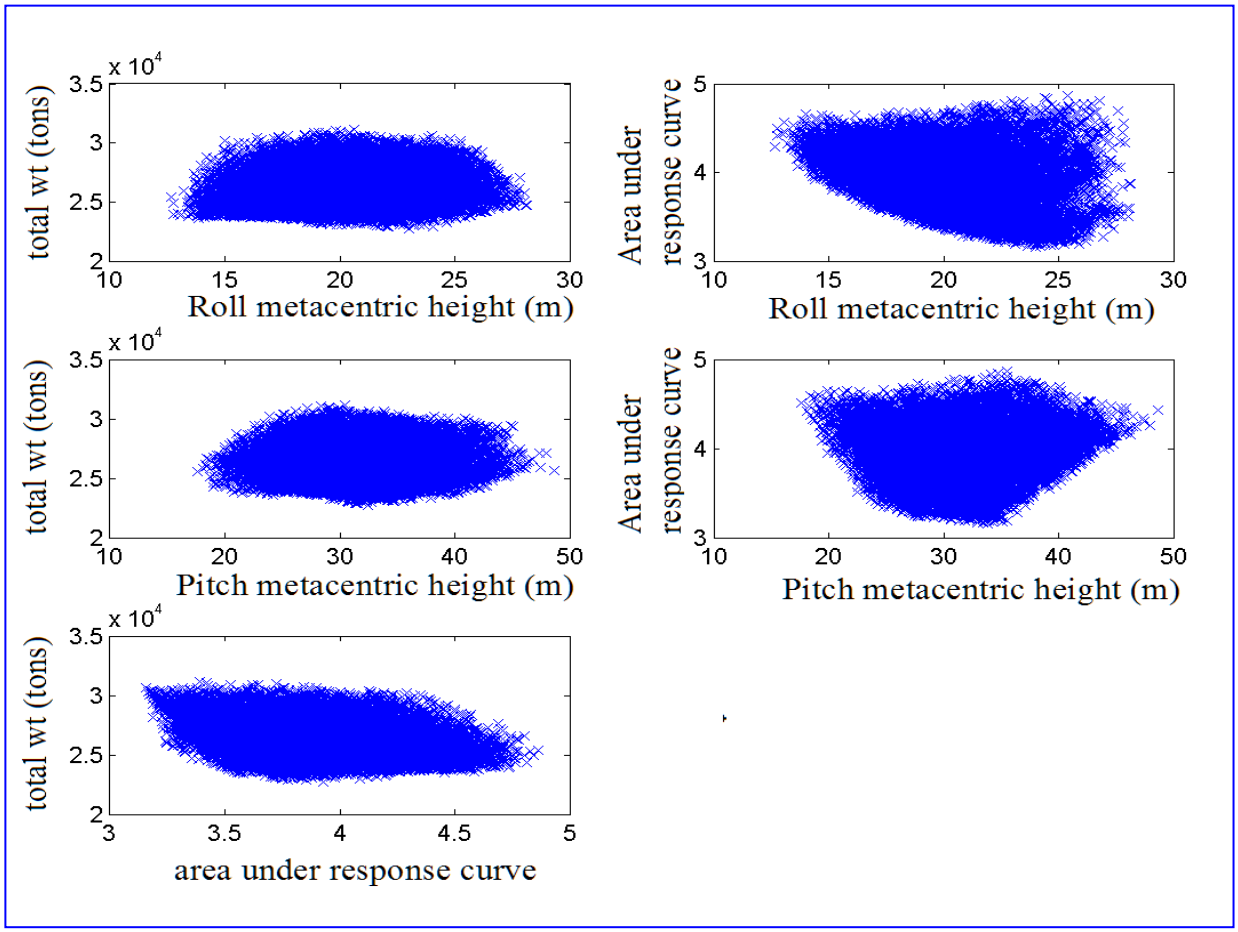

Figure 14: Feasible solution space sets computed by the NSGA-II.

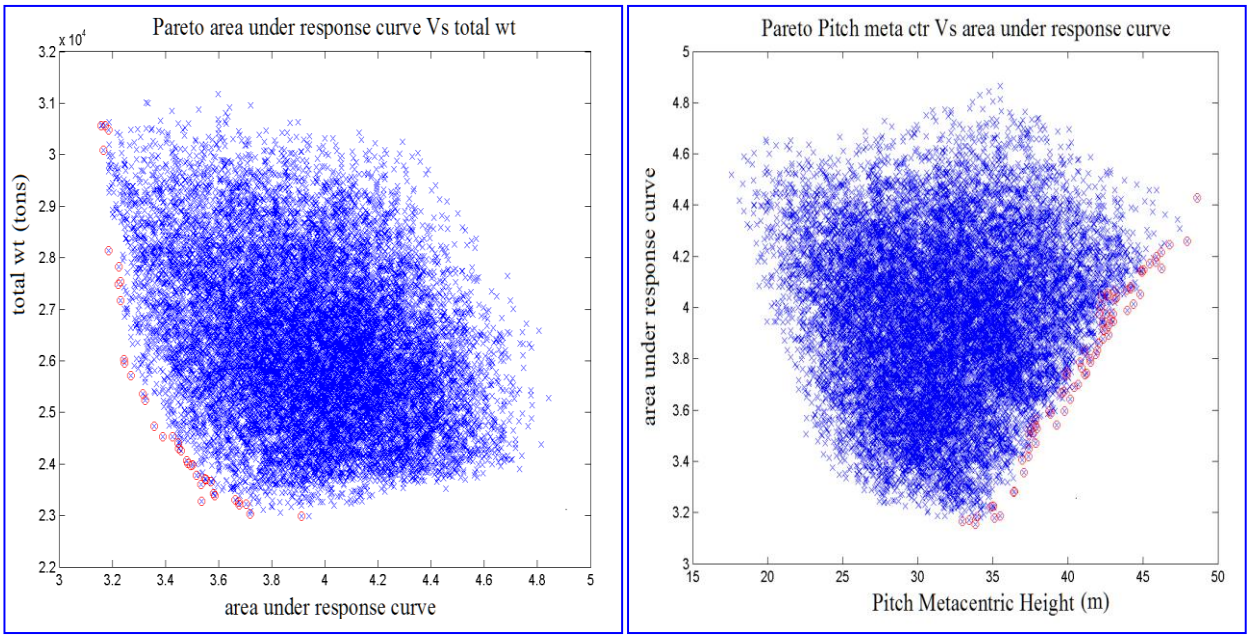

(a) POF for area under the heave response curve and total weight.

(b) POF for area under heave response curve and pitch meta-centric height.

Figure 15: Computed POF for the area under heave response curve versus total structural steel weight and versus meta-centric height in pitch.

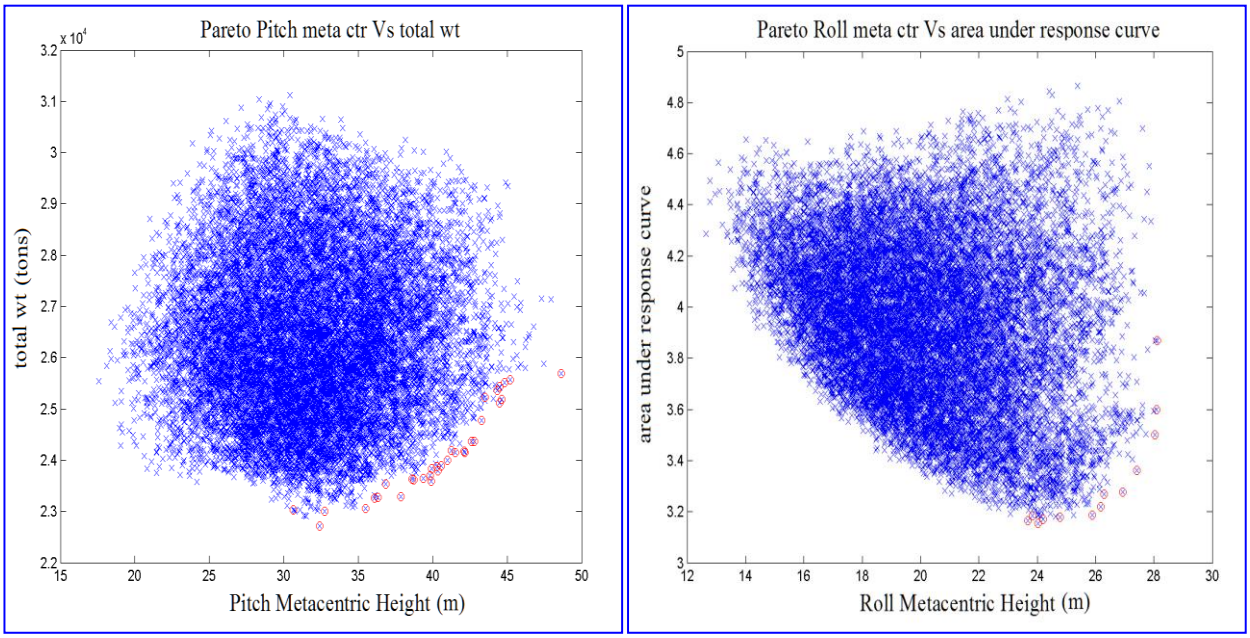

(a) POF for the total weight and pitch meta-centric height.

(b) POF for area under the heave response curve and roll meta-centric height.

Figure 16: Computed POF for the total structural steel weight versus meta-centric height in pitch and the area under heave response curve versus meta-centric height in roll.

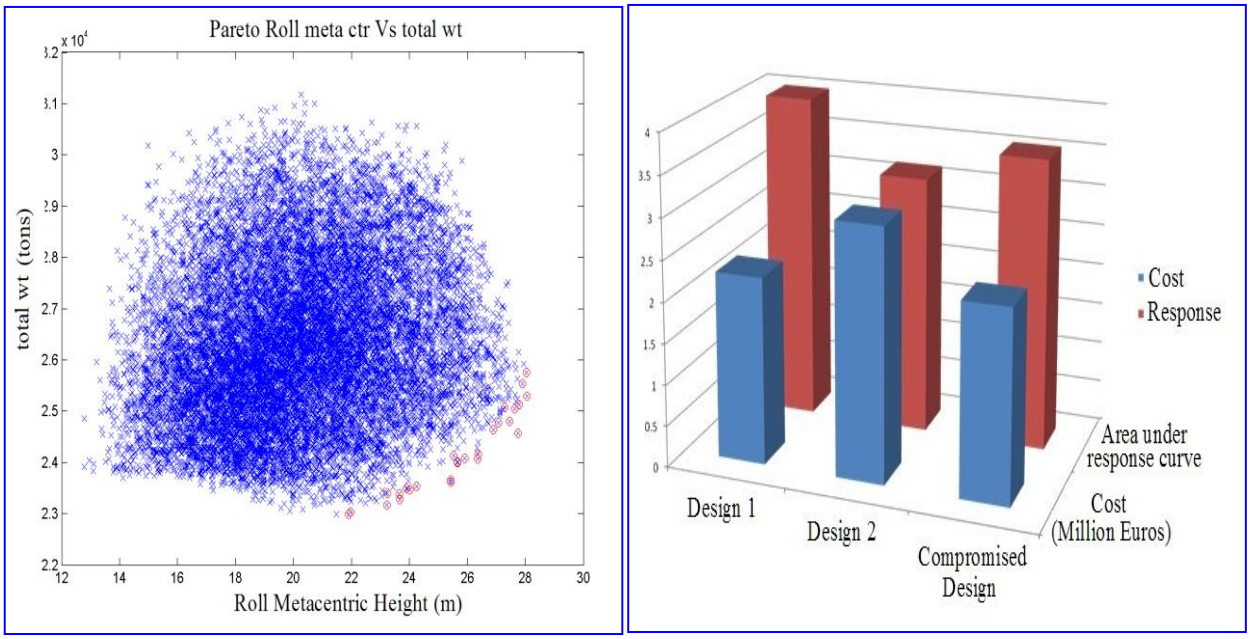

(a) POF for the total weight and roll meta-centric height.

(b) Cost and response result analysis for the solutions obtained from POFs.

Figure 17: Computed POF for the total structural steel weight versus meta-centric height in roll and cost and response result analysis for the solutions obtained from POFs.

EVALUATION METHODOLOGY ON TRAJECTORY OF INBOUND SINGLE SHIP USING SIMILARITY MEASUREMENT BETWEEN PLANAR CLOUDS

(DOI No: 10.3940/rina.ijme.2017.a3.425)

C Fang, Dalian Maritime University, Zhejiang Institute of Communications, China, **H Ren**, Dalian Maritime University, China, **Y Jin**, Dalian Maritime University, China and **C Dong**, University of Tennessee, USA

SUMMARY

In order to evaluate the ship trajectory more reasonable based on the quantitative information. This paper presents a new approach to evaluate the inward-port single ship trajectory quantitatively based on ship-handling simulator. First, a ship tracking points generating algorithm is proposed to generate sufficient tracking points in order to address the issue that the sample information is not enough on the ship simulator. Second, three reference tracking belts are established based on the sample data and cloud drop contribution degrees for the scenario that the collected samples information are enough. Finally, a quantitative score evaluation method that combines the qualitative information and the quantitative information is proposed, the similarity measurement results verify that the MES algorithm is more reasonable, the evaluation results of inward-port single ship trajectory illustrative that the proposed method is effective when applied to quantitative evaluation problems.

NOMENCLATURE

IMO	International Maritime Organization
STCW	International Convention on standards of Training, Certification and Watch keeping for Seafarers
SVM	Support Vector Machine
BP	Back Propagation
CS	Cloud Similar
VTS	Vessel Traffic System
IBCSC	Interval Based Cloud Similarity Comparison
MMCM	Maximum and Minimum based Cloud Model
LICM	Likeness comparing method based on cloud model
ECM	Expectation based cloud model
MCM	Maximum boundary based Cloud Model
ES	Expectation Surface
MBS	Maximum Boundary Surface
MES	Modified Expectation Surface
Ex	Expectation: the distribution of droplet expectations in the domain
En	Entropy: the uncertainty of qualitative concept determined by the concept of randomness and fuzziness.
He	Hyper Entropy: the uncertainty of Entropy, namely the entropy of entropy

1. INTRODUCTION

At present, ships developed to be large-sized, intelligent and specialized, then the more advanced requirements of comprehensive quality crews are needed, such as the ship manoeuvring ability and the bridge resource management ability, thus the IMO promulgated the Manila amendment of the STCW convention to strengthen the skill training of the crew (Jin & Yin, 2010), especially, to strengthen the ship navigator manoeuvring ability training. However, in the training practice, the problem is "how to reasonably evaluate the ship navigator manoeuvring ability when the ship is navigating in the fairway", In order to deal with this problem, the traditional evaluating method only consider the expert experience or the personal subjective experience, the reasonable evaluating method should consider both the subjective information and objective information, and the ship trajectory provides important quantitative objective information when the single ship is navigating an inward-port fairway (Chen, Ren, & Yi, 2011) (Roberge, Tarbouchi & Labonte, 2013) and if enough sample ship trajectories are collected which are navigated by the different experts or captains, then, these samples contain both objective information and subjective information, because of the partial related subjective information comes from these samples. The evaluation of ship trajectory is an effective way to deal with the evaluation of the ship navigator's manoeuvring ability.

In the navigational research field, some researchers pay attention to the research of route plan or route optimization, such as: compare the ship trajectory of not-under command vessel navigating nearby the bridge water area by using SVM (Wang, 2010), learn the optimal route by using genetic algorithm (Yang, 2012) (Zhang, Zhang, & Zheng, 2015) (Zhang & Zhang, 2015). Some researchers focus on the prediction of ship route, such as: analysis of the ship trajectory and prediction of Vessel Traffic System based on the improved adaptive trajectory estimation algorithm and BP neural network prediction algorithm (Xu, 2012). Very seldom research on the evaluation of ship trajectory can be found.

From the analysis of algorithm point of view, the existing references and algorithm always focuses on route planning algorithm and parameter learning. First, determine the objective function, the constraint conditions, and then, learn parameters by the corresponding machine learning algorithm. From the route evaluation and using information a point of view, the existing research results always focus on the route planning, dead reckoning and route prediction, however, the route planning reference standard are highly

subjective, model selection is often set in advance, and the best evaluation selection is chosen from a variety of programs based on the expert experience or subjective information.

In order to make the ship trajectory evaluation more objective, an effective way to evaluate the ship trajectory is based on using and learning the existing sample information. However, in navigation practice, it is difficult to evaluate the ship trajectory due to the large number of ships, sailing on the same waters in different times, the navigation path are overlap and cross, evaluation objects are complicated, and the evaluation of the inward-port single ship trajectory is the most simple and typical state. Therefore, the study of the evaluation of the inward-port single ship trajectory is the basis of the evaluation of other navigation conditions.

2. PROBLEM FORMULATION AND PRELIMINARIES

2.1 PROBLEM FORMULATION

For the inward-port single ship trajectory, the position point of the ship trajectory is determined by the longitude and latitude in the electronic chart based on the ship simulator, it is difficult to collect the certainty degree of position in the sample information. Therefore, the suitable backward cloud algorithm is the algorithm of backward cloud without certainty degree.

When evaluating the inward-port single ship trajectory, it is necessary to establish the reference tracking belt with different requirements owning to the ship tracking points that may navigate outside of the fairway, and it is can be obviously concluded that the more excellent sample information the more reasonable results. However, in practice, there is always not thousands of sample information, because the one inward-port navigation procedure always last more than an hour and the experiment are not always acceptable. So the inward-port single ship tracking points generating algorithm is needed.

In order to generate the inward-port single ship tracking points cloud chart, first, set the same ship condition, the same environment condition, then, invite the excellent captains or pilots to test the inward-port navigation, after finishing the navigation, check whether the ship trajectory has obviously problem or not, such as collided with the other objects, ship aground. If there are problems, reset the exercise and try again, if there is no problem, save it as a sample ship trajectory, all these exercises are based on ship simulator. Collect the samples, setup the sample information database. If there are enough samples in the database according to the evaluation requirement, then directly generate the inward-port single ship tracking points cloud chart. If there are no enough samples, then use the inward-port single ship tracking points generating algorithm to generate enough ship tracking points. Finally, generate the inward-port single ship tracking points cloud chart.

2.2 PREMILINARIES

The cloud model (Li and Du, 2005) that was first proposed by Li *et al*. The related definitions are as follows:

Cloud drop: suppose U is a quantitative domain with exact numerical value, C is a qualitative concept on U ,if qualitative value $x \in U$,and x is a stochastic realization of the qualitative concept C , $\mu(x) \in [0,1]$ is the certainty degree of x belonging to C , which is a random number with stable tendency $\mu : U \to [0,1]; \forall x \in U;\ x \to \mu(x)$

The distribution of x can be defined as a cloud, and each x is a cloud drop.

The cloud model describes the quantitative characteristics of qualitative concept by using the three digital features: Expectation, Entropy, and Hyper Entropy.

The cloud model algorithms mainly divide into two kinds of algorithm: the forward cloud generator and the backward cloud generator, and the normal distribution is one of the commonly used distribution in the navigational research field, thus, the two typical cloud algorithms are the forward normal cloud generator and the backward normal cloud generator.

Some researchers propose another forward normal cloud generator (Zhang, Li and Li, 2007) to revise the parameter He , for example, in the solution process of He , the thickness variation of the cloud satisfies two the half-normal distributions:

$$f_1(x) = He \exp(-\frac{(x-Ex_1)^2}{2(En_1^{\ 2})}),\ f_2(x) = He \exp(-\frac{(x_i-Ex_2)^2}{2(En_2^{\ 2})})$$

$$\text{Where } En_1 = (3-(\ln 8)^{1/2})En/4,\ Ex_1 = 0,\ Ex_2 = 0,$$
$$En_2 = (\ln 8)^{1/2} En/4.$$

According to the sample information whether the uncertainty of the information or not, divide the backward normal cloud generator into two categories, One is the algorithm of backward cloud with certainty degree, and the other is the algorithm of backward cloud without certainty degree.

For the algorithm of backward cloud with certainty degree research, Yu Shaowei proposes an algorithm of backward cloud based on normal distribution interval number (Yu and Shi, 2011). Li Deyi proposes an algorithm of backward cloud based on mean method (Li, Wang, and Li, 2016). Wang Hui proposes an algorithm

of backward cloud based on improved curve fitting (Wang, Qin, Liu, *et al*, 2014). Luo Ziqiang proposes an algorithm of backward cloud based on curve fitting (Luo. and Zhang, 2007), and so on.

Few researches discuss the algorithm of backward cloud without certainty degree: Liu Changyu first proposes the algorithm of backward cloud without certainty degree (Liu, Feng, Dai, *et al*, 2004). Hu Shenping proposes the cloud model based on the Monte Carlo Algorithm (Hu, Huang and Zhang, 2012).

The algorithm of backward cloud without certainty degree is as follows:

Set Sample information (N cloud drops (x_i)).as input,

Set Ex , En , He as output, first, calculate the sample mean, absolute centre distance of first order sample, sample variance

$$\overline{x} = \frac{1}{\mathrm{N}}\sum_{i=1}^{\mathrm{N}} x_i \ , \frac{1}{\mathrm{N}}\sum_{i=1}^{\mathrm{N}}\left|x_i - \overline{x}\right| , S^2 = \frac{1}{\mathrm{N}-1}\sum_{i=1}^{\mathrm{N}}(x_i - \overline{x})^2$$

Then calculate estimated expected value, estimated entropy, and estimated Hyper Entropy

$$E\hat{x} = \overline{x} \ , E\hat{n} = \sqrt{\frac{\pi}{2}} \times \frac{1}{\mathrm{N}}\sum_{i=1}^{\mathrm{N}}\left|x_i - E\hat{x}\right| , H\hat{e} = \sqrt{S^2 - E\hat{n}^2}$$

3. EVALUATION METHODOLOGY

3.1 THE SHIP TEACKING POINTS GENERATING ALGORITHM

The ship tracking points generating algorithm is as follows: first, set S samples, each sample select P position points as input, set N ship tracking points position and its degree as output. One select the same time interval points with the same numbers of points from each sample ship tracking line, that is, each sample tracking line has P position points, select each sample S_i the position of the same time S_iT_j , thus, the set of T_j tracking position points is A_{T_j} :

$A_{T_j} = \{drop(\varphi_{S_1T_j}, \lambda_{S_1T_j}), drop(\varphi_{S_2T_j}, \lambda_{S_2T_j})..., j = 1, 2...P\}$, according to A_{T_j} , calculate $E\hat{x}_{T_j}$, $E\hat{y}_{T_j}$

$E\hat{x}_{T_j} = \overline{\varphi_{T_j}} = \frac{1}{S}\sum_{i=1}^{S}\varphi_{S_iT_j}, E\hat{y}_{T_j} = \overline{\lambda_{T_j}} = \frac{1}{S}\sum_{i=1}^{S}\lambda_{S_iT_j}$ Calculate Enx_{T_j} and Eny_{T_j}

$Enx_{T_j} = \sqrt{\frac{\pi}{2}}\frac{1}{S}\sum_{i=1}^{S}\left|\varphi_{S_iT_j} - \overline{\varphi_{T_j}}\right|, Eny_{T_j} = \sqrt{\frac{\pi}{2}}\frac{1}{S}\sum_{i=1}^{S}\left|\lambda_{S_iT_j} - \overline{\lambda_{T_j}}\right|$, calculate $S\hat{x}_{T_j}$ and $S\hat{y}_{T_j}$

$(S\hat{x}_{T_j})^2 = \frac{1}{S-1}\sum_{i=1}^{S-1}(\varphi_{S_iT_j} - \overline{\varphi_{T_j}})^2 , (S\hat{y}_{T_j})^2 = \frac{1}{S-1}\sum_{i=1}^{S-1}(\lambda_{S_iT_j} - \overline{\lambda_{T_j}})^2$, next, calculate $He\hat{x}_{T_j}$ and Hey_{T_j}

$Hex_{T_j} = \sqrt{(S\hat{x})^2 - (Enx)^2}, Hey_{T_j} = \sqrt{(S\hat{y})^2 - (Eny)^2}$

Then, generate two dimensional normal random number $(Enx_{T_j}^{'}, Eny_{T_j}^{'})$ based on the expectation of (Enx_{T_j}, Eny_{T_j}) , and the standard deviation of (Hex_{T_j}, Hey_{T_j}) .and generate two dimensional normal random number $drop(\varphi_{Nk}, \lambda_{Nk})$ based on the expectation of (Ex_{T_j}, Ey_{T_j}) , and the standard deviation of $(Enx_{T_j}^{'}, Eny_{T_j}^{'})$., next, calculate μ_{Nk} : the degree of $drop(\varphi_{Nk}, \lambda_{Nk})$

$$\mu_{Nk} = e^{-[\frac{(\varphi_{Nk} - Ex_{T_j})^2}{2(Enx_{T_j}^{'})^2} + \frac{(\lambda_{Nk} - Ey_{T_j})^2}{2(Eny_{T_j}^{'})^2}]}$$

if N is the total ship tracking position points, each select time T_j generate N/P tracking points, so, repeat it until you generate N/P ship tracking cloud position points. Finally, repeat each sample points until you generate N ship tracking cloud position points (Fang, Ren and Jin, 2016).

3.2 THE INWARD-PORT SINGLE SHIP REFERENCE TRACKING BELT

In ship navigating alter-course situations, the generated position points are more discrete, therefore, to determine the present navigation situation compare the present position point with the history position point cloud chart. This is a good way to set the inward-port single ship reference tracking belt with different requirements.

According to the normal cloud drops group of concept contribution (Figure.1), the cloud drops in [Ex-0.67En, Ex+0.67En] accounted for 22.33% of cloud chart, the contribution of the concept is the total contribution of 50%, known as the key element. The cloud drops in [Ex-En, Ex+En] accounted for 33.33% of cloud chart, the contribution of the concept is the total contribution of 68.26%, known as the basic element. The cloud drops in [Ex-2En, Ex+2En] accounted for 66.66% of cloud chart, the contribution of the concept is the total contribution of 95.44%, the cloud drops in [Ex-2En, Ex-En] and [Ex+En, Ex+2En] known as the peripheral element. The cloud drops

in [Ex-3En, Ex+3En] accounted for 99.99% of cloud chart, the contribution of the concept is the total contribution of 99.97%, the cloud drops in [Ex-3En, Ex-2En] and [Ex+2En, Ex+3En] known as the weak peripheral element (Lu, Wang, Li, *et al*, 2003) (Yang, Yan, Zeng, 2013). Therefore, set the area of key element, the area of basic element and the area of including peripheral element as the requirement condition.

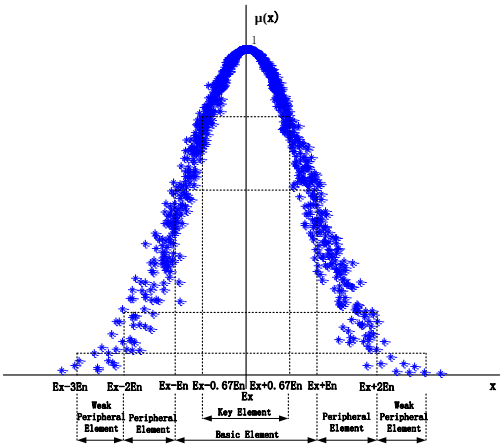

Figure 1. The normal cloud drops group of concept contribution chart

3.3 THE SIMILARITY MEASUREMENT ALGORITHM OF INWARD-PORT SINGLE SHIP TRAJECTORY

The existing cloud similarity measurement evaluation algorithms divide into three kinds, the first kind of algorithm is the cloud drop measurement algorithm, such as CS algorithm (Zhang, Zhao, Li, 2004), IBCSC algorithm (Cai, Fang, and Zhao, 2011), and MMCM algorithm (Jin and Tan, 2014). This kind algorithm selects the suitable cloud drops from the generated cloud, and calculates the similarity of the drop based on distance. The second kind of algorithm is a vector measurement algorithm, such as LICM algorithm (Li, 2012). This kind of algorithm uses the cosine value to calculate the similarity of two clouds by the cloud parameters. The third kind of algorithm is public space measurement algorithm, such as ECM algorithm (Li, Guo, and Qiu, 2011), MCM algorithm (Sun, 2015). This kind algorithm uses pubic space to calculate the similarity of cloud. Most of the above algorithms and references focus on the one dimension cloud, but for the two dimensions or higher dimensions, there are seldom relevant reference and supporting tests.

As for the evaluation of inward-port single ship trajectories based on the ship simulator, referring to the relevant literature, combining with the assessment of an actual situation, it is more reasonable to describe the navigating situation by using the course deviation and displacement difference in two-dimensions.

The evaluation algorithm of inward-port single ship trajectory is as follows:

Set S --sample tracking line, H --a tracking line to be evaluated as input,

Set $Sim(H,H')$ --The cloud similarity value of H and the reference tracking line H' select from the S sample tracking line as output.

Step 1: Select the same time interval points with the same numbers F of points from each sample ship tracking line, select each sample S_i the position of the same time S_iT_j, thus, the set of T_j tracking position points is A_{T_j} ,the related course information set know as C_{T_j} ,

$$A_{T_j} = \{drop(\varphi_{S_1T_j}, \lambda_{S_1T_j}), drop(\varphi_{S_2T_j}, \lambda_{S_2T_j}), ... , drop(\varphi_{S_iT_j}, \lambda_{S_iT_j}), i = 1,2...S\}$$

$$C_{T_j} = \{C_{S_1T_j}, C_{S_2T_j}, ..., C_{S_iT_j}, i = 1,2...S\}$$

Step 2: according to A_{T_j} , C_{T_j} , calculate $E\hat{x}_{T_j}$ and $E\hat{y}_{T_j}$

$$\bar{\varphi}_{T_j} = \frac{1}{S}\sum_{i=1}^{S}\varphi_{S_iT_j}, \bar{\lambda}_{T_j} = \frac{1}{S}\sum_{i=1}^{S}\lambda_{S_iT_j}, \bar{C}_{T_j} = \frac{1}{S}\sum_{i=1}^{S}C_{S_iT_j}$$

Step 3: according to the T_j moment of sample tracking point position $drop(\varphi_{HT_j}, \lambda_{HT_j})$ in H , and course C_{HT_j} , calculate the course deviation ΔC_{T_j} and displacement difference ΔD_{T_j} (R is the radius of earth, about 6378137 meters). $\Delta C_{T_j} = C_{HT_j} - \bar{C}_{T_j}$

$$C = \sin(\varphi_{HT_j}\pi/180)\sin(\bar{\varphi}_{T_j}\pi/180) + \cos(\varphi_{HT_j}\pi/180)\cos(\bar{\varphi}_{T_j}\pi/180)\cos((\lambda_{HT_j} - \bar{\lambda}_{T_j})\pi/180)$$

$$\Delta D_{T_j} = \arccos(C)\cdot R\cdot\pi/180$$

Step 4: for the course deviation dimension, calculate $Ex(\Delta C)$, $En(\Delta C)$, $He(\Delta C)$, for the displacement difference dimension, calculate $Ex(\Delta D)$, $En(\Delta D)$, $He(\Delta D)$:

$$Ex(\Delta C) = \Delta\bar{C} = \frac{1}{F}\sum_{j=1}^{F}\Delta C_{T_j}$$

$$Ex(\Delta D) = \Delta\bar{D} = \frac{1}{F}\sum_{j=1}^{F}\Delta C_{T_j}$$

$$En(\Delta C) = \sqrt{\frac{\pi}{2}}\frac{1}{F}\sum_{j=1}^{F}\left|\Delta C_{T_j} - \Delta\bar{C}\right|$$

$$En(\Delta D) = \sqrt{\frac{\pi}{2}}\frac{1}{F}\sum_{j=1}^{F}\left|\Delta D_{T_j} - \Delta\bar{D}\right|$$

$$(S(\Delta C))^2 = \frac{1}{\text{F-1}}\sum_{i=1}^{\text{F-1}}(\Delta C_{T_j} - \Delta\bar{C})^2$$

$$(S(\Delta D))^2 = \frac{1}{\text{F-1}}\sum_{i=1}^{\text{F-1}}(\Delta D_{T_j} - \Delta\bar{D})^2$$

$$He(\Delta C) = \sqrt{(S(\Delta C))^2 - (\text{En}(\Delta C))^2},$$

$$He(\Delta D) = \sqrt{(S(\Delta D))^2 - (\text{En}(\Delta D))^2}$$

Step 5: generate two dimensional normal random number $(En(\Delta C_t)', En(\Delta D_t')), t = 1, 2, ..., \text{N}$ based on the expectation of $(En(\Delta C), En(\Delta D))$, and the standard deviation of $(He(\Delta C), He(\Delta D))$; generate two dimensional normal random number $\text{drop}(\Delta C_t, \Delta D_t), t = 1, 2, ..., \text{N}$ based on the expectation of $(Ex(\Delta C), Ex(\Delta D))$, and the standard deviation of $(En(\Delta C)', En(\Delta D)')$, and calculate the degree of membership μ_t

$$\mu_t = \text{e}^{-[\frac{(\Delta C_t - Ex(\Delta C))^2}{2(En(\Delta C)'^2)} + \frac{(\Delta D_t - Ex(\Delta D))^2}{2(En(\Delta D)'^2)}]}$$

Step 6: for the course deviation dimension, the cloud drops in $[Ex(\Delta C)\text{-}2En(\Delta C), Ex(\Delta C)\text{+}2En(\Delta C)]$ accounted for 66.66% of cloud chart, the contribution of the concept is the total contribution of 95.44%, the distribution of cloud drops are relevant concentrate and the drop density change are relevant low, the same to the displacement difference dimension, so define the set $B = \{drop(\Delta C_t, \Delta D_t, \mu_t), t = 1, 2, ..., N\}$, when the drop both satisfy the condition $Ex(\Delta C)\text{-}2En(\Delta C) \le \Delta C_t \le Ex(\Delta C)\text{+}2En(\Delta C)$ and $Ex(\Delta D)\text{-}2En(\Delta D) \le \Delta D_t \le Ex(\Delta D)\text{+}2En(\Delta D)$, and these drops form the set K.

Step 7: in order to find the largest degree of membership in the certain area with the same interval delta distance and delta course, divide the delta distance dimension into M parts, and divide the delta course dimension into M parts, then form the M*M mesh area, and find the drop with the largest degree of membership in each small part, and all these drops form set Y.

Step 8: for the course deviation dimension, calculate $Ex_Y(\Delta C)$, $En_Y(\Delta C)$, $He_Y(\Delta C)$, for the displacement difference dimension, calculate $Ex_Y(\Delta D)$, $En_Y(\Delta D)$, $He_Y(\Delta D)$.

$$Ex(\Delta C_Y) = \Delta\bar{C}_Y = \frac{1}{\text{M}^2}\sum_{j=1}^{\text{M}^2}\Delta C_{YT_j}$$

$$Ex(\Delta D_Y) = \Delta\bar{D}_Y = \frac{1}{\text{M}^2}\sum_{j=1}^{\text{M}^2}\Delta C_{YT_j}$$

$$En(\Delta C_Y) = \sqrt{\frac{\pi}{2}}\frac{1}{\text{M}^2}\sum_{j=1}^{\text{M}^2}\left|\Delta C_{YT_j} - \Delta\bar{C}_Y\right|,$$

$$En(\Delta D_Y) = \sqrt{\frac{\pi}{2}}\frac{1}{\text{M}^2}\sum_{j=1}^{\text{M}^2}\left|\Delta D_{YT_j} - \Delta\bar{D}_Y\right|$$

$$(S(\Delta C_Y))^2 = \frac{1}{\text{M}^2\text{-}1}\sum_{i=1}^{\text{M}^2-1}(\Delta C_{YT_j} - \Delta\bar{C}_Y)^2$$

$$(S(\Delta D_Y))^2 = \frac{1}{\text{M}^2\text{-}1}\sum_{i=1}^{\text{M}^2-1}(\Delta D_{YT_j} - \Delta\bar{D}_Y)^2$$

$$He(\Delta C_Y) = \sqrt{(S(\Delta C_Y))^2 - (\text{En}(\Delta C_Y))^2}$$

$$He(\Delta D_Y) = \sqrt{(S(\Delta D_Y))^2 - (\text{En}(\Delta D_Y))^2}$$

Step 9: choose a typical ship tracking line as reference tracking line H', repeat step1 to step 8.

Step 10: calculate the value of $Sim(H, H')$ by different method, such as vector measurement algorithm, public space measurement algorithm and so on.

The similarity of Vector measurement formula:

$$\overrightarrow{U_H} = vector(Ex(\Delta C_{HY}), En(\Delta C_{HY}), He(\Delta C_{HY}), Ex(\Delta D_{HY}), En(\Delta D_{HY}), He(\Delta D_{HY}))$$

$$\overrightarrow{U_{H'}} = vector(Ex(\Delta C_{H'Y}), En(\Delta C_{H'Y}), He(\Delta C_{H'Y}), Ex(\Delta D_{H'Y}), En(\Delta D_{H'Y}), He(\Delta D_{H'Y}))$$

$$Sim(H, H') = \cos(\overrightarrow{U_H}, \overrightarrow{U_{H'}}) = \frac{\overrightarrow{U_H} \cdot \overrightarrow{U_{H'}}}{\left\|\overrightarrow{U_H}\right\|\left\|\overrightarrow{U_{H'}}\right\|}$$

The similarity of public space measurement formula:

S_H is the cloud area based on H tracking line, $S_{H'}$ is the cloud area based on H' tracking line, S_{public} is the pubic area between the H tracking line and the H' tracking line

$$Sim(H, H') = \frac{2S_{public}}{S_H + S_{H'}}$$

Therefore, the evaluation score of inward-port single ship trajectory can be calculated by three steps: first, judge whether the sample information is sufficient or not, if not enough, use the ship tracking points generating algorithm to generate enough sample information, and then construct the inward-port single ship reference tracking belt with the different requirement condition, and calculate the outside-belt score. Next, use the similarity measurement algorithm to evaluate the similarity score by comparing the reference tracking line with the target tracking line. Finally, calculate the total score of the inward-port single ship trajectory.

4. EXPERIMENTAL STUDIES

Generally, in order to make evaluation results more comparable, the evaluation of the inward-port single ship trajectory need lots of navigational samples in the same ship condition, the same traffic condition, and the same starting point, but it is very difficult to collect these kinds of sample information in the real port, because the environment and condition always change.

The ship simulator is formed from a collection of navigational equipment simulator, the system can simulate the expected navigational environment (Fang and Ren, 2015) (Fang and Ren, 2015b), in order to test the algorithm effectiveness, when collecting the samples information of the inward-port single ship trajectory, we set up the same ship condition, the same traffic environment, and the same starting point based on the ship simulator.

Set the oil tanker "CHANGHANGXIWANG" entering into the Dalian port as an example, set NE wind 1kn, E current 0.5kn, the starting point is latitude $38°55.812'$ longitude $121°47.028'$. Select about an hour period of navigation ship trajectory, for each tracking line select 127 position points with the same time interval, in this case, invite 32 different experienced captains and 20 different experienced pilots to test the navigation, collect 50 valid exercises ship tracking lines for the sample information database. According to the ship tracking points generating algorithm, the input information S is 50, and P is 127. These 127 sample point at the same time generates 100, 1000 and 10000 tracking points are shown in Figure.2, and the overall situation of inward-port single ship tracking point's generation cloud chart is shown in Figure.3.

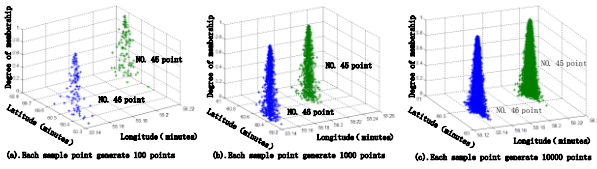

Figure.2. The cloud chart of a single sample point generate tracking points

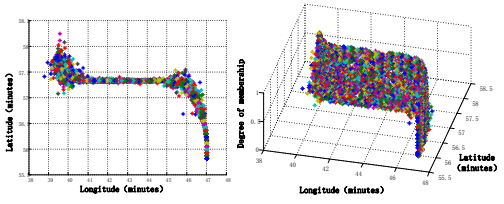

Figure.3. the overall situation of inward-port single ship tracking points generation cloud chart

According to the results of Figure.3 and the cloud drop contribution of Figure.1, set the area of key element, the area of basic element and the area of including peripheral element as the requirement condition when determining the inward-port single ship reference tracking belt. As Figure.4 shows, the key element area tracking belt, the basic element area tracking belt and the including peripheral element tracking belt.

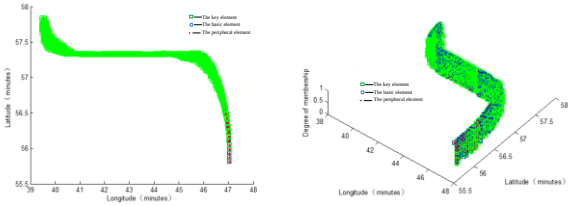

Figure 4. the inward-port single ship reference track belt chart

Based on Figure 3 information, according to the evaluation algorithm of inward-port single ship trajectory, set input information S=49, the tracking line to be evaluated, after step 1-step 6, then set K is as the circle drop points in Figure.5 shows, then continue to step 7, form the set Y is as the selected maximum points in Figure 5 shows, after step 8 calculate the six parameters of the two-dimension cloud, and it is easy to draw the mathematic equation surface based on the six parameters of the two-dimension cloud. Figure 6 shows that the ES, MBS and MES on set Y cloud drops, z_{ES} is the degree of membership based on ES, z_{MES} is the degree of membership based on MES, z_{MBS} is the degree of membership based on MBS.

$$z_{ES} = e^{-\left[\frac{(x-Ex(\Delta C_Y))^2}{2(En(\Delta C_Y)'^2)}+\frac{(y-Ex(\Delta D_Y))^2}{2(En(\Delta D_Y)'^2)}\right]}$$

$$z_{MES} = e^{-\left[\frac{(x-Ex(\Delta C_Y))^2}{2(He(\Delta C_Y)^2+En(\Delta C_Y)'^2)}+\frac{(y-Ex(\Delta D_Y))^2}{2(He(\Delta D_Y)^2+En(\Delta D_Y)'^2)}\right]}$$

$$z_{MBS} = e^{-\left[\frac{(x-Ex(\Delta C_Y))^2}{2(3He(\Delta C_Y)+En(\Delta C_Y)')^2}+\frac{(y-Ex(\Delta D_Y))^2}{2(3He(\Delta D_Y)+En(\Delta D_Y)')^2}\right]}$$

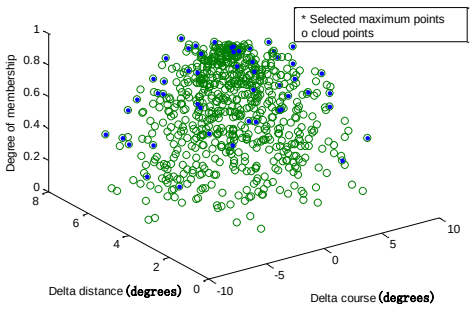

Figure.5. the set K and set Y cloud drops chart

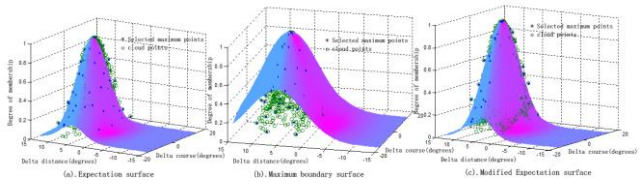

Figure.6. the ES, MBS and MES curve fitting based on set Y cloud drops

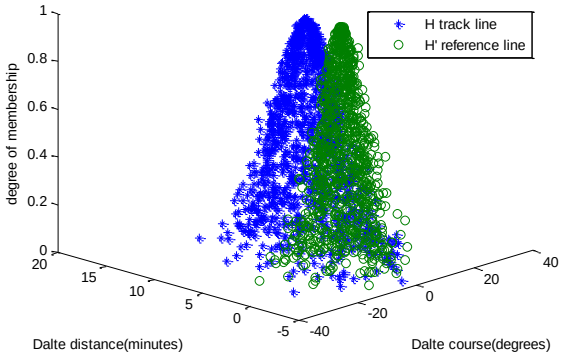

Figure.7. the relationship between the selected reference line cloud and the target track line cloud

Figure.7 shows the relationship between the selected reference line (H') cloud and the target tracking line (H) cloud. by using different mathematic equation surfaces, the similarities of the cloud are different, according to the experiment of one-dimension cloud, the modified expectation is more reasonable (Zhang, Li & Sun, *et al.* 2014) (Gong, Jiang and Liang, 2015). However, for the two-dimension cloud, it is necessary to compare these four algorithm's test results to each other (Dong, Hong, & Xu, *et al*., 2011) (Zhang and Sanderson, 2009). In this case study, select five typical track lines as target track lines to be evaluated in the S sample information, and evaluate the similarity based on the S sample information, the results are seen in Table 1.

From the similarity of the selected five target lines based on COSINE, ES, MBS, MES algorithm in the Table 1, it can be concluded that :H2 has the highest similarity of H4, H3 has the highest similarity of H5, H1 has the lowest similarity of H2 and has the higher similarity of H5. Although the value differences are different, the tendency conclusion is the same. It also can be concluded that the MES algorithm is better than the ES and the MBS algorithm when compared H2 to H5, because the similarity value difference between the ES and MBS algorithm is small, and the difference of similarity value is larger by using the MES algorithm.

Table 1 the similarity of selected five target lines based on COSINE, ES, MBS, MES algorithm

		H1	H2	H3	H4	H5
COSINE	H1	1	0.7142	0.8328	0.7438	0.8715
	H2	0.7142	1	0.7546	**0.9104**	0.7919
	H3	0.8328	0.7546	1	0.8316	**0.9126**
	H4	0.7438	0.9104	0.8316	1	0.8236
	H5	0.8715	0.7919	0.9126	0.8236	1
ES	H1	1	0.6857	0.7896	0.6904	0.8578
	H2	0.6857	1	0.7027	**0.8432**	0.8225
	H3	0.7896	0.7027	1	0.7946	**0.8410**
	H4	0.6904	0.8432	0.7946	1	0.7858
	H5	0.8578	0.8225	0.8410	0.7858	1
MBS	H1	1	0.6214	0.8012	0.7102	0.8136
	H2	0.6214	1	0.7324	**0.8360**	0.7908
	H3	0.8012	0.7324	1	0.8127	**0.8349**
	H4	0.7102	0.8360	0.8127	1	0.7735
	H5	0.8136	0.7908	0.8349	0.7735	1
MES	H1	1	0.7263	0.8231	0.7325	0.8869
	H2	0.7263	1	0.7641	**0.9018**	0.8035
	H3	0.8231	0.7641	1	0.8019	**0.9028**
	H4	0.7325	0.9018	0.8019	1	0.8002
	H5	0.8869	0.8035	0.9028	0.8002	1

Therefore, when evaluating the inward-port single ship tracks quantitatively, first, it is necessary to set the track line belts with different requirements, for example, in Figure.6, suppose: the total score is 100, if the evaluator needs a strict rule during the navigation, and there are 127 sample points in the track line, when the ship track point navigating outside the green track belt, it should be minus 1 score, when the ship track point navigating outside the blue track belt, it should be minus 0.5 score. Secondly, by using the evaluation algorithm of inward-port single ship track, and comparing them, and make sure the score-calculating reference track line is under the numbers of experts' supervision, for example, in table1, suppose the H5 is the score-calculating reference track line, use the similarity with the other track line, it is easy to calculate the score of the others track line by multiplying the similarity, and the total score is the similarity score minus the outside-belt score. The quantitative score results of the other track line are obtained by using the MES algorithm is shown in Table 2.

Table 2 the quantitative score results by using the MES algorithm

	H1	H2	H3	H4	H5
The similarity score	+88.7	+80.4	+90.3	+80.0	+100
The outside-belt score	-4.5	-5.0	-2.5	-6.5	-1.5
The total score	+84.2	+75.4	+87.8	+73.5	+98.5

In addition, if the experts group think the score of H5 is another score not 100, then the others score will change according to the score of H5. Therefore, this method combines effectively the qualitative information with quantitative information based on the ship handling simulator.

5. CONCLUSIONS

This paper has outlined a feasible approach in which historical and sample information were used to evaluate the inward-port single ship tracking line based on the ship-handling simulator. Once an adequate sample trajectory information by excellent captains or pilots were obtained, a reasonable inward-port single ship reference tracking belt will be formed, then the evaluation score should be more reasonable, however, if there are not adequate sample trajectory information, the inward-port single ship tracking points generating algorithm can be used. When evaluating the inward-port single ship tracking line, by using the evaluation algorithm of inward-port single ship trajectory, calculate the similarity of different measurement algorithm (COSINE, ES, MBS, MES), and choose the more suitable algorithm result, set the score-calculating reference tracking line under the numbers of expert's supervise, calculate the outside-tracking score, then the total quantitative score of each tracking line can be obtained. Therefore, this similarity of cloud model algorithm combines effectively the sample information and the expert's experience.

It can be concluded that if sufficient information is available, the evaluation results will be more reasonable, so future work will involve collecting more sample information, and integrating the evaluation algorithm with the expert's human-computer interaction based on the navigational simulation system.

6. ACKNOWLEDGEMENTS

The authors would like to thank the captains and pilots, XuDong, Mao, Liang, Li and all the other participating members for their patiently participating in the single ship navigating in Dalian port based on the ship simulator. They like to thank Prof. Yin Yong for his valuable suggestions. They like to thank Meyers Danielle for her patiently revision and valuable suggestions. They would also like to thank Prof. David B. Clarke as the first author Fang's visiting scholar supervisor, who is working at the University of Tennessee, respectively, for his revision and some valuable suggestions to this paper. This work is supported by scientific research fund of The National High Technology Research and Development Program of China (863) under Grant 2015AA016404, The Traffic Department of Applied Basic Research Project under Grant 2015329225240 and Zhejiang Province Department of Education Research Project under Grant Y201533096.

7. REFERENCES

1. JIN, Y.C., YIN, Y., "*Maritime simulator: convention and technology*", Navigation of China, vol. 33, no. 1,pp.1-6, 2010
2. CHEN, L.N., REN, H.X., JIN, Y.C., "*On ship radar/ARPA intelligent examination system*", Journal of Chongqing Jiaotong University (natural science), vol.30, no.5, pp.1049-1053, 2011
3. ROBERGE, V., TARBOUCHI, M,. and LABONTE, G., "*Comparison of parallel genetic algorithm and particle swarm optimization for real-time UAV path planning*," IEEE Transactions on Industrial Informatics, vol.9, no1, pp.132-141, 2013
4. WANG, Y.F., (2010), "*Contrasting track out of control ship based on SVM bridge water*", Wuhan: Wuhan University of technology, pp.23-47, 2010
5. YANG, X., "*Research of key technology and practical application of intelligent vessel traffic system*", Dalian maritime university, pp.73-110, 2012
6. ZHANG, G., ZHANG, X., ZHENG, Y., *Adaptive neural path-following control for under actuated ships in fields of marine practice*, Ocean Engineering, vol.104, no.1, pp.558-567, 2015
7. ZHANG, G., ZHANG, X., *A novel DVS guidance principle and robust adaptive path-following control for under actuated ships using low frequency gain-learning*, ISA Transaction, vol.56, pp.75-85,2015
8. XU, T.T., "*Study on new technology of vessel tracking and track prediction in vessel traffic services system*". Dalian: Dalian maritime university, pp.17-71, 2012
9. LI, D.Y., DU Y., "*Artificial intelligent with uncertainty*", National Defense Industry Press, pp.136-145, 2005.
10. ZHANG, G., LI, D.Y., LI, P., *et al*, "*A collaborative filtering recommendation algorithm based on cloud model*", Journal of software, vol.18, no.10, pp. 2403-2411, 2007
11. YU, S.Z., SHI, Z.K., "*New algorithm of backward cloud based on normal interval*

number", Systems Engineering-theory & practice, vol.31, no.10, pp. 2021-2026, 2011
12. LI, D., WANG, S., LI, D.Y., "*cloud model*", spatial data mining, pp.187-201, 2016
13. WANG, H., QIN, S., LIU, S.Y., YU, L.J., WANG, K.J., "*An improved algorithm of backward cloud based on curve fitting*", CAAI Transactions on intelligent systems, vol.9, no.5, pp. 590-594, 2014
14. LUO, Z.Q., ZHANG, G.W., "*A new algorithm of backward normal one-variant cloud*", Journal of frontiers of computer science and technology, vol.1, no.2, pp. 234-240, 2007
15. LIU, C.Y., FENG, M., DAI, X.J., LI, D.Y., "*A new algorithm of backward cloud*", Journal of system simulation, vol.1, no.2, pp. 2417-2410, 2004
16. HU, S., HUANG, C., ZHANG, H., *Cloud Model-based Simulation of System Risk of Marine Traffic by Monte Carlo Algorithm*, China Safety Science Journal, vol.22, no.4, pp. 20 – 26, 2012
17. FANG, C., REN, H., JIN, Y., *New Evaluating Algorithm of the Single Ship Track When Inward/outward Port Based on Ship-Handling Simulator Training*, Journal of System Simulation, vol.28, no.9, pp. 2201 – 2206, 2016
18. LU, H., WANG, Y., LI, D.Y., *et al*, "*The application of backward cloud in qualitative evaluation*", Chinese Journal of Computer, vol.26, no.8, pp. 1009 – 1014, 2003
19. YANG, X., YAN, L., ZENG, L., "*How to handle uncertainties in AHP: The Cloud Delphi hierarchical analysis*", Information Sciences, vol.222, pp. 384–404, 2013
20. ZHANG, Y., ZHAO, D., LI, D.Y., "*The similar cloud and its measurement analysis method*", Information and control, vol.33, no.2, pp. 129-132, 2004
21. CAI, S., FANG, W., ZHAO, J., *et al*, "*Research of interval-based cloud similarity comparison algorithm*", Journal of Chinese Computer Systems, vol.32, no.12, pp. 2456-2460, 2011
22. JIN, L., TAN, S., "*Similarity measurement between cloud models based on close degree*", Application Research of Computers, vol.31, no.5, pp. 1308-1311, 2014
23. LI, H., "*Research on feature representations and similarity measurements in time series data mining*", Dalian University of Technology, pp.45-75, 2012
24. LI, H., GUO, C., QIU, W., "*Similarity measurement between normal cloud models*", Acta Electronica Sinica, vol.39, no.11, pp. 2561-2567, 2011
25. SUN, N., "*Research and application of similarity measurement between normal cloud models based on overlap degree*", Taiyuan University of Technology, pp. 21-23, 2015
26. FANG, C., REN, H., "*The Evaluating Simulation System of Ship Anchoring Operation*", Control Conference (CCC), 34th Chinese, pp. 8834-8837, 2015
27. FANG, C., REN, H., "*A Review of Intelligent Evaluation Methods in Ship Simulator*", Navigation of China, vol.38, no.4, pp.48-52, 2015b
28. ZHANG, H., LI, Z., SUN, Y., ZHANG, H., "*New similarity measure method on time series*", computer engineering and design, vol.35, no.4, pp. 1279-1284, 2014
29. GONG, Y., JIANG, Y., LIANG, X., "*Similarity measurement for normal cloud models based on fuzzy similarity measure*", System engineering, vol.33, no.9, pp. 133-137, 2015
30. DONG, Y.C., HONG, W.C., XU, Y.F., YU, S. *Selecting the individual numerical scale and prioritization method in the analytic hierarchy process: a 2-tuple fuzzy linguistic approach*, IEEE Transactions on Fuzzy Systems 19 (1) 13–25.2011
31. ZHANG, J. Q., SANDERSON, A. C. *Adaptive differential evolution with optional external archive*. IEEE Transactions on Evolutionary Computation, 13(5) pp. 945-958.2009

CFD STUDY OF SHIP-TO-BANK INTERACTION

(DOI No: 10.3940/rina.ijme.2017.a3.426)

Y K Kim, Lloyd's Register Global Technology Centre, Singapore and **E Y K Ng,** School of Mechanical & Aerospace Engineering, Nanyang Technological University, Singapore

SUMMARY

Ship-to-bank interaction is a complex physical phenomenon that involves not only in the asymmetric pressure field near banks or channels but also shallow water effect. Traditionally many experimental studies were carried out in this field. As numerical method is getting popular, there were various computational approaches as well. In this study, flow around a container ship in confined water is investigated with the open source CFD (Computational Fluid Dynamics) toolbox, OpenFOAM. Computations with several bank arrangements and different settings are performed. The OpenFOAM results are also compared to experiment results for validation.

NOMENCLATURE

P	Pressure (N m^{-2})
Fx	Longitudinal force / Resistance (N)
Fy	Transverse force / Sway force (N)
g	Acceleration of gravity (m s^{-2})
k	Turbulence kinetic energy (m^2 s^{-2})
*p**	Dynamic pressure kg/(m·s2)
t	time (s)
U	Speed vector *(*m s^{-1})
w	Artificial velocity normal to the interface of volume fraction *(*m s^{-1})
Mz	Yaw moment (N m)
y_B	Distance from bank wall to the centreline of ship (m)
y+	Non-dimensional distance from the wall to the first grid point
α	Scalar field of volume fraction
κ	Surface curvature (m^{-1})
μ	Dynamic viscosity (kg m^{-1} s^{-1})
ρ	Density of fluid (kg m^{-3})
σ	Surface tension coefficient (N m^{-1})
ω	Specific turbulence dissipation rate (s^{-1})
CFD	Computational Fluid Dynamics
RANS	Reynolds Averaged Navier Stokes
SST	Shear Stress Transport
VOF	Volume of Fluid

1. INTRODUCTION

When a ship navigates in the proximity of banks or harbours, the pressure field near the ship becomes asymmetric and ship experiences repelling or attracting forces. It makes hard for the ship to manoeuvre and can lead to an accident. In such cases, it is advised to travel at the middle of water to minimise any interaction from the bank or the harbour. However, as this is not always possible, it is important to understand the phenomenon to prevent any dangerous situation. Basically ship-to-bank interaction causes sway force and yaw moment on the ship when separation from the bank wall is small. Moreover, small under keel clearance in confined water allows the interaction even stronger due to the shallow water effect. In addition, there are several other factors such as propeller effect and bank shape that contribute to the bank effect. Because ships have been increased in size and length in recent years, the importance of prediction and understanding of ship-to-bank interaction are thus getting more critical.

Nowadays, ship-handling simulators play an important role in training captains and crew for safe operation and preventing from accidents. In the mathematical model of the ship-handling simulator, various forces and moments that arise from hull, rudder, propeller, wind, wave, bank effect, etc have to be carefully modelled for realistic simulations. The best way to obtain those forces and moments is to carry out model tests. Captive model test such as HPMM (Horizontal Planar Motion Mechanism) test enables measuring of each force and moment components. However, the test is costly and time consuming. Therefore, it is normal to use empirical methods that are based on the regression formulas from database to estimate these forces and moments. When the accuracy is concerned, CFD (Computational Fluid Dynamics) analysis can give better accuracy to predict those forces and moments. Nowadays, it is not much to say that CFD technology became essential in marine industry. As CFD methodology is being developed, the accuracy and reliability of CFD analysis are also getting better. There were many studies to calculate hydrodynamic forces and moments of mathematical model in ship-handling simulator using CFD approach. In this study, it is decided to work on an open source CFD code to analyse ship-to-bank interaction from various bank arrangements and compare them to the experiment results.

In early days, many experimental studies have been carried out to investigate ship-to-bank interaction and researchers developed empirical formulas that could predict ship-to-bank interaction. It was found that sway force and yaw moment vary in proportion to the square of ship speed. Based on this finding, empirical formulas were suggested from model test results (Norrbin, 1974).

Li *et al.* (2001) found ship-to-bank interaction occurs in a more complex manner. The study suggested there is a point where the sway force is switched from suction to

repulsive force when under keel clearance is extremely small, approximately at about 10% of water draught. Moreover, unlike the study in early times, it turns out that the sway force tends to increase in a higher order than two with respect to the ship speed when under keel clearance is very small. Even in some cases, it became more than order of two at 40% of under keel clearance. At a sloped bank with 30 degrees angle, it tends to reduce force and moments at low speeds but bank effects increase at high speeds as compared to a vertical bank at a low under keel clearance. Moreover, a suction force arises from a rotating propeller compared to the cases without propeller according to the experiments. It was found the more propeller loading caused the larger contribution of suction force.

Expansive shallow water tank tests were carried out at FHR (Flanders Hydraulics Research) in Belgium (Lataire *et al.*, 2009). More than 10,000 model tests of the bank effect were performed and many factors that influence the bank effect were investigated. Through the experiments, it was confirmed that there is a transition point from attraction sway force to repulsion force in shallow water. Small difference from the test results of Li *et al.* (2001) is that the transition happened at slightly higher under keel clearance which is in range of 15% to 20%. Therefore, it is understood that the transition from attraction to repulsion force appears at the under keel clearance of 10~20% water draught. The test results also indicated that propeller action increased the bank effect. Similarly to the results of Li *et al.* (2001), propeller action changed repulsion force into suction force in shallow water where under keel clearance is less than 35% of water draught. These tests results are also developed into empirical formulas. Several sets of test data are made available for the bench marking purpose of simulation model (Lataire *et al.*, 2009). These open test results are used for the validation the CFD calculations in this study.

As numerical technique was being developed, there were many computational studies on the bank effect. In early times, numerical method based on potential theory was used to evaluate the bank effect. When the free surface condition is linearised by double model solution, it was good enough to show qualitative predictions only when the draught and water depth ratio is not too small, such that the ratio is greater than 1.5 (Q. Miao and J. Xia, 2003 and Lee and Lee, 2008). When non-linear boundary condition is applied, panel method was also able to calculate ship-to-bank interaction in extreme shallow water with qualitative agreement (Park *et al.*, 2014). With this non-linear potential method, even the transition point from suction force to repulsion force was found at 40% of the draught-water depth ratio which is slightly higher than the experiment results reported by Li *et al.* (2001) and Lataire *et al.* (2009).

As computational capability is rapidly improving, RANS based finite volume methods were also getting popular. However, it was quite recent that RANS based method was started to be used in this topic.

Lo *et al.* (2009) carried out transient analysis on the bank effect. Trajectory of a containership travelling near the bank was illustrated. Sway force and yaw moment with time variations at various velocities were calculated at about 30% of the draught-water depth ratio. However, there was no comparison with experiment result.

Wang *et al.* (2010) studied viscous analysis around series 60 hull with k-ω SST turbulence model from 50% to 1000% of the water depth – draught ratio and showed good agreement with experiments in sway forces but over prediction with the very short distance to the bank wall.

Zou *et al.* (2011) used validation and verification method including a grid convergence study to evaluate RANS based CFD prediction of ship-to-bank interaction. The bank effect between KVLCC hull and a sloped bank was analysed with an overlapping grid of structured mesh and k-ω SST turbulence model. CFD calculations in the comparison with model tests were done at 50%, 35% and even 10% of the draught-water depth ratio. Furthermore, not only sway force and yaw moment but also rolling, sinkage and trim moment were calculated and compared with potential flow analysis. Because sinkage and trim moment did not show big difference between the potential method and CFD calculation result, free surface effect at slow speed is considered to be insignificant for sinkage and trim. In the study, slip boundary condition was applied on the bank wall instead of no slip condition. The rationale for this boundary condition is not clear and the author also states that the boundary condition may not be accurate. The bank effect analysis gave good agreement in tendencies of yaw and roll moments but with under prediction of sway force.

Mehdi *et al.* (2013) carried out simulation of the viscous flow around LNG ship using RANS method with unstructured hybrid mesh and k-ω turbulence model. Yaw moment was compared with the experiment results at various velocities and distance from a bank wall but sway force results were not presented in their paper. Calculated yaw moments at different distance from the bank wall and 60% of the draught-water depth ratio were compared to the tank test results and showed qualitative agreement with some under prediction.

From the various studies done in the past, it is still a big challenge to use CFD for ship-to-bank interaction analysis with extreme shallow water. Many studies failed to simulate extreme conditions such as 10% of under keel clearance or did not predict bank effect correctly.

Moreover, during the literature review about numerical studies of the bank effect, viscous flow analysis including free surface effect on the bank effect was not found so far. When a ship travels at slow speed, it is no doubt that free surface elevation is not so high and the importance from

free surface might be relatively low. However, it is believed to be worthwhile to carry out viscous flow analysis with free surface for more accurate prediction of the flow near the proximity of banks. It is also expected to see the difference between the analysis with and without free surface.

2. COMPUTATIONAL SETTINGS

2.1 CASE SETTING

Numerical setup for confined water analyses was established according to the experimental setup done by FHR (Lataire *et al.* 2009). The test cases with several bank arrangements and different under keel clearances were chosen for numerical analysis. As found in the experimental research, a 8000TEU container ship in model scale was used for the simulations with a scale ratio of 80. Table 1 is the principle dimension of the model ship.

Table 1: Principle dimension of the model ship

Length overall (m)	4.332
Breadth (m)	0.530
Draught (m)	0.149 ~ 0.180
Block Coefficient	0.65 ~ 0.66 (depending on the draught)

The solver used for the simulations is *interFoam* which is a solver for transient solutions of two incompressible, isothermal and immiscible fluids using a VOF (volume of fluid) phase-fraction. The governing equations applied in the solver are the continuity equation (1) and momentum equation (2):

$$\nabla \cdot U = 0 \tag{1}$$

$$\frac{\partial \rho U}{\partial t} + \nabla \cdot (\rho U U) = -\nabla p^* - g \cdot h \nabla \rho + F_S + \nabla \cdot (\mu \nabla U) + (\nabla U) \cdot \mu \tag{2}$$

where μ is dynamic viscosity, p^* is the dynamic pressure, g is acceleration of gravity, ρ is density, U is velocity vector and h is hydrostatic height of the fluid. Hence, first term in the right hand side represents dynamic pressure and second term hydrostatic pressure. F_S is the source momentum of surface tension, which is expressed as;

$$F_S = \sigma \kappa \nabla \alpha \tag{3}$$

where σ represents the surface tension coefficient, κ is the surface curvature and α is volume fraction which is bounded in $0 \le \alpha \le 1$ (0 for air and 1 for water). Surface curvature can be modelled as the boundary condition of wall surfaces by setting the contact angle. In this simulation, surface tension between the interface and walls are neglected because the effect from surface tension is not significant.

To capture the sharp free surface where α is between 0 and 1 from VOF method, OpenFOAM adopts artificial compression velocity (w) to the transport equation of α:

$$\frac{\partial \alpha}{\partial t} + \nabla \cdot (U\alpha) + \nabla \cdot \{w\alpha(1-\alpha)\} = 0 \tag{4}$$

The artificial compression does not affect the solution when the volume fraction is either 0 or 1 so that it can be used for the free surface compression.

For the turbulence model, *k-ω* SST has been chosen because it is proven in many of marine applications and in the most of past CFD studies in state of the art review by Wang *et al.* (2010), Zou *et al.* (2011) and Mehdi *et al.* (2013).

The coordinate system to describe settings and forces/moments of the simulation is defined as body fixed and right handed system and that is different from the experiment. The origin is located at the amidships, centreline and keel for x, y and z, respectively. Longitudinal axis (x) is towards the bow, transverse axis (y) towards port side and vertical axis (z) upwards. Therefore, positive sway force directs to the outside the bank and yaw moment is positive when the bow is away and the stern towards the bank (Figure 1). The negative heading angle of the case A means that bow of the ship is toward the bank and the stern is away from the bank.

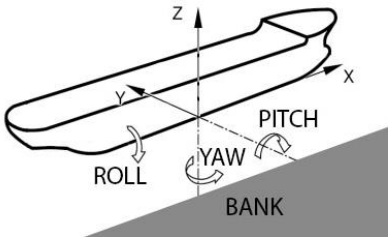

Figure 1: Coordinate system of the CFD simulations

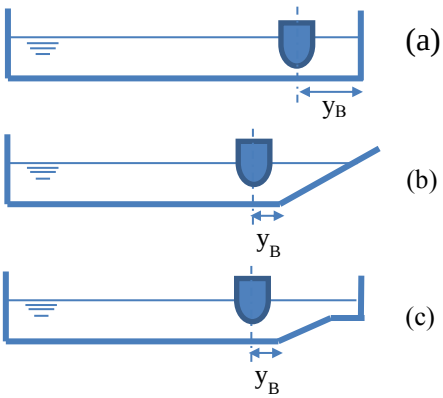

Figure 2: The types of the bank

As can be seen in Figure 2, three types of the banks were used. The arrangement (a) has a straight vertical bank wall. The bank type (b) has an inclined bank wall and type (c) has a bank wall that is inclined and submerged. All three types have 7 meters width.

Three cases were chosen among the experiment results for CFD simulations. Table 2 includes the details of the case arrangements. Under keel clearance from 10% to 100% of the draught and various lateral position of the ship from the bank are included in the test cases. The test cases without propeller thrust have been chosen firstly to see the bank effect merely from asymmetric flow field. If propeller is rotating, it may affect the force and the moment values. In these test cases, propeller was prevented from rotating and there was no thrust. The trim and the sinkage of the ship were not taken into account in the simulation.

Table 2: Test cases without propeller thrust

Test cases		A	F	H
Under keel clearance	[%]	100	100	10
Draught	[m]	0.180	0.180	0.149
Water depth	[m]	0.360	0.360	0.163
Forward component of speed vector	[m/s]	0.6842	0.8012	0.4578
Transverse component of speed vector	[m/s]	-0.0599	0.0	0.0
Lateral separation (Y_B)	[m]	0.265	1.435	1.965
Heading angle	[deg]	-5.0	0.0	0.0
Propeller rate	[rpm]	-1	-1	-1
Propeller thrust	[N]	-1.10	-0.93	-0.37
Propeller torque	[Nmm]	-27.09	0.84	7.28
Type of bank	-	(b)	(b)	(a)
Bank inclination		8:1	3:1	1

The case A has slight heading angle with small separation from the bank wall. The case F does not have extreme clearance from the bank wall or the bank bottom, however, the velocity of the ship is relatively high. The case H has very small under keel clearance but moderate distance to the bank wall. Figure 3 is the graphical view of simulations cases without propeller thrust, A, F and H (looking from the forward).

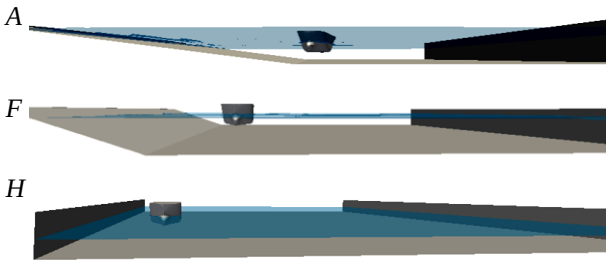

Figure 3: Graphical view of simulation cases

There is a need to understand the contribution of propeller to the bank effect. Although propeller rotation is not modelled in this study, another set of simulations has been compared with the test cases with propeller thrust but without modelling the propeller or thrust in the simulations. This means the ship is simply towed in the simulations to achieve the velocity of the ships but the propeller thrusts and rotations are not modelled. This will indicate the significance of propeller contribution to the bank effect. The purpose of this set of simulations is not to validate the CFD results with the experiment results but to see the contribution of propeller thrust assuming the hypothesis of CFD is realistic enough. They will show the difference as much as propeller rotation contributes to the bank. Table 3 is the detailed experiment conditions of the set of test cases with propeller thrust. The propeller is not modelled in the simulations, hence, propeller thrust is not applied.

Table 3: Test cases with propeller thrust

Test cases		D	I	J
Under keel clearance	[%]	100	35	100
Draught	[m]	0.149	0.149	0.149
Water depth	[m]	0.297	0.200	0.297
Forward component of speed vector	[m/s]	0.6868	0.5723	0.8012
Transverse component of speed vector	[m/s]	0.0	0.0	0.0
Lateral separation	[m]	1.340	0.565	0.530
Heading angle	[°]	0.0	0.0	0.0
Propeller rate	[rpm]	540	359	539
Propeller thrust	[N]	3.30	1.46	3.16
Propeller torque	[Nmm]	53.78	20.65	62.35
Type of bank	-	(b)	(c)	(c)
Bank inclination		8:1	8:1	5:1

2.2 SIMULATION MODELLING

Efforts were made to model the mesh finer and prism boundary layers properly because having a certain number of mesh layers would be important in the narrow gap between the bank and the ship as well as in the under keel clearance. The OpenFOAM mesher was prone to fail to generate more than three layers especially on the surface with the big curvature of the hull. The number of the mesh are 0.8~1.4 million for all the cases. The computation domain has been modelled up to the deck height of the ship, however, the deck height is slightly extended to have enough area in the air domain. After some testings, it was found that the freeboard height is sufficient to cover the air domain because the confined water cases have relatively slow speeds.

The mesh size was carefully determined from separate grid independence test in open sea without bank. It was because usual grid dependence tests for the confined water cases were limited due to the small gaps between the hull and the bank. Too fine mesh at the hull surface was not appropriate because it caused y+ value too small, thus compromising between the cell sizes next to the hull surface and the y+ value was important for proper modelling of the narrow gap. The meshes were modelled in such a way that y+ values ranged between 30 and 300 on all the area of the hull surface except the case H due to the narrow gap between the hull and the bank. The more details about the case H will be discussed later. The mesh generation of the single-phase simulations is basically equal to those used for two-phase solver below the water level.

As for the boundary conditions, a fixed value is applied at the inlet for velocity and turbulence properties. At the outlet, zero gradient is applied for velocity and turbulence properties. No slip condition is applied to the hull surface. For the velocity at the bank boundary, the same fixed value with the inlet velocity was used so that no-slip condition can be applied on the bank wall. This is reasonable for no-slip condition on the bank wall of body fixed coordinate system because the point of view is on the ship, and undisturbed water and the bank should have the same velocity. Wall function is applied for k and ω on the ship and the bank wall.

For the single-phase solver, a slip condition is used for the velocity on the top which is free surface level.

3. COMPUTATIONAL RESULT

The numerical results of two-phase solver showed that pressure component dominates over the viscosity with large oscillations. It is presumed that the oscillation is caused from the interaction between the bank and the ship because such oscillation did not appear when the simulation is carried out in open water (using the same settings but in deep water without banks) in spite of relatively slow speed. Even the resistance in x direction revealed much bigger oscillating behaviour compare to the simulation in open water. Reducing Courant number was also helpful to suppress the oscillation. The average was taken for capturing force and moment values after substantial calculations.

A single-phase steady-state solver *simpleFoam* was tested to compare the result from *interFoam* which is a VOF transient solver. Table 4 is the comparison table of forces and moments between the CFD results and the experiment (Lataire *et al.*, 2009). Comparing the different gradient schemes having 2nd order accuracy, least square generally showed slightly better results compared to Gauss linear. Therefore, the results from least square scheme were presented. *simpleFoam* also allowed good accuracy although they were single-phase simulations without free surface. Least square method also allowed better accuracy for single-phase calculations.

3.1 RESULT SUMMARY

Case A: The two-phase solver over-predicted the Fx and Fy values by 17.8% and 9.8% respectively, but yaw moment suggested good accuracy with 1.4% error. The single-phase solver also showed good accuracy compared to the experiment.

Case F: The two-phase solution gave the good accuracy for longitudinal force and yaw moment, however, sway force was under-predicted by 39%. Single-phase solver predicted better sway force but not for other values.

Table 4: Comparison of the 3 cases (A, F, H) to the experimental results without thrust (Lataire *et al.*, 2009)

Solver	Force /Moment	A	F	H
interFoam (VoF)	Fx(N)	4.866	5.512	2.239
	Fy(N)	-5.646	-1.008	1.963
	Mz(Nm)	-9.067	1.305	5.561
simpleFoam (single-phase)	Fx(N)	3.922	3.794	1.880
	Fy(N)	-5.343	-1.300	1.245
	Mz(Nm)	-8.665	1.053	4.017
EXP	Fx(N)	4.130	5.354	2.935
	Fy(N)	-5.139	-1.648	2.545
	Mz(Nm)	-8.939	1.804	6.959

Case H: This case has small under keel clearance which is 10% of water draught, but the separation from the bank wall is however, not small. Unlike the other cases in which the difference was insignificant between two and many prism boundary layers applied near the ship, all the values were under-predicted in this case when two prism layers were used. The details will be discussed in the next section. The values presented in Table 4 were of the

refined mesh with 8 prism boundary layers. Fx represents resistance, Fy sway force and Mz yaw moment.

3.2 UNDER KEEL SPACE MODELLING OF THE CASE H

Because of small under keel clearance of the case H, it was hard to model the mesh in the narrow space properly. If many layers are modelled in the under keel space, y+ values become too low, i.e. below 30. In that case, the wall function may not be valid. To keep y+ values bigger than 30, the optimum number of layer in the under keel clearance had to be only about two or three in the case H. The small under keel clearance is known to affect the bank effect significantly, therefore, too few number of layers in the under keel would not be enough to capture the effect. In this case, the best way would be to model y+ values less than 1 throughout the hull surface and resolve the whole boundary layer without using wall functions. However, this was not successful by the OpenFOAM mesher.

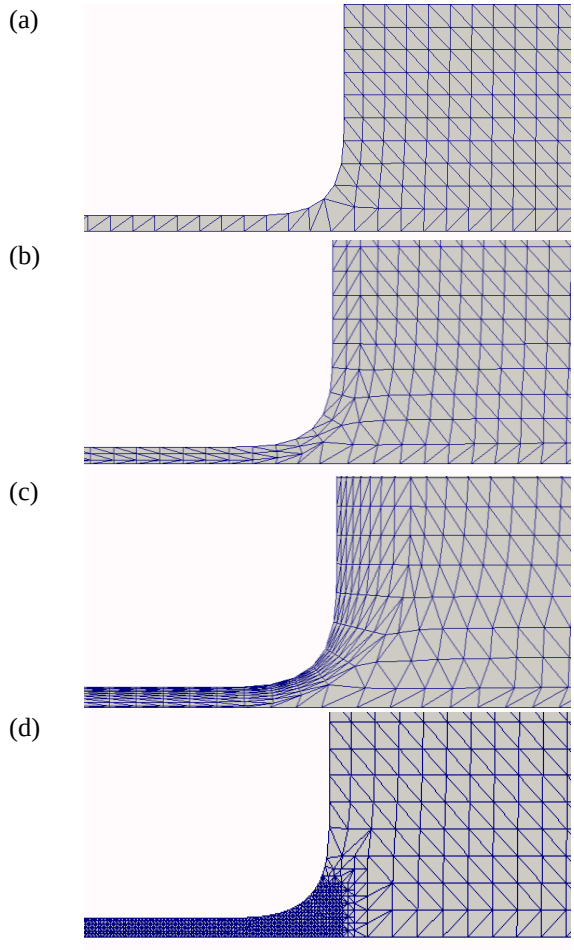

Figure 4: Different meshing of case H with no layer (a), two prism layers (b), eight layers (c) and fine mesh (d)

To compromise between the number of mesh layers and valid y+ value for the wall function in the under keel space, a comparison has been made. Four different meshes are tested for the case H. They have same mesh size in other areas but different size in boundary layers or in the under keel space. The tested meshes are shown in Figure 4 as the midship sections near the bilge radius are zoomed in.

Type (a) has no specific modelling for the prism boundary layer, (b) has two prism boundary layers and total three layers in the under keel, (c) has eight prism boundary layers and total nine in the under keel, and (d) has very fine refinement in the under keel clearance without modelling overall boundary layer. The (b) type meshing shows good y+ distribution to use wall function. Figure 4 illustrates y+ distribution near the bilge keel area for each of the four meshing type.

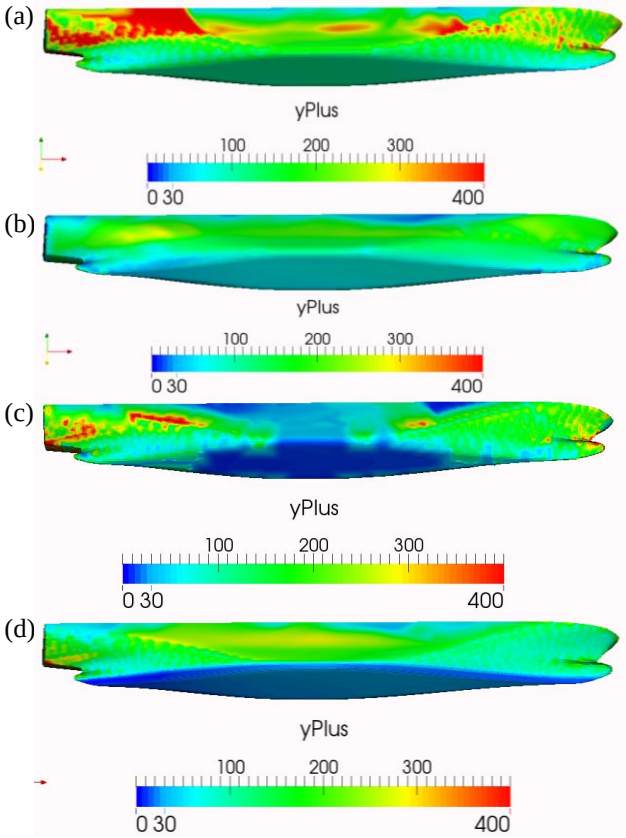

Figure 5: y+ distribution of the case H with different meshing in the underkeel - no layer (a), two prism layers (b), eight layers (c) and fine mesh in the under keel(d)

Type (a) and (b) have y+ values above 30 and all are in good range. OpenFOAM mesher has problem when many prism layers have to be created at the boundary layer especially at large curvature. For this reason, it failed to generate complete eight prism layers at fore and aft area of (c) where curvature appears. However, expected number of prism layers has been created in the boundary layer near the parallel middle body where under keel clearance is most significant. This is clearly shown in Figure 5. In (d), very fine mesh was used only in the underkeel space, hence, very low y+ distribution can be seen on the bottom hull surface. Since majority of area was still modelled with y+ value above 10 for (d), wall function is applied to all four cases.

Table 5 is the forces and moments from different boundary layer modelling. The (c) type meshing showed the best accuracy in spite of low y+ distribution at the bottom of the hull. Therefore, it is important to model enough number of prism layers in the under keel clearance to capture the bank effect. Enough number of prism layers at the boundary layer was the most effective modelling. Moveover, the result suggests the importance of under keel clearance modelling. Because (d) shows much better accuracy of sway force than (a), although they have similar cell size at the side wall of the ship.

Table 5: Results with different boundary layer modelling

	(a)	(b)	(c)	(d)	EXP
No. of mesh (mil.)	1.11	1.13	1.15	5.21	-
Fx (N)	1.484	2.239	2.236	2.247	2.935
Fy (N)	0.368	1.104	1.963	1.037	2.545
Mz (Nm)	4.004	3.734	5.561	3.647	6.959

3.3 COMPARISON OF THE CASES WITH PROPELLER THRUST

Table 6 is the comparison results of the cases (D, I and J) with propeller thrust. Sway forces and yaw moments are compared with the experimental results.

As can be seen in the comparison, when the propeller rotations are not modelled, all the sway forces are under predicted compared to the experiment result. The directions of the sway forces were mostly correct but the magnitudes were all under-estimated. When the ship was towed without propeller thrust in both the simulations and the experiments, the deviation between them was 10%-40%, however, the cases with propeller thrust show at least 2.5 times bigger in suction of sway force than the simulations where the ships were simply towed without propeller thrust. This ascertains propeller loading causes more suction force (Li et al., 2001). Moreover, for the cases with propeller thrust, sway forces were all in suction direction to the bank wall. This is in line with the fact that the propeller rotation either affects the magnitude of sway force or causes suction in sway force (Lataire *et al.*, 2009). However, further comparison of these cases are not reliable but would become speculation, hence, it is not meaningful to discuss further and more study is required to confirm the capability of CFD and the propeller effect. Another limitation is that propeller rotation and the bank locations are all in the same direction in these cases. The predicted yaw moment values indicated reasonable accuracy with the VoF solver even without modelling propeller. For these cases, Gauss linear method provided relatively better results than least square method for both sway force and yaw moment. Single-phase solver showed poor accuracy even for yaw moments.

Table 6: Comparison of the cases (D, I, J) with thrust to the experimental results (Lataire *et al.*, 2009)

Solver	Force /Moment	D	I	J
interFoam (VoF)	Fy (N)	-2.011	-0.201	-0.894
	Mz (Nm)	19.280	9.750	2.169
simpleFoam (single-phase)	Fy (N)	-2.683	-1.080	-1.427
	Mz (Nm)	4.692	1.960	1.688
EXP	Fy (N)	-8.056	-3.682	-2.264
	Mz (Nm)	16.407	8.312	2.065

3.4 FREE SURFACE ELEVATION

Free surface elevations were compared with the experimental results. It was measured at three points of the cases F, I and J which are the same in the simulations and the experiments. Table 7 displays the locations of the wave gauges from the centreline of the ship according to the experiment. Wave gauges measure the wave elevation at the defined transverse distances from the centreline of the ship. Figure 6, Figure 7 and Figure 8 are the comparisons of wave elevation with the model test measurement.

Table 7: The locations (m) of the wave gauges with reference to the centreline of the ship (Lataire *et al.*, 2009)

	Gauge 1	*Gauge 2*	*Gauge 3*
Case F	*0.475*	*1.005*	*1.535*
Case I	*0.875*	*1.215*	*2.115*
Case J	*0.920*	*1.320*	*1.785*

The simulations captured the free surface elevation in confined water with reasonable accuracy. The further wave gauges from the ship showed less accuracy of the wave elevation. A steep wave is observed in the case I and it is continued from the hull to the bank wall. This was also found in the experiment but over-predicted in the simulation result at the gauges 1 and 2. In addition, phase delay was observed, especially at the furthest wave gauge from the ship, i.e. wave gauge 3. This phase delay was also found at the gauge 3 of the case F. The phase of wave trough was deviated by about a quarter of trough length. The case J showed relatively good accuracy, however, reason was not found for the better accuracy of the case J compared to the case F and I in terms of the bank arrangement and speed. As the CFD solvers used in these simulations are known to capture free surface elevation quite accurately, the difference in these comparisons is presumed to arise from the under-predicted bank effect that causes asymmetric flow field.

Lastly, the computations did not capture the oscillation of the wave elevation correctly. The experiment showed more oscillation but this was not captured or captured differently in the simulated results.

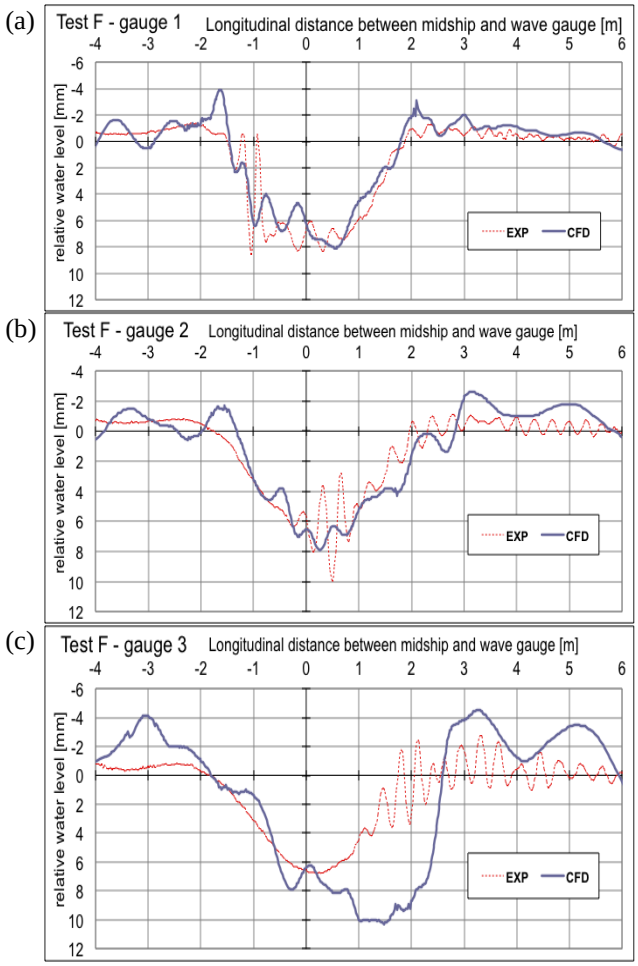

Figure 6: Wave elevation of the case F at (a) gauge 1, (b) gauge 2 and (c) gauge 3 (Lataire *et al.*, 2009)

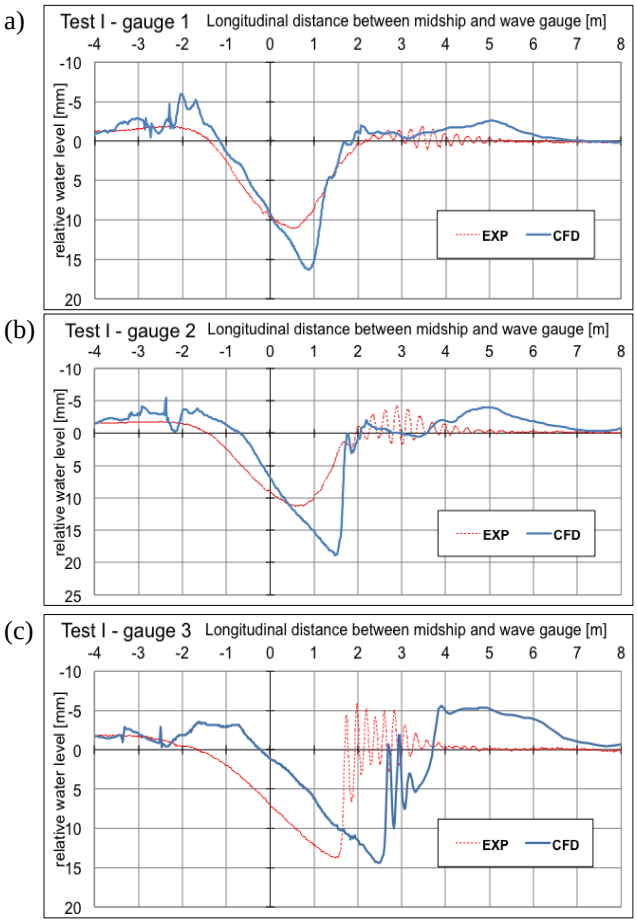

Figure 7: Wave elevation of the case I at (a) gauge 1, (b) gauge 2 and (c) gauge 3 (Lataire *et al.*, 2009)

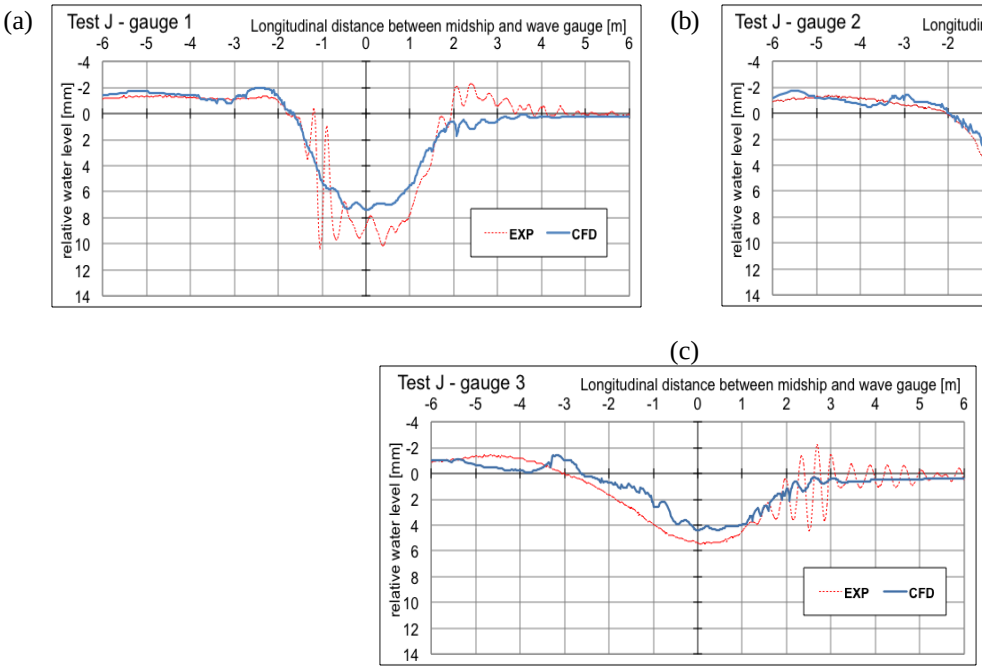

Figure 8: Wave elevation of the case J at (a) gauge 1, (b) gauge 2 and (c) gauge 3 (Lataire *et al.*, 2009)

4. CONCLUSIONS

In this study, flow around a ship in confined water with several bank arrangements was computed by incompressible RANS solvers of OpenFOAM. The results from single-phase and two-phase solver were compared to the experiment result. The hydrodynamic forces and moments due to the bank effect, and wave elevation in confined water were compared to the experimental results. Under keel clearance modelling was evaluated and suggested to compromise between mesh fineness and y+ distribution.

CFD analysis was good in qualitative prediction of the forces and the moment from bank effect. However, the computation tended to under-predict forces and moment for most of cases. This is most obvious in sway force. These can be led to several reasons. Firstly, there is limitation of meshing in the narrow gap. One thing can be tried is resolving whole boundary layer by modelling y+ below 1. However, this requires huge computational cost and is hard to achieve with the OpenFOAM mesher. Secondly, fixed heave and pitch motion of CFD calculations could have caused this under-prediction because the two motions were free in the model tests. This assumption of fixed motion neglects squat effect, therefore, better accuracy can be expected if the 2 DOF motions are allowed. However, mesh motion with fine mesh and small keel clearance is a big challenge.

The under-prediction of sway force was more obvious in the cases with propeller rotation although yaw moments were predicted with reasonable accuracy. This explains what experimental study discovered (Li *et al.*, 2001) on how propeller rotation affects the sway force. More study is needed to see whether propeller intervention causes additional sway force to specific direction or affects magnitude of sway force. In this set of experiments, all the cases with propeller rotation resulted in suction forces and the computation without propeller modelling predicted the sway forces to the correct direction but in smaller magnitude. From this comparison, it is noted that propeller rotation seems to affect the magnitude of sway forces but does not give significant contribution to yaw moment. Overall, the calculated sway forces and yaw moments from the bank effect are all in correct directions for all the types of bank shapes and arrangement although ship-to-bank interaction is very complex and difficult to predict the directions.

Free surface elevation was captured reasonably well except the difference in the wave phase. Such a phase delay was more obvious in the case where the water depth is shallow. Less oscillation on the free surface level was observed in the computation than the experimental result. However, from the comparison between the single phase and two phase simulations free surface effect does not give significant contribution. There was no clear improvement of the accuracy of forces and moment in the bank effect prediction by adding free surface in the CFD simulation. Therefore, single phase solver which is faster and more stable can be useful solution to predict bank effect.

Unfortunately, the experiment results open to the public were only available to limited cases, therefore, systematic parametric study was not possible.

5. REFERENCES

1. LATAIRE, E., VANTORRE, M., LAFORCE, E., ELOOT, K. and DELEFORTRIE G., *Navigation in Confined Waters: Influence of Bank Characteristics on Ship-Bank Interaction*, International Conference on Ship Manoeuvring in Shallow and Confined Water, page 135~143, Antwerp, Belgium, 2007
2. LATAIRE, E., VANTORRE, M. and ELOOT, K., *Systematic Model Tests on Ship–Bank Interaction Effects*, International Conference on Ship Manoeuvring in Shallow and Confined Water: Bank Effect, Antwerp, Belgium, 2009
3. LEE, K. and LEE, S. G., *Investigation of ship maneuvering with hydrodynamic effects between ship and bank*, Journal of Mechanical Science and Technology, No. 22, page 1230~1236, 2008
4. LI, Q., LEER-ANDERSEN, M., OTTOSSON, P. and TRÄGÅRDH, P., *Experimental Investigation of Bank Effects Under Extreme Conditions*, Proceeding of PRADS 2001, page 541-546, Shanghai, China, 2001
5. LO, C., SU, DONG-TAUR and LIN, I-FU, *Applying Computational Fluid Dynamics to Simulate Bank Effects*, 19th International Offshore and Polar Engineering Conference, page 466~471, Osaka, Japan, 2009
6. MIAO, Q., and XIA, J., *Numerical Study of Bank Effect on a Ship Traveling in a Channel*, The 8th International Conference on Numerical Ship Hydrodynamics, Busan, Korea, 2003
7. NAKISA, M., MAIMUN, A., YASSER M. AHMED, SIAN, A.Y., PRIYANTO, A., BEHROUZI, JASWARAMD F., *RANS Simulation of the Viscous Flow around Hull of LNG Ship in Confined Water*, 15th Mathematical and Computational Methods in Science and Engineering, page 133~137, Kuala Lumpur, Malaysia, 2013
8. NORRBIN, *Bank Effect on a Ship Moving through a Short Dredged Channel*, Proceedings of 10th Symposium on Naval Hydrodynamics, page 71~88, Cambridge, MA, USA, 1974
9. PARK, D. W., CHOI, H. J. and PAIK, K. J., *Bank Effect of a Ship Operating in a Shallow Water and Channel*, Journal of Navigation and Port, Volume 38, No. 1, page 19~27, 2014
10. RUSCHE, H., *Computational Fluid Dynamics of Dispersed Two-phase Flows at High Phase*

Fractions, PhD thesis, Imperial College, London, 2002

11. VANTORRE, M., and DELEFORTRIE, G., *Experimental Investigation of Ship-Bank Interaction Forces*, Proceeding of International Conference on Marine Simulation and Ship Manoeuvrability, MARSIM'03, page RC-31-1~9, Kanazawa, Japan, 2003
12. WANG, H., ZOU, Z., XIE, Y., and KONG, W., *Numerical Study of Viscous Hydrodynamic Forces on a Ship Navigating near Bank in Shallow Water*, Proceedings of the 20th International Offshore and Polar Engineering Conference, page 523~528, Beijing, China, 2010
13. ZOU L., LARSSON, L., DELEFORTRIE, G. and LATAIRE, E., *CFD Prediction and Validation of Ship-bank Interaction in a Canal*, 2nd International Conference on Ship Manoeuvring in Shallow and Confined Water: Ship to Ship Interaction, May 18-20, Trondheim, Norway, 2011

MANAGING INTERNATIONAL COLLABORATIVE RESEARCH BETWEEN ACADEMICS, INDUSTRIES, AND POLICY MAKERS IN UNDERSTANDING THE EFFECTS OF BIOFOULING IN SHIP HULL TURBULENT BOUNDARY LAYERS

(DOI No: 10.3940/rina.ijme.2016.a3.428)

B Nugroho and **B Ganapathisubramani**, University of Southampton, UK, **I K A P Utama** and **I K Suastika**, Institut Teknologi Sepuluh Nopember (ITS), Indonesia, **F A Prasetyo**, PT Biro Klasifikasi Indonesia (Persero), Indonesia, **M Yusuf**, PT Dharma Lautan Utama (DLU), Indonesia, **M Tullberg**, Hempel A/S, Denmark, **J P Monty** and **N Hutchins**, University of Melbourne, Australia

SUMMARY

This report documents a large scale joint research project with the aim of improving the efficiency of ship operations and management by providing a methodology and technology that can quantify the emission and fuel usage penalty due to bio-fouling on ship hull. This can be obtained through better understanding of turbulent boundary layer flows over rough surfaces that cause skin friction drag. Here six different institutions from four countries (Australia, Denmark, Indonesia, and UK) that consist of universities, a passenger ship company, a manufacturer of anti-fouling coatings, and the Indonesian Classification Society are formed. They represent three fields, namely: academic, industrial, and an independent party that supports policy makers. Each of them has different objectives and interests that are interconnected. The research collaboration uses an *in-situ* laser-based measurement technique of the water flow over the hull of an operating ship combined with under-water image-based surface scanning techniques. The shipboard experiments are accompanied by detailed laboratory experiments to provide further validation. This paper will discuss the importance and challenges of managing such collaboration and the significance of satisfying individual objectives from each three fields in order to achieve the overarching aim.

NOMENCLATURE

[Symbol]	[Definition] [(unit)]
v	Kinematic viscosity (N s m^{-2})
ρ	Density of water (kg m^{-3})
U	Mean velocity (m s^{-1})
U_τ	Skin friction velocity (m s^{-1})
L	Characteristic length scale (m)
δ	Boundary layer thickness (m)
k	Roughness height (m)
k_s	Sand grain equivalent roughness height (m)
k_a	Average roughness height (m)
e	Roughness offset (m)
z	Wall normal distance (m)
ES_x	Effective slope

1. INTRODUCTION

There are approximately more than 100,000 ships (including cargo, military, tanker, and passengers) operating worldwide, together consuming around 200 – 300 million metric tons of fuel per year (Corbett et al 1999, Erying *et al*, 2010). To put it into perspective, this is equivalent to 5% - 8% of world's oil production in 2015. Much of the oil that is consumed by these ships is low grade and contains harmful materials such as: sulphur, asphaltenes, leads, various metals, and ash (Corbett *et al*, 1999, Winebrake *et al*, 2009). When this type of oil is fed into a ship's internal combustion engine, its by-product is gas emission that contains particulate matter (PM), sulphur oxides (SOx), nitrogen oxides (NOx), black carbon (BC), carbon dioxide (CO_2), carbon monoxide (CO), and other harmful properties. The air pollution from ship-related emission has direct impact to human's health and well-being. Recent studies indicate that around 60,000 – 90,000 premature death annually are caused by shipping air pollution, particularly at the coastal area of Europe, East Asia, and South Asia (Corbett *et al*, 2007, Winebrake *et al*, 2009). Further studies by Erying *et al*, (2010) show that aerosol pollution and their derivative species from ships combustion can be transported high in the atmosphere and carried further inland by airstreams, resulting in increased pollution in locations that are far from coastal areas. Therefore, the exact number of mortality caused by ships emission may be even higher. Furthermore, many studies also show that the global shipping industries contribute towards climate change. Hence this industry has a large economic, environmental, and health footprint (see Erying *et al* 2010 and Miola and Ciuffo 2011 for recent reviews on ship impacts on climate).

The issue of health, global warming, and energy crisis have prompted efforts by policy makers, academics, and industries representative to find new ways to reduce energy consumption in the shipping industries (Davies, 2006; Longva *et al*., 2010, Molland *et al*. 2014). This is particularly crucial for countries that rely heavily on ships, such as archipelagic countries (Indonesia, Japan, Malaysia, Philippines, UK, Pacific nations), and countries that are geographically isolated from major trading partners (Australia, New Zealand). From the listed countries, it is clear that the issue affects both developing and developed countries. This is even more important for countries that subsidise fossil fuel. A recent report by Coady *et al* (2015) from the IMF (International

Monetary Fund) reveals that global petroleum subsidies amount to $1.6 trillion (2.2 percent of global GDP) in 2013. Many marine dependant developing countries such as Indonesia provide subsidies for passenger ships and ferries. Such subsidiaries burden the country's budget and slow the growth of other infrastructure.

Hull roughness due to biofouling (marine organisms that settle on the ship's hull) is an important, but largely unquantifiable contributor to the overall energy expenditure, emissions, and pollution from the shipping industry. Many studies have shown that biofouling contributes significantly to the ship's overall drag resulting in excess use of fuel to propel the ship forward (see Schultz *et al* (2004, 2007, 2011) and Monty *et al* (2016) for recent studies). Unfortunately, currently there are no reliable techniques that allow ship owners and operators to quantify a ship's drag penalty due to biofouling accurately.

In an effort to understand the skin friction drag on ship hulls due to biofouling and to improve the efficiency of ship operations by providing a methodology and technology that can accurately quantify the emission and fuel usage penalty, a large-scale research collaboration is currently underway. The research involves an in-situ laser-based measurement of the water flow over the hull of a ship coupled with a detailed under-water image-based surface scanning techniques. These techniques allow direct measurement of the increase in drag experienced by the ship under different fouling conditions. The two novel shipboard experiments are accompanied by detailed laboratory investigation to provide further validation. The outcome of the study will allow policy makers and ship industries to make more informed decisions in terms of operations at operational or regulatory level.

The project involves six institutions from four different countries, namely: Institute of Technology Sepuluh Nopember, Biro Klasifikasi Indonesia (Indonesian classification society), and Dharma Lautan Utama passenger ship company from Indonesia; the University of Melbourne from Australia; the University of Southampton from the United Kingdom (UK); and Hempel A/S an anti-fouling paint company from Denmark.

In general the six institutions can be categorized into *three major fields*, namely: academic, industry, and classification society to support policy maker. Each of these three fields has different interests and expected outcomes that form the base of the overall main objective of the research collaboration. To accomplish the challenging objectives, the six different participants need to collaborate closely and effectively, particularly because each of them has a different role and unique set of expertise for the project.

In this paper, we discuss the importance of collaborative research in tackling biofouling, which is one of the most challenging issues in the shipping industry. This includes the motives and details of the joint research, the role of each institution, the expected outcome or results from individual fields, and how these individual field's objectives are correlated and satisfied to achieve the overarching goal. This paper will also discuss some challenges that we have experienced. Note that the current report is based on, and also serves as an extension of our recent conference paper (Utama *et al*, 2016) that was presented at the RINA International Conference on the Education and Professional Development of Engineers in the Maritime Industry (Singapore 20-21 September 2016).

2. RESEARCH GROUP FORMATION AND ROLE

Research collaboration is an essential part of any modern scientific endeavour, particularly for complex and large-scale projects. With the ever increasing cost of scientific apparatus and materials, lower cost of travel and communication (internet and telephone), and the need for division of work in interdisciplinary research, it is only natural that many scientists resort to collaboration, both nationally or internationally (Katz and Martin, 1997; Subramanyam, 1982; Melin and Persson, 1996). Our proposed research project requires a large quantity of resources such as: lab facilities, field experiment equipment, travel funds, and personnel salary. To the best of our knowledge there have not been many attempts for this type of research. One such study is by Lewthwaite *et al*. (1984) where it also involved several different institutions. Learning from their previous experience, we have assembled a likeminded group of institutions to tackle the issue of biofouling.

The large scale research collaboration is initiated by the University of Melbourne and Institute of Technology Sepuluh Nopember (ITS), in response to the newly formed Australian-Indonesian Centre (AIC) program aimed to strengthen collaboration between Australian and Indonesian universities. The University of Melbourne approached ITS in the late 2014 to propose novel boundary layer study that involves access to an operational ship. The research idea has been formulated by academics in Melbourne over the last decades or so, however the difficulty in obtaining access to an operational ship in Australia hindered realisation of the concept. From several formal and informal meetings between the academics from the University of Melbourne and ITS, a collaboration plan finally materialized.

For this research, the University of Melbourne is responsible for the management of the overall research plan and contributes in the form of field research equipment, such as the LDA, surface scanner, and other supporting research apparatus. Furthermore, the University has a very strong fluid mechanics background and extensive laboratory facilities, therefore it is an ideal place for the laboratory experiment. The relatively short

distance between Indonesia and Australia is another reason for the University of Melbourne to host the laboratory experiment.

As one of Indonesia's leading marine research universities, ITS has a very strong marine faculty and is well-linked to various Indonesian marine intuitions (both in industry and government). The main role of ITS is to host the field experiment and use their extensive contacts in the Indonesian maritime industry to assist with the import of various scientific apparatus from overseas, and liaise with local government representatives. The university is also responsible in providing Masters and final year Undergraduate students to assist in this project.

With its strong alumni connection, ITS has invited PT Dharma Lautan Utama (DLU), an Indonesian passenger ship and ferry company, to be involved in the research project. PT DLU is one of the largest passenger ship operator companies in Indonesia and is actively involved in many ITS activities. The company has agreed to lend the all-important ship as test bed. The ship is a RO/RO passenger ferry called Dharma Kencana IX (figure 1) that serves between Merak (Java island) and Bakaehuni (Sumatra island), Indonesia's busiest lines. The two islands are the most densely populated in Indonesia (note that Indonesia is the 4th largest country in the world in term of population - approximately 250 million people).

Figure 1 : Dharma Kencana IX ferry from PT Dharma Lautan Utama (PT DLU)

Field experiments in an operational ship pose certain risks, particularly for our proposed experiment where there will be an optical access at the bottom of ship. Therefore, to ensure the safety of the scientists (and ship) for the entire duration of the investigation, ITS has invited Biro Klasifikasi Indonesia (BKI), Indonesian classification society, to be part of the research team. BKI is a recognized organization by the Indonesian Government that is tasked to classify any Indonesian flagged marine transport both domestic and international that operates in Indonesian water and/or world wide voyage [DJPL, 2016]. BKI assist the research collaboration via technical evaluation regarding ship design, building, reconstruction, maintenance, modification, and other dry-docking activities as well as periodical survey, in accordance with BKI technical standards (rules and regulations).

The field experiment involves a laser-based velocity measurement (laser Doppler anemometery). Two crossed lasers shine through an optical access on the bottom of the hull and measure the velocity gradient in the turbulent boundary layer formed over the ships hull. Because such method is novel and un-proven it requires repeated test under constant environment, i.e. constant hull condition over a period of time. Therefore, the University of Melbourne invited Hempel A/S, a multinational antifouling company to be part of the research collaboration. They contribute in the form of antifouling paint that is applied on the hull of Dharma Kencana IX during dry docking when the hull is in clean state. The paint allows the ship hull to remain clean for longer period of time permitting the field researchers to test the LDA during the initial stages of this project.

Although the University of Melbourne and ITS have secured the necessary lab and field facilities and equipment, they still lacked the necessary personnel to perform the experiments and guide the ITS Undergraduate and Masters students. Therefore, the two universities invited the University of Southampton as part of the research team. ITS and the University of Southampton have a long history in academic cooperation, particularly in naval research. Many senior ITS academics have received higher education from the University of Southampton. Furthermore, the University of Melbourne and the University of Southampton have previously performed similar collaborative laboratory experiments, where they scanned a sample of tubeworm type fouling and characterised the drag using a wind tunnel (see Monty *et al*, 2016).

In early 2015 ITS and the University of Southampton secured funding from the British Council via the Newton Fund program, leveraging the previous subsidy from the Australian-Indonesian Centre. This cooperation also acts as a realisation of the cooperation between the government of Indonesia and UK that was signed on 1st November 2012 at 10 Downing St, London, and witnessed by the then Indonesian President and The Prime Minister of England. This funding allows the University of Southampton to recruit a Postdoctoral research fellow (Post-doc) to perform the field and laboratory experiment, and train the Undergraduate and Masters students from ITS.

There are two crucial lessons arising from the research group formation. The first is the importance of networking, where it allows scientists to learn about each other's research, facilities, etc, particularly in many different channels/levels. Without proper networking, such large international research would not materialize. The second is inter-government cooperation. Without close relationship between the Indonesian-Australian and Indonesian-UK governments, such funding would not exist. It is an evidence that proper international relationship and policy between governments can influence the more grass root level, i.e. people-to-people engagement.

3. CORRELATION BETWEEN INDIVIDUAL FIELD OBJECTIVES

From the previous section it is clear that this research project involves many different institutions that can be grouped into three different fields. Each of these fields has their own individual objectives that together form the overarching goal. The challenge for this collaboration is to satisfy each field's individual objective without sacrificing the overall goal. This section will discuss each individual field's objective and how they correlate with each other.

3.1 ACADEMIC FIELD OBJECTIVES

The three academic institutions: ITS, the University of Melbourne, and the University of Southampton have two main objectives, the first is to obtain further understanding about turbulent boundary layer flows over rough surfaces that cause skin friction drag. The expected outcome from the project is a database with high research value. These results will be published in peer-reviewed journals and conference papers, allowing the three academic institutions to communicate their results to the scientific communities and wider audiences.

Figure 2: One of ITS Masters student examining fouled ship hull

The second objective is to educate and train higher degree students via this international research. The University of Melbourne uses this research opportunity to construct a capstone/final year project for Master students. The project is to perform an initial study and design for the image based surface scanner, allowing the students to learn digital image reconstruction techniques. The project also serves as an initial study for the Postdocs from the University of Southampton to continue and expand. These objectives are similar with Bruneel *et al* (2010) and Dasgupta and David's (1994) arguments that university is mostly driven with scientific and academic excellence.

For ITS, the funding from AIC and Newton fund is particularly beneficial. The research collaboration allows their two Masters students to experience international research collaboration and broaden their view. The two students are from the "Pre to Post MSc" program which is funded by the Indonesian Ministry of Research, Technology and Higher Education. Figure 2 shows one of the Masters students examining a fouled ship hull (note that this particular fouled hull is not from our test bed ship). The program is aimed at training and educating high achieving students, that originate from other smaller or younger Universities that are located in the eastern part of Indonesia, at ITS. In developing countries such as Indonesia there is a considerable gap in education quality between different areas. The program is aimed to reduce such gap. The two Master students are expected to return to their respective universities and work as university lecturers. The international collaboration project also paves ways for ITS to allow more Undergraduates and Masters students to be involved, particularly those aiming to continue their study in PhD at The University of Melbourne and The University of Southampton, and expected to return to ITS as lecturers. This is part of the effort by ITS to be a world-class research university. Furthermore, it also strengthens the relationship between the three universities beyond the current joint research.

Finally, for ITS the collaborative project also represents the three core roles for higher education in Indonesia, namely: (1) education and teaching, (2) research and development of science, technology and arts, (3) community service. The three philosophies are more commonly known as TRI DHARMA PERGURUAN TINGGI (Utama and Pribadi, 2011).

3.2 INDUSTRIAL FIELD OBJECTIVES

The two industrial representatives, namely: PT DLU (passenger ship company) and Hempel A/S (manufacturer of antifouling coatings) are from different industries that complement each other. For passenger ship companies such as PT DLU their fixed costs are crew and staff salary, fuel, and maintenance (including dry docking and anti-fouling paint). To improve earnings, many shipping companies require effective and efficient operation management. Fouled hulls are one of the main sources of expenses for PT DLU. Apart from causing excess fuel usage during operations, it forces the ship to undergo a relatively expensive dry docking process, during which it is unable to generate revenues. The passenger ships are required to perform dry docking once a year (DJPL, 2014; BKI, 2016).

For PT DLU, having a more informed decision in terms of operations (particularly related to dry docking) will be economically beneficial. The LDA measurement technique also has the potential to be developed and downsized to be part of the standard sensor suite on a modern ship, providing a constantly updating report on the health of the hull. The surface scanner data when considered together with the LDA results can potentially form a single system to predict a ship's excess fuel usage.

For anti-fouling companies (i.e. Hempel A/S), the prospect of the availability of a workable correlation/equation that allows the hull fouling penalty to be calculated directly from surface scan information is desirable. It provides them information as a basis for the maximum allowed fouling properties (height, effective slopes, sand grain equivalent roughness) over a certain period from their anti-fouling technology. Hence it allows anti-fouling producers to provide more precise information regarding their product performance to their customers.

3.3 POLICYMAKER FIELD OBJECTIVES

Biro Klasifikasi Indonesia (BKI) is an institution that is tasked by the Indonesian Government to classify any Indonesian flagged marine transport that operates both in Indonesian and International waters. The institution has an important role in advising the Indonesian Government regarding various marine safety, environmental protection, and procedures. Various marine rules and codes including docking schedules are governed by BKI and Ministry of Transportation, many of which are also based from the International Maritime Organization (IMO) regulations.

One of the major outcomes from this research collaboration is more detailed information regarding the energy and economic ramifications of a fouled ship hull. Such information can be used by BKI as a scientific basis to review Government policy regarding the management of biofouling treatment procedure. For example, modifying regulations regarding the periodical inspection of antifouling application during scheduled dry docking for passenger ships or other types of ship. The timeline should be based more on the proper calculation of hull roughness condition. Hence it will benefit ship operators that adhere to the regulation of using proper anti-fouling technology and prevent heavily fouled ships from using excess fuel. In short, it would allow more economical and efficient ship operations. This is particularly important for Indonesia because the country is still subsidising fuel for passenger ships and ferries. Such research intensive based policy is difficult to perform in developing countries due to the low national research budget. Hence this research is an excellent opportunity for BKI to implement such research results into policy. Furthermore, the policy can also be submitted internationally through IMO, allowing other IMO member states or flag administrators to study and implement it for their respective countries.

4. TURBULENT BOUNDARY LAYERS

In order to understand the reason behind the proposed research, this section will provide a short background on turbulent boundary layers, particularly over rough surfaces.

As a ship moves through the water, the no-slip condition at the solid boundary will generate a thin region of shear close to the hull boundary where the fluid is pulled along with the ship. The velocity gradients within this region give rise to tangential stresses or skin friction drag which provides a major component of the total drag or resistive force that the ship propulsion systems must overcome. The energy consumption to overcome skin friction drag is relatively costly. For example, for a large ship such as a Very Large Crude Carriers (VLCC) up to 80%-90% of the total drag is due to skin friction (Lackenby, 1962). Hence a large amount (or in many cases the majority) of the fuel which is used to propel the vehicle is expended purely to overcome skin-friction drag. The motions within the thin shear layer, particularly in large engineering applications such as ships, are highly turbulent, hence it is generally described as a turbulent boundary layer. If one considers the large contribution that sea transportation makes to global emissions, it is easy to see that drag from turbulent boundary layers constitutes a very pressing engineering and societal problem.

4.1 REYNOLDS NUMBER

The study of turbulent boundary layers is closely related to Reynolds number,

$$Re = UL/v \tag{1}$$

where U is mean velocity, L is a characteristic length scale, and v is kinematic viscosity. For the hull of moving ship, with hull lengths of 100 to 250 m and cruising speed of 5 – 10 m/s, Reynolds numbers on the order of 10^9 can result. With the high Reynolds numbers such as this, turbulent boundary layers are unavoidable.

For canonical wall bounded turbulent flow (i.e. pipe flow, channel flow, and turbulent boundary layer flow), it is desirable to use Friction Reynolds number

$$Re_\tau = U_\tau \delta/v \tag{2}$$

where U_τ is skin friction velocity, and δ is boundary layer thickness. The skin-friction velocity U_τ is proportional to the skin-friction drag, hence higher skin-friction velocity translates to higher skin-friction drag.

Adding to the complexity of the problem, the already high contribution of skin friction drag due to high Reynolds number flow in large ships is exacerbated by the issue of surface roughness. Although the hull of a large ship can often seem relatively smooth, particularly when it is just recently cleaned and painted, it is generally not so from the perspective of the flow. When the height of surface irregularities become appreciable in term of viscous length scale (v/U_τ), the flow will "see" the roughness and start to interact with it. Nikuradse (1932) considers that a surface is "smooth" when the viscous scaled roughness height $k^+ < 5$, where

$$k^+ = U_\tau k/v. \tag{3}$$

here k is roughness height. Hence this translates to a maximum permissible physical roughness for ship

moving at cruising speed of 5 – 10 m/s to be around 20 – 50 μm, which is exceedingly small. Therefore, the seemingly smooth ship hull is in fact dynamically rough (from the perspective of the flow). When we take biofouling, which have roughness heights orders of magnitude greater into consideration, it is clear that the drag will be much higher.

5.2 ESTIMATING SKIN FRICTION VELOCITY (U_τ) AND SAND GRAIN EQUIVALENT ROUGHNESS (k_s)

In canonical wall bounded turbulent flow, skin friction velocity U_τ can be estimated from a measured velocity distribution over some wall normal distance z (using either hot-wire, Pitot-tube or Laser Doppler Anemometer) by fitting the mean velocity profile to a logarithmic law:

$$\frac{U}{U_\tau} = \frac{1}{\kappa} log\left(\frac{z\,U_\tau}{\nu}\right) + A \qquad (4)$$

where κ is the Karman constant and A is the wall intercept (both considered to be universal constants). However, due to the non-smooth nature of the surface, the entire profile will be shifted downwards by the Hama roughness function $\Delta(U/U_\tau)$. Hence equation 4 will become:

$$\frac{U}{U_\tau} = \frac{1}{\kappa} log\left(\frac{(z+e)\,U_\tau}{\nu}\right) + A - \Delta\left(\frac{U}{U_\tau}\right) \qquad (5)$$

here e is the necessary roughness offset (see Clauser, 1954, 1956 for further reading regarding the estimation method).

An important component in estimating drag is the sand grain equivalent roughness height k_s, first introduced by Nikuradse (1932). Although both k_s and k have dimensions (in meter), unlike k that is directly measurable from the surface topography, k_s can only be estimated by exposing the rough surface to turbulent flow at various different free-stream velocities (because k_s is a measure of the influence a surface has on the flow). Currently, the most common technique to estimate k_s is through laboratory testing (in wind tunnels, water channels etc), where k_s can be determined by assuming "fully rough" conditions of the form:

$$\Delta\left(\frac{U}{U_\tau}\right) = \frac{1}{\kappa} log\left(\frac{k_s\,U_\tau}{\nu}\right) + A - B \qquad (6)$$

The issue with this technique to determine k_s is the cost. One would need to perform many rough surface wall-normal measurements at different Reynolds number in the laboratory facility to obtain various $\Delta(U/U_\tau)$ values. For realistic roughness such as the "orange peel" pattern of a freshly cleaned and painted ship hull or the complex surface topography of a bio-fouled hull, one would need to scan or imprint the surface, replicate it (through 3D printing or CNC machine), and lay it in the wind tunnel or water channel. This manufacturing process itself is time consuming. Furthermore, it is important to scale the roughness dimension, to account for the difference in Reynolds number between the flow of a ship and the fluid flow in a laboratory wind tunnel or water tunnel (see Monty *et al*, 2016).

Apart from the manufacturing process, the time required to complete rough surface boundary layer experiments is also relatively costly. For illustration, a typical wall-normal experiment in a wind tunnel over a rough surface (such as sand paper or replica of ship hull roughness) at a respectable $Re_\tau \approx 1500$ will take around three hours to measure using hot-wire. From this experiment we can obtain one value of $\Delta(U/U_\tau)$. In order to obtain sufficient values of $\Delta(U/U_\tau)$ to estimate k_s via equation (6), more wall-normal measurements at higher Re_τ are required. The required rule to accurately estimate k_s is the need to attain "fully-rough" condition where $k_s{}^+$ has to be in the order of 70 – 100. Furthermore, δ/k has to be greater than 40 in order to minimise the effect of blockage (Jimenez, 2004). Hence the range of Reynolds numbers required is considerable high. Therefore, one would need to have access to large and costly wind-tunnel/water channel facilities to perform the investigation. Considering the challenge in measuring U_τ and k_s from laboratory activities, it is desirable to develop techniques and methodology that by-pass this need.

5. THE COLLABORATIVE RESEARCH METHODOLOGY

To meet the overarching aims of the research collaboration, the research methodologies are divided into four research strands.

5.1 RESEARCH STRAND 1: LASER DOPPLER ANEMOMETER (LDA) MEASUREMENT

Here we intend to directly measure the boundary layer development over a ship's hull under sailing conditions to monitor the influence of the accumulation of bio-fouling on the skin friction drag. The flow measurement will be made using a Laser Doppler Anemometer (LDA), which is a non-intrusive measurement technique that requires only optical access and does not require a full hull-penetration (see Tropea 1995 for further reading regarding LDA). Lewthwaite *et al*. (1984) attempted a similar study using pitot tubes.

Figure 3 shows the schematic of the experiment, where a small glass window is placed on the double-bottom hull of an operating ship. The actual set up can be seen in figure 4. The LDA measures the velocity gradient in the turbulent boundary layer formed over the ship's hull (during steady sailing) across some traversable distance from close to the hull surface, to at least the end of the logarithmic region. From the velocity gradient and traverse distance we can estimate the skin friction velocity U_τ and Hama function various $\Delta(U/U_\tau)$, allowing a direct measure of local skin friction

coefficient on the operating ship. The flow over the ship hull will be monitored (along with other key data - GPS coordinates, fuel data, etc) during the entire inter dry-docking period.

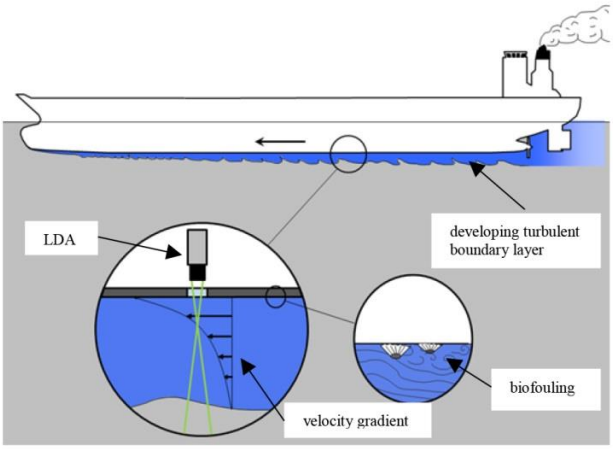

Figure 3: Illustration of the LDA with turbulent boundary layer and surface roughness in ships

Figure 4: LDA experiment set up

5.2 RESEARCH STRAND 2: IMAGE BASED SURFACE SCANNER

The pioneering work of Lewthwaite *et al* (1984) demonstrated for the first time, a successful attempt in studying the skin friction drag of an operational ship under the influence of bio-fouling. The results confirm the challenges faced by the naval industry in overcoming the deleterious effects of bio-fouling. However, one thing that was lacking in Lewthwaite *et al.*'s (1984) work is the absence of the hull-condition record.

To avoid similar drawbacks, here we propose an image-based surface scanner (via digital camera) to monitor the state of the hull surface finish (figure 5). The surface scanner is made of four digital underwater cameras that are attached to a frame. Photos taken by the cameras can be used to reconstruct the 3D topology, allowing us to investigate the roughness in detail. Figure 6 shows sample of biofouling reconstruction.

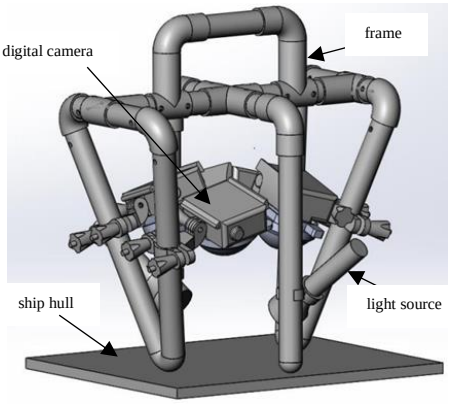

Figure 5: Surface scanner

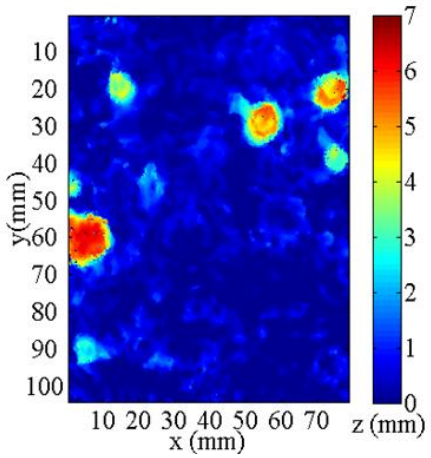

Figure 6: Digitally reconstructed biofouling from image based surface scanner

The surface scanner will record the hull condition regularly, starting during dry-docking and continuing (via dive inspections) until the following scheduled dry-docking (typically a period of one year). This allows a direct comparison between the physical dimension of the biofouling and its effect on the ship skin-friction drag. The scan data can be used to predict the Hama Roughness $\Delta(U/U_\tau)$ from the known average roughness height k_a and effective slope ES_x (Chan *et al*, 2015). Hence the prediction of Hama roughness from this surface scanning can be compared with the estimation from the LDA experiment. Furthermore, the scanned data will later be used in the third and fourth strands of this research.

5.3 RESEARCH STRAND 3: AERODYNAMICS TESTING

Here we intend to validate the efficacy of the LDA measurement technique under controlled laboratory conditions. As previously discussed, generally to predict the drag caused by biofouling, one needs to perform experiments on the surface roughness using a laboratory wind tunnel/water channel at various Reynolds numbers.

From the wind tunnel experiment we can obtain the skin friction velocity U_τ and the Hama roughness function $\Delta(U/U_\tau)$, that can lead to the determination of k_s.

There are two common methods to investigate the effects of biofouling on turbulent boundary layers using wind tunnels. The first forms a test surface from the actual bio-fouling that has been grown in their natural habitat and then removed to a laboratory for experiment (Walker *et al*, 2013). However, this technique is relatively difficult to perform due to the challenges in preserving them for lab environments, particularly the effect of change from their natural habitat, such as from sea, river or lake to lab water tunnel or channel. The second method involves replicating the bio-fouling through casting, machining, rapid-prototyping or combinations of the three (see section 3.2). The second method is often desirable because we can rescale the surface to perform tests under more convenient fluid conditions (i.e in air rather than sea-water), and it also avoids the need to introduce fouling (marine organisms) into expensive laboratory facilities.

Figure 7: Scaled replica of "orange-peel" pattern from freshly cleaned and painted Dharma Kencana IX ship hull inside a wind tunnel

Using the digitally reconstructed and scaled biofouling data from the surface scanner (from strand 2), a detailed master model is manufactured and replicated using a CNC-Machine, the material can be from plastic, engineering wax, or aluminium. From the master model, a moulding from silicone rubber is made and can be used to produce multiple epoxy casts that are identical with the master model. A similar manufacturing method was used by Nugroho *et al* (2013, 2014) and Monty *et al* (2016) for their surface roughness experiment.

Figure 7 shows epoxy casts of "orange-peel" pattern from freshly cleaned and painted Dharma Kencana IX ship hull inside a wind tunnel at the University of Melbourne. Note that the orange peel pattern was obtained via imprint from silicone rubber during dry dock, and then scanned using triangulation laser scanner. We did not use the image based surface scanner, as the apparatus was still under development in Melbourne during that period.

5.4 RESEARCH STRAND 4: DATA CORRELATION

The information from the LDA, surface scanner, and wind tunnel can be used to predict the drag of the entire ship. A recent report by Monty *et al* (2016) shows that by using information such as k_s, ship speed, kinematic viscosity, and hull length (or boundary layer length), one could numerically predict the drag on a fouled full scale ship. When combined with ship-board data such as GPS coordinates, velocity, sea-state, fuel usage, draft, this will allow us to produce a full scale prediction of the fuel drag penalty. The end result of this planned project is a catalogue of data taken over a certain period of time that will help us to produce a workable correlation/equation that will ultimately enable the hull fouling penalty to be calculated directly from just surface scan information.

From the above discussion, it is clear that this project requires substantial logistic and monetary resources. The situation is the reflection of the earlier argument by Katz and Martin (1997) regarding the need of collaboration to combine resources. Our research endeavour is currently still on its early phase. We expect further results from the LDA and wind tunnel experiment to be available in the next available report. This includes the development of the image based surface scanner.

6. CONCLUSIONS

A large scale international research collaboration with an overarching aim to understand the negative effect of biofouling on the turbulent boundary layers of ship's hull and to improve the productivity of ship operations by providing a technique and technology that can measure the emission and fuel usage penalty more precise is currently underway. The research involves six institutions from four different countries that represent academic, industry and policy maker fields. Each of them has different and specific roles that complement each other. The three universities act as initiator and provide the necessary scientific expertise, research personnel, and equipment. The ship company provides the ship as an experimental test bed and the anti-fouling producers provide the necessary technology to repel biofouling on the ship's hull. Finally, the classification society provides technical advice, ensures the safety of the project, and provides avenues for the research to impact government policy.

In this report we have shown that it is possible to form a large scale international collaboration despite the differences in interest and expected results for each of the three fields. The three academic institutions are interested to obtain better understanding in rough wall turbulent boundary layers, to educate higher degree students, and to have their research exposed to the broader community. The two industrial firms are interested with the possibility of having more efficient ship operation management and new technology that can

be applied. Finally, the Classification Society is interested to have a better government policy based on the research outcomes. From the individual objectives of each field, one can see immediately that they are complementary and synergistic, making this a well-structured project. By satisfying the requirements and objectives of each field, the overall aims of this project can be attained.

There are four important research strands that form the pillars of the research collaboration. The first strand is to measure the effect of roughness on ship's hull in-situ using the Laser Doppler Anemometer (LDA). The second strand is to develop an image based surface scanner that allows divers to record the development of biofouling on the ship's hull. The proposed LDA experiment from the first strand is novel and un-tested, therefore to validate the technique a wind tunnel experiment is needed. The wind tunnel validation will form the third research strand. Finally for the fourth research strand we are interested to correlate the data from strand one-to-three with ship performance data (GPS coordinates, ship velocity, fuel usage, etc). This will ultimately allow us to provide a correlation that enables the hull fouling penalty to be calculated directly from just surface scan information. The research collaboration is currently underway and still on its early stage. Initial results will be available in the next round of publication.

7. ACKNOWLEDGEMENTS

The authors would like to thank the Australian Research Council (ARC), the Australia Indonesia Center (AIC) and the Newton Fund from the British Council for financial support. We also grateful to Merak Port Authority for the ship tracking data.

8. REFERENCES

1. BIRO KLASIFIKASI INDONESIA, BKI, (2016), *Rules for classification & surveys*, volume 1, Part 1.
2. BRUNEEL, J., D'ESTE, P., SALTER, A., (2010*), Investigating the factors that diminish the barriers to university–industry collaboration*. Research Policy. 39: 858 -868
3. CHAN, L., MACDONALD, M,. CHUNG, D., HUTCHINS, N., OOI, A., (215). *A systematic investigation of roughness height and wavelength in turbulent pipe flow in the transitionally rough regime*. J. Fluid Mech., 771:743–777.
4. CORBETT, J. J., FISBECK, P. S., PANDIS, S. N. (1999*) Global nitrogen and sulfur inventories for oceangoing ships.* J. Geophys. Res. 104(D3) 3475 – 3470
5. CLAUSER, F. H., 1954. *Turbulent boundary layers in adverse pressure gradients*. J. Aeronaut Sci. 21, 91–108.
6. CLAUSER, F. H., 1956. *The turbulent boundary layers*. Adv. Appl. Mech. 4,1–151.
7. COADY, D., PARRY, I., SEARS, L., SHANG, B. (2015) *How large are global energy subsidies?* IMF Working Paper
8. CORBETT, J. J., WINEBRAKE, J. J., GREEN, E. H., KASIBHATLA, P., ERYING, V., LAUER, A., (2007) *Mortality from ship emissions: A global assessment*. Environ. Sci. Technol., 41(24) : 8512 – 8518
9. DASGUPTA, P., DAVID, P., (1994). *Towards a new economics of science*. Research Policy, 23: 487–522.
10. DAVIES, M., (2006) *Emissions trading for ships- a european perspective*. Naval Eng. J. 118(3): 131– 138.
11. DJPL (2014), Peraturan Direktur Jenderal Perhubungan Laut Nomor. HK.103/I/4/DJPL-14 tentang Pengedokan (Pelimbungan) Kapal Berbendera Indonesia. Direktorat Jenderal Perhubungan Laut.
12. DJPL (2016), Surat Keputusan Direktur Jenderal Perhubungan Laut Nomor PK.204/1/3/DJPL-16 tentang Penunjukan Biro Klasifikasi Indonesia (Persero) sebagai Recognized Organization untuk melaksanakan survey dan sertifikasi Statutoria atas nama Pemerintah pada kapal Berbendera Indonesia. Direktorat Jenderal Perhubungan Laut.
13. ERYING, V., ISAKSEN, I., BEMSTEN, T., COLLINS, W. J., CORBETT, J. J., ENDERSEN, O., GRAINGER, R. G., MOLDAVONA, J., SCHLAGER, H., STEVENSON, D. S. (2010) *Transport impacts on atmosphere and climate: Shipping*. Atmos. Environ., 44(37):4735–4771
14. JIMENEZ, J. (2004) *Turbulent flows over rough walls*. Annu. Rev.Fluid Mech., 36:173–196
15. KATZ,J. S., MARTIN, B. R., (1997) *What is research collaboration?*. Research Policy. 26: 1 – 18
16. LACKENBY, H (1962) '*Resistance of Ships, With Special Reference to Skin Friction and Hull Surface Condition*. Proceedings of the Institution of Mechanical Engineers, 176 (981–1014).
17. LEWTHWAITE, J.C., MOLLAND, A.F., THOMAS, K., (1984) *An investigation into the variation of ship skin frictional resistance with fouling*. The Royal Institution of Naval Architects.
18. LONGVA, T., EIDE, M. S., SKJONG, R., (2010) *Determining a required energy efficiency design index level for new ships based on a cost-effectiveness criterion*. Maritime Policy and Management. 37:2, 129–143.
19. MELIN, G., PERSSON, O., (1996) *Studying Research Collaboration Using Co-authorships*. Scientometrics. 36 (3): 363 - 377
20. MIOLA, A., CIUFFO, B., (2011) *Estimating air emissions from ships: Meta-analysis of*

modelling approaches and available data sources. Atmos. Environ, 45: 2242 – 2251

21. MOLLAND, A. F., TURNOCK, S. R., HUDSON, D. A. and UTAMA, I. K. A. P. (2014) *Reducing ship emissions: a review of potential practical improvements in the propulsive efficiency of future ships*. Transactions of Royal Institution of Naval Architects Part A. 156, 175-188
22. MONTY, J. P., DOGAN, E., HANSON, R., SCARDINO, A. J., GANAPATHISUBRAMANI, B., HUTCHINS, N., (2016) *An assessment of the ship drag penalty arising from light calcareous tubeworm fouling*. Biofouling, 32(4): 451-64
23. NIKURADSE, J. (1932) *Gesetzmassigkeiten der turbulenten stromung in glatten rohren*. Forsch. Auf Dem Gebiet des Ingen.,3:1–36.
24. NUGROHO, B., HUTCHINS, N., MONTY, J. P., (2013) *Large-scale spanwise periodicity in a turbulent boundary layer induced by highly ordered and directional surface roughness*. Int J Heat Fluid Flow, 41:90 -102.
25. NUGROHO, B., GNANAMANICKAM, E. P., KEVIN, MONTY, J. P., HUTCHINS, N., (2014) *Roll-modes generated in boundary layers with passive surface modification*. AIAA Paper 2014-0197
26. SCHULTZ, M. P. (2004) *Frictional resistance of antifouling coating systems*. J. Fluids Eng. 126, 1039.
27. SCHULTZ, M. P. (2007) *Effects of coating roughness and biofouling on ship resistance and powering*. Biofouling 23(5-6), 331–341
28. SCHULTZ, M. P., BENDICK, J. A., HOLM, E. R. & HERTEL, W. M. (2011) *Economic impact of biofouling on a naval surface ship*. Biofouling 27, 87–98.
29. SUBRAMANYAM, K. (1982) *Bibliometric studies of research collaboration: A review*. Journal of Information Science. 33 – 38
30. TROPEA, C., (1995) *Laser doppler anemometry: recent developments and future challenges*. Meas. Sci. Technol. 6 : 605-619.
31. UTAMA, I. K. A. P., and PRIBADI, T. W., (2011). *Three in one education concept, an Indonesian perspective*. The Royal Institution of Naval Architects. Education and Professional Development of Engineers in the Maritime Industry, Newcastle University, UK.
32. UTAMA, I.K.A.P., GANAPATHISUBRAMANI, B., HUTCHINS, N., NUGROHO, B., MONTY, J. P., PRASETYO, F. A., YUSUF, M., TULLBERG, M., (2016). *International collaborative work to improve research quality and enhance academic achievement.* The Royal Institution of Naval Architects. Education & Professional development of Engineers in the Maritime Industry conference, Singapore.
33. WALKER, J. M., SARGISON, J. E., and HENDERSON, A. D., (2013). *Turbulent boundary-layer structure of flows over freshwater biofilms*. Exp. Fluids, 54:1–17.
34. WINEBRAKE, J. J., CORBETT, J. J., GREEN, E. H., LAUER, A., ERYING, V., (2009) *Mitigating the health impacts of pollution from oceangoing shipping : An assessment of low-sulfur fuel mandates*. Environ. Sci. Technol. 43 (13) 4776 – 4782

EXPERIMENTAL INVESTIGATION INTO THE EFFECTS OF REDUCED VERTICAL CENTRE OF GRAVITY OF AN ARTICULATED CONCRETE MATTRESS IN CURRENT FLOW

(DOI No: 10.3940/rina.ijme.2017.a3.433)

A Neville, **R McLaren**, **J Weber**, **C Chin**, **J Binns**, and **A Taylor,** Australian Maritime College, Australia

SUMMARY

An articulated concrete mattress model has been utilised to investigate the effects of reduced vertical centre of gravity on the stability of a 400 series block. Experimental testing was conducted at the AMC CWC, Beauty Point. To determine the effects that a reduced centre of gravity has on stability, the 3 by 3 articulated concrete mattress model was subject to pure uniform current flow. The subsequent forces were analysed with a six degree of freedom underwater force sensor. In order to gain a range of real world scenarios, the experimental model was tested at six flow angles ranging from -15 degrees through to 60 degrees, at 15 degree increments. Additionally, five fluid velocities starting at 0.6 m/s through to 1.4 m/s, at 0.2 m/s increments were investigated. These results explain how the inversion of a 400 series block increases its hydrodynamic coefficients and subsequently decreases its stability performance in current flow. Ultimately, this study provides experimental information for the installation of 400 series articulated concrete mattresses in the inverted orientation.

NOMENCLATURE

Symbol	Definition (unit)
A	Area (m^2)
A_D	Drag area (m^2)
A_L	Lift area (m^2)
ACM	Articulated Concrete Mattress
AMC	Australian Maritime College
C	Force Coefficient
C_D	Drag Coefficient
C_{INT}	Confidence interval (%)
C_L	Lift Coefficient
C_{OVT}	overturning moment coefficient
CWC	Circulating Water Channel
F	Force (N)
F_D	Drag force (N)
F_L	Lift force (N)
g	Acceleration due to gravity (m/s^2)
H_{MP}	Height to pivot point (m)
M_{OVT}	overturning moment (N m)
n	number in the sample
s	standard deviation of the sample
t	confidence interval of the distribution
v	velocity (m/s)
V_{ACM}	ACM volume (m^3)
$v_{F,A}$	Failure velocity at A (m/s)
$v_{F,B}$	Failure velocity at B (m/s)
W_S	Submerged Weight (N)
ρ	density (kg/m^3)

1. INTRODUCTION

The implementation of manufactured and naturally formed marine structures in rivers and oceans has led to the issue of scouring, which occurs where the structure meets natural or unnatural fluid flow. In the case of a structure meeting fluid flow, its presence can alter the field of flow around its immediate environment. Scouring occurs as induced vortices around the structure remove seabeds, sand and mud (Young & Testik 2009). Pipelines are susceptible to scouring and can fail due to the removal of sand or sediment along the length of the pipe. This is a common issue in industry as pipelines can fail at the scoured location, due to bending under self-weight and contents. There are many ways to mitigate the destruction that scouring creates. Riprap, is a common countermeasure on bridge abutments and embankments to prevent scour, but possess negative traits as it is subject to dislodgment and slump; as well as slide failures (Melville 2006). Due to the economic cost of this method of pipeline protection and associated problems, new methods of technologically advanced protection have been developed.

Articulated concrete mattresses (ACM) are one such option that can provide stability throughout design life. An ACM is comprised of a series of individual concrete blocks placed to form a matrix revetment with specific hydraulic performance characteristics (Abt *et al.* 2001). They can provide a flexible alternative to riprap or rigid revetments; individual units are commonly held together by either steel rods, cables or rope. Typical failure modes of ACM's are the overturning and rollup of the edge exposed most to the flow, or the leading edge of the mattress. In addition, the uplift at the centre of the mattress is also a possible mode of failure. The uplift occurs when the leading edge is incorrectly anchored (Lagasse 2007). There is no industry standard stability design methodology to appropriately estimate the hydrodynamic forces of drag and lift (Godbold, Sackmann & Cheng 2014). Recommended practice outlines in situ conditions and requirements that need to be taken into consideration when calculating pipeline stability, in environmental conditions such as typical wave and current loads (Veritas 1988). The knowledge gap between predicted and encountered forces acting on an ACM still exists as recommended practices only contains design methods for dynamic lateral stability of pipelines. Recommended practice acknowledges that

ACMs are to be engineered to the correct shape, size, flexibility, density and ultimate strength (Veritas 2007). It is common industry practice to implement pipeline stability design equations and large safety factors that have the potential to over engineer ACM design. In the interest of improving the design procedure for ACMs, experimental and numerical research is necessary to determine non-dimensional hydrodynamic coefficients of drag and lift. In doing so, realistic estimations of these forces can be calculated that have the potential to reduce the cost of materials and labour in the build and installation process.

When an ACM is placed in protective environments such as pipeline protection, it will require specific minimum properties such as size, submerged mass, flexibility as well as overall concrete density. The stabilisation effects that an ACM possesses is generated by the submerged mass resting on the sea floor or object, as well as its geometric profile that can reduce overall drag and lift acting on the block itself. Companies such as Subcon produce three full ACM blocks that are 300, 400 and 500 mm high, as well as half ACMs that are 150 and 250 mm high. These are illustrated in Figure 1. Offshore stabilisation companies deploy these ACMs in situations specific to requirements of the environment; as economical and cost effective practices are of high importance to clients. Therefore, if a cheaper and lighter option is more viable, the company is able to compete for more business. Thus, to be less conservative in the design stage, research is required in the hydrodynamic properties of these ACMs so that large safety factors are not required.

Initial research investigated current forces on a 2 by 4, 300 series ACM in the Australian Maritime College (AMC) Circulating Water Channel (CWC) (Francis 2013). Typical lift coefficients for the mattress were much lower than predictions from literature and much lower than that recommended by industry practice (Veritas 2007). In addition, the coefficients were lower than that predicted in computational fluid dynamics (CFD) due to the effects of diminished lift and drag forces located in the critical region where high drag occurs (Francis 2013). Further numerical research (CFD) was also performed on a simplified 500 series model that investigated a 3 by 8 matrix at flow angles of 0 and 45 degrees at varied current velocities (Griggs 2014). Recent research has included the testing of these forces on all block types 300, 400 and 500, which investigated the overall performance on each of these types of ACM and their relevant implications in industry (Mclaren 2015). Final conclusions showed that the 400 series ACM outperformed the 500 series, ultimately leaving the 500 series a less viable solution if the stability of the block is the underlying requirement. However, the 500 series can be used if weight is the requirement (such implications are pipeline protection and support), whilst the 300 series may be used if low drag and lift forces are present on them due to their smaller geometry.

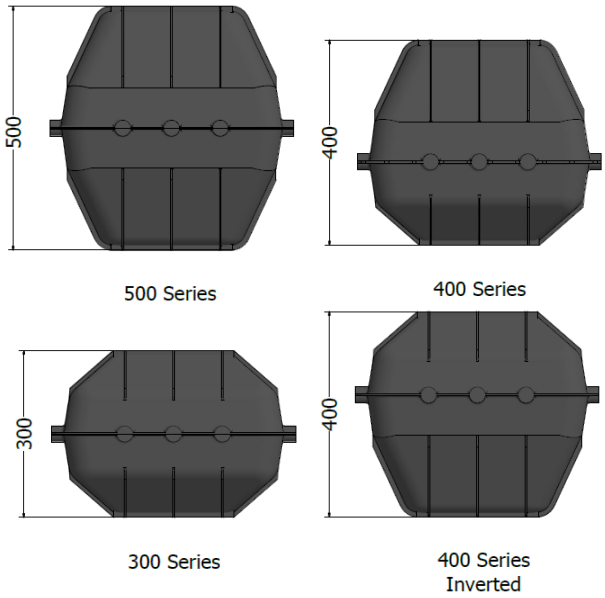

Figure 1: Summary of block types used for comparison in this paper

This paper will investigate how the stability of a 400 series ACM is affected by both the vertical shift upwards in the centre of gravity (COG) and a change in the centre of buoyancy (COB). The inverted 400 series will also be compared to other ACM sizes, to understand how it performs under the same experimental conditions, as well as investigating if it is a plausible option when compared with other block types. The increased COG position is to be achieved by inverting the geometry of a 400 series block. The inverted 400 series will be tested using the same model and procedure as Mclaren (2015).

2. THEORY

2.1 HYDROSTATIC AND HYDRODYNAMIC PROPERTIES

The COG of the submerged ACM block will be a contributing factor to the overall stability of the inverted 400 series block. It is assumed that the geometry of the block is consistent in shape, size and density; that is, it is a uniform object of mass. The centre of buoyancy of the object acts at the centre of the overall volume, which in this case, acts at the same position as the COG with the above condition. This is important for the calculation process as it is assumed the mass acts as point load through the COG, for simplification purposes in analysis.

2.2 FAILURE METHODS

A free body diagram of the forces acting on a submerged ACM is shown in Figure 2. Points A and B show the expected failure locations of an ACM in current flow. It is expected that in a matrix formation, the failure mode occurs at location A, due to the uplift of the most frontal block. Uplift occurs on the front row of the ACM, and causes the frontal blocks to flip over the second row

about point A. In this paper, failure is assumed and defined to be any movement off the datum. This definition is required as it is too difficult to quantify small uplifts that do not cause the front row of the ACM to fail.

Failure at point B is also taken into consideration due to the possibility that the ACM is disconnected or the joining articulation has failed. This failure method causes the ACM to rotate about point B, and turn over about this touch down position at the datum.

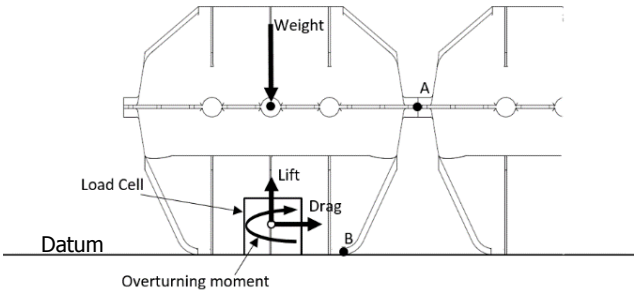

Figure 2: Summary of forces and failure locations (A and B) acting on an ACM due to failure methods

2.3 DRAG AND LIFT COEFFICIENTS

The non-dimensional coefficients of drag C_D and lift C_L can be used as a means of quantifying the hydrodynamic effects acting on an object. In this case, by rearrangement of the simplified Morrisons equation (Veritas 2010) shown in Equation (1), the coefficient can be calculated. Here F is force, ρ is the fluid density, A is projected area, v is the fluid velocity and C is a coefficient of the force.

$$F = \frac{1}{2}\rho A v^2 C \tag{1}$$

Equations (2) and (3) are used to evaluate the drag coefficient C_D and lift coefficient C_L (Veritas 2010). Here, ρ_{water} is density (in this case taken as 999.1 kg/m^3 (Mclaren 2015)), v is the water particle velocity, A_D is the drag area and A_L is lift area. The drag area of the block is taken as the frontal exposed area of the ACM block. In addition, the lift area is simply the top area of the ACM and the drag and lift areas are kept constant. The drag force F_D, and lift force F_L are the measured forces acting on the experimental load cell.

$$C_D = \frac{2F_D}{\rho_{water} A_D v^2} \tag{2}$$

$$C_L = \frac{2F_L}{\rho_{water} A_L v^2} \tag{3}$$

2.4 COEFFICIENT OF OVERTURNING MOMENT AND SUBSEQUENT FAILURE VELOCITY

A method of quantitatively measuring the stability is required and was proposed. A proposed overturning coefficient C_{OVT} is, in its most simple form, the combination of asymmetrical drag and lift about the centre of the load cell, or about the point acting as a hinge (Mclaren 2015). Due to the relationship of the overturning moment M_{OVT} to drag and lift, a simple area is not used. Thus, the volume of the object V_{ACM} is used for non-dimensionality, in this case, the volume of the ACM block. The formula for the overturning moment coefficient is given by Equation (4).

$$C_{OVT} = \frac{2M_{OVT}}{\rho V_{ACM} v^2} \tag{4}$$

The failure velocity is determined where the fluid creates an overturning moment equal to or greater than the submerged weight about the point of failure. This is determined by the summation of moments about the failure points A and B in Figure 2 and is defined as $v_{F,A}$ and $v_{F,B}$ respectively. Summation of moments includes drag force, lift force as well as the moment generated about the base of the ACM block. The summation of these forces give the failure velocities A and B and these are shown in Equations (5) and (6).

$$v_{F,B} = \sqrt{\frac{0.25W_{Submerged}}{\rho_{water}(C_{OVT}V_{ACM} + 0.038C_D A_D + 0.125C_L A_L)}} \tag{5}$$

$$v_{F,A} = \sqrt{\frac{0.50W_{Submerged}}{\rho_{water}(C_{OVT}V_{ACM} - (H_{MP} - 0.038)C_D A_D + 0.25C_L A_L)}} \tag{6}$$

Here, $W_{Submerged}$ is the submerged weight of an individual ACM block, other keys terms in Equations (5) and (6) have been defined in Equations (2) and (3), as they are kept consistent throughout this paper. The submerged weight of the ACM block is evaluated by the formula shown in Equation (7). It is important to note that H_{MP} is the height measured from the datum to the pivot point of the moment and is not simply half the height of the block in a 400 series. The numerical values for the failure velocity are simply a means of evaluating the performance of the block relative to one another. This will not be equal to the exact velocity at which a block will fail at in situ. Lastly, g is defined as the gravitational constant, $\rho_{concrete}$ is the density of concrete (taken as 2400 kg/m^3, as per McLaren (2015)) and V_{ACM} is the volume of the ACM block.

$$W_{Submerged} = gV_{ACM}(\rho_{concrete} - \rho_{water}) \tag{7}$$

The importance of these calculations is to determine and gauge the performance of each block type relative to each other. It is important to note environmental loads that the ACMs are exposed to in operation cannot be fully replicated in the CWC, and therefore do not accurately represent failure velocities expected whilst in operation. A better understanding of hydrodynamic coefficients of lift and drag will broaden industry knowledge and design processes. The research conducted in this paper will aid in mattress placement with respect to the type of ACM installed as well as its position with respect to the incident flow direction.

2.5 UNCERTAINTY ANALYSIS

In order to approximate the level of deviation in the experimental data, an uncertainty analysis is required. This can be achieved by evaluating the confidence interval at 97 % of the mean, of the non-dimensional coefficients at each velocity and angle. The sample confidence interval is determined using Equation (8) (Figliola & Beasley 2015), where s is the standard deviation of the sample, t is the confidence interval of the distribution and n is the number of samples in the source.

$$C_{Int} = t\frac{s}{\sqrt{n}} \qquad (8)$$

3. METHODS

The AMC CWC was used in the experimental investigation. The CWC is a large test facility that is 11m long, 5m wide and 2.5m deep that can produce water velocities up to 1.7 m/s (Australian Maritime College 2016). A glass window on the side of the tank allows for test viewing, as well as a means of inspection for problems or issues occurring during experiments.

3.1 EXPERIMENTAL CONFIGURATION AND PROCEDURE

The model scale used in the experimental testing of the inverted 400 series block was a full scale (1:1) Subcon concrete block mould. The mould consists of two half shells that are clipped together and fixed to a steel plate using threaded bar and a top plate. The top shell is a 150mm shell, and the bottom is a 250mm shell. The testing apparatus is an adaptation of that used by Mclaren (2015). It is important to note that the initial set up was fabricated by Francis (2013) and has been further modified for this experiment. The initial 2x4 mattress and plate has been improved to allow for a uniform 3 by 3 matrix shown in Figure 3. One block is constructed to mount the load cell for 6 degrees of freedom (Figure 4) within the block, whilst also simultaneously being secured to the steel plate. In addition, the block itself is positioned so that it does not interact with adjacent blocks.

The load cell was located in the centre block facing the flow, shown by the arrow in Figure 3. The load cell cable was tied down to the plate and surrounding blocks, and at the back to prevent movement and any possible interference from its vibrations in the fluid flow.

The load cell was located in the central block at the leading edge of the flow, as failure at the leading frontal block occurs first (Mclaren 2015). Thus, there was little reason to investigate the corner block of the matrix. The load cell was internally fitted within the centre block at the leading edge of the mattress, in order to measure forces when it was displaced. This requires the block itself to suspend off the steel plate and have the ability to move in all degrees of freedom. Lastly, it was imperative that the blocks did not touch and interfere with each other at any point, as this would induce forces previous experiments have not included or accounted for.

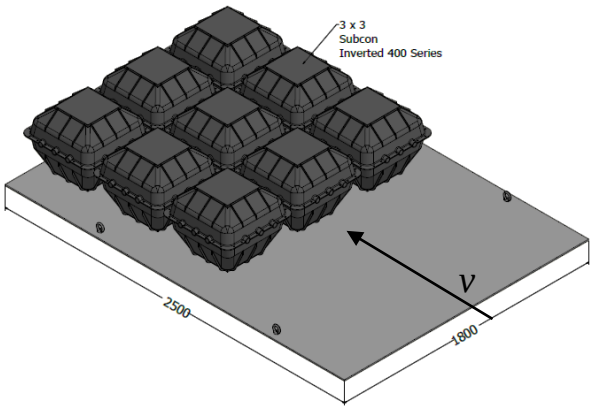

Figure 3: Experimental set up in mm, where the arrow indicates flow direction, *v*

This experiment was conducted such that the front row of the ACM was subjected to flow from the frontal side (load cell location). A summary of the testing regime for each angle of attack is shown in Table 1, where at the beginning of all angle runs, a zero value was recorded. The zero value takes into account all forces including hydrostatic pressure acting on the load cell at the bottom of the CWC. Testing procedure occurred such that two, 180 second readings of each pump velocity was recorded at each angle of attack. To reduce testing time, data was recorded whilst the water velocities were increased from the lowest to the largest and subsequently decreased in the reverse manner. Double readings were required to gain an average of the force over the testing duration.

Repeatability in the experiment is crucial in order to verify and cross check final data. The first set of repeatability checks conducted were the angles of attack. In the experiment, -15 and 15 degrees are theoretically the same angle assuming the model was positioned symmetrically in the CWC. The drag, lift and overturning moment coefficients were cross checked with the repeated 15 degree angle. The water velocity

within the tank was repeated after the maximum velocity was produced, with velocities of 0.8, 0.6 and 0 m/s. This action also aids in slowing down the velocity within the tank, in order to record another 0 m/s run.

Table 1: Testing regime at flow angles of attack -15, 0, 15, 30, 45 and 60 degrees

Run	Velocity(m/s)	RPM	Run	Velocity(m/s)	RPM
1	0	0	**8**	1.2	145
2	0.6	75.1	**9**	1.2	145
3	0.6	75.1	**10**	1.4	170
4	0.8	100.1	**11**	1.4	170
5	0.8	100.1	**12**	0.8	100.1
6	1	120.1	**13**	0.6	75.1
7	1	120.1	**14**	0	0

3.2 DATA ACQUISITION AND CALIBRATION

The underwater load cell was a six component force sensor with a stainless steel body that operates with an oil filled pressure compensation bladder to enable short term (less than 24 hours) immersion in fresh water (AMTI Force and Motion 2009). The six degrees of freedom load cell and calibration equipment are shown in Figure 4.

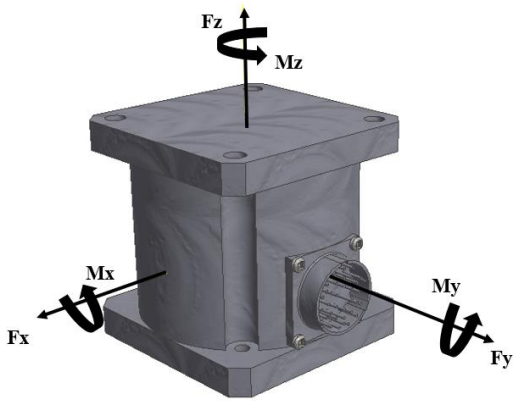

Figure 4: MC3-SSUDW underwater load cell used in the experimental procedure

Without a load cell calibration, the experiment would not be accurate or credible. Calibration is required to read accurate hydrodynamic forces whilst testing is in operation. The calibration technique involved taking registered readings of forces and moments in known directions including forces in Fx, Fy and Fz and moments in Mx, My and Mz. A relationship was generated by plot between the load applied and the output voltage. The relationship created is linear, and the resultant gradient is the calibration conversion from volts [V] to Newtons [N]. The voltage reading from the load cell can be converted to a force with the known calibration matrix K. Table 2 describes the calibration matrix used to process the raw data.

Table 2: Calibration matrix for the underwater load cell

Channel	1	2	3	4	5	6
	Fz	Fx	Mz	My	Mx	Fy
K [N/V]	30.045	7.793	0.211	0.146	0.140	8.135

4. RESULTS AND DISCUSSION

4.1 STABILITY

To gain an estimation of the change in the COG in a 400 series ACM block, its computer animated geometry was investigated. The COG can be measured from the datum or ground the block rests on. An increase in the COG leads to an overall reduction of the GM. As per Figure 5, the COG for an upright block is 203mm and the inverted block has a COG of 218mm. An overall change upwards of 15mm in the value of COG was measured.

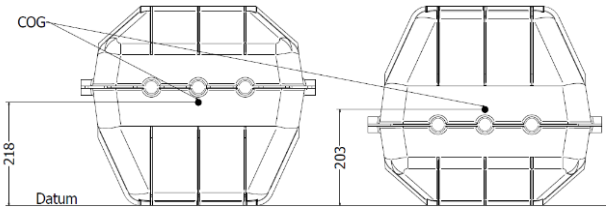

Figure 5: Location of COG (black circle) for; the inverted (left), and upright 400 series (right)

This 15mm shift upwards in COG translates to an overall increase of 6.88 %, measured from the datum. Although this is a relatively small variance in COG, the overall stability of the inverted 400 series is still expected to reduce. The likelihood of failure due to overturning increases when the COG shifts upwards from the datum. As the mass of the object acts through the COG, less overturning force is required to generate a moment greater than its submerged weight. This is due to a higher moment lever the 400 series ascertains after inversion, leading to increased instability.

4.2 BLOCK TYPE VALIDATION

Data collected from previous experimental analysis from Mclaren (2015) can be used to compare the performance of the inverted 400 series ACM. This data contains the same experimental methods of 300, 400 and 500 series.

4.3 DRAG AND LIFT COEFFICIENTS

Figure 6 and Figure 7 show the post processing results for the drag and lift coefficients respectively, using Equations (2) and (3). The repeatability angles of -15 and 15 degrees showed similar values of drag coefficient of 0.5 and lift coefficient of 0.3 as expected. The inverted 400 series shows the highest coefficient of drag at 0 degrees angle of attack and can be accounted for due to the large exposed frontal area of the block. As the drag coefficient is proportional to exposed frontal area, when

altering the angle, the drag force changes respectively, whilst the projected drag area remains consistent.

The study shows that the drag coefficient of the inverted 400 series is only higher than the upright 400 at this 0 degrees angle of attack. To verify the data, implementation of a 97% confidence interval in the load cell data was produced and shows little deviation from the mean result. Therefore, the drag coefficient determined in this paper is within an acceptable range, as the data does not deviate significantly from the mean. Uncertainty bars can be used to show this confidence interval and it is clear that varying degrees of overlap occur within the four sets of data as shown in Figure 6. It is also apparent that the difference between the 400 series and the inverted 400 is minimal, as significant overlapping occurs whilst increasing the angle of attack. For ease of analysis and clarity, Figure 6 is the only plot that indicates the uncertainty of the coefficients for simplicity and ease of analysis. It is assumed that other load cell channels used for the lift and overturning coefficients carry the same sample uncertainty. Therefore, the uncertainty bars illustrated in Figure 6 will not be present throughout the data plotted in this paper, due to congestion that prevent clear understanding of data points.

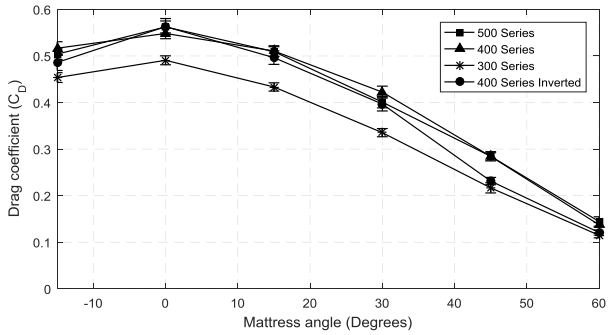

Figure 6: Drag coefficient comparison with 97 % confidence interval showing significant overlap between inverted 400 and upright 400 series, whilst the inverted 400 has higher drag at 0 degrees angle of attack

Overall, the change in drag force is not significant enough to simply imply the instability of the inverse 400 series. To quantify the instability, the lift force must also be examined, as this lift force significantly contributes to the failure mechanisms in conjunction with overturning moment.

The study shows that the lift coefficient of the inverted 400 series is higher than the upright 400 series in all angles of flow incidence. This is due to the geometry of the block, as it experiences higher differential pressure around the larger bottom area. The high pressure differentials in the xy plane (refer to Figure 4) acting between the bottom and top section of the block also causes this increased lift force. There is a significant difference in lift forces acting on the two 400 series shown in Figure 7. The difference in geometry between the two blocks causes large lift forces acting on the 250 mm section of the block and is mainly accounted for due to the large pressure on the face of the bottom shell as the velocity at the face reduces significantly. Figure 7 suggests decreased stability, resulting from a difference in lift coefficient of 0.1 that is clearly present between the upright and inverted 400 series. At angles of attack up to 30 degrees, this 0.1 differential in the trend is a common difference. It is clear that the inverted 400 series has similar lift forces when compared to the 500 series despite having considerably less weight. It is possible that the geometry of the 250 mm half shell induces these large lift forces. The impact of significantly larger lift forces in the lower 250 mm region causes the instability of the inverted 400 series to increase. High instability occurs due to more force that is able to lift the block off the datum. Another verification of reduced instability can be produced upon investigation of the moment (Mx) generated about the centre of the load cell. Although it is not a true representation of the failure moment force at the failure location, it gives a qualitative analysis between the upright and inverted 400 series.

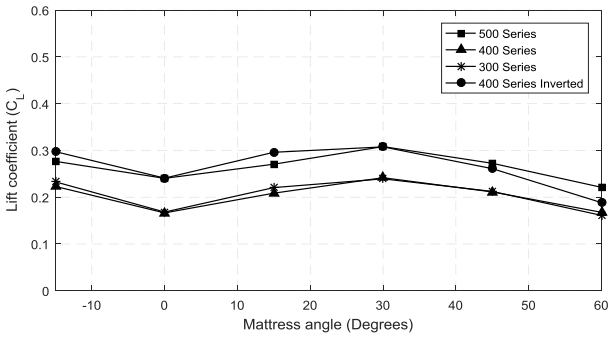

Figure 7: Lift coefficient comparison showing significantly higher lift for the inverted 400 series compared to the 400 series due to the 250mm bottom half section of the block

4.4 OVERTURNING AND FAILURE VELOCITY

The qualitative method of comparison mentioned in section 4.3 is the overturning moment coefficient. The overturning moment coefficient in the xz axis was calculated using Equation (4), and is plotted against the angle of attack shown in Figure 8. The overturning moment coefficient is a maximum at 0 degrees angle of attack. This is highest at this location due to large forces acting at this angle. It is evident that the inverted 400 series has higher moment coefficients at all angles of attack. Again, as the geometry of the 400 series suggests, a greater portion of the body resides at a higher location above the datum. Hence, the higher the force lever, the greater the moment for the same applied load. Higher moment forces suggest that the increased COG has an effect on the overall stability of the ACM. However, as the coefficient difference is only 0.08, the increase in COG has a lesser effect to the stability than originally hypothesised. It is important to note that the data presented in Figure 8 follows expected theory. The 500 series ACM has the highest overturning moment

coefficient as it is the largest block. Conversely, the 300 series has the least as it is the smallest block. The location of the overturning moment coefficients gives credibility to the location of the moment acting on the inverted 400 series, as the 400 series' data lies just below the 500 series, yet, above the upright 400 series.

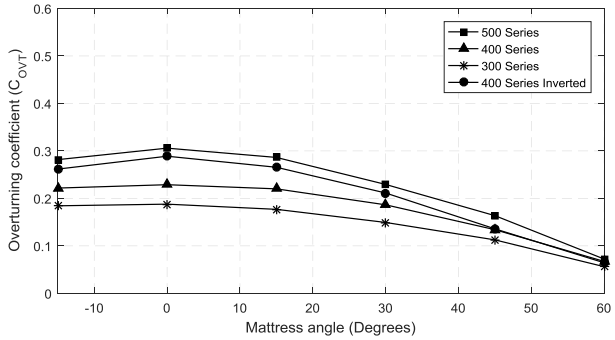

Figure 8: Overturning coefficients showing higher moment forces acting on the inverted 400 series

Failure flow rate is the fluid velocity required to cause enough hydrodynamic force of drag, lift and overturning moment that will result in the ACM failure at points A or B shown in Figure 2. For this reason, the failure velocity is a comprehensive way of comparing the stability of each ACM block size, as it takes into account the submerged mass of the block, as well as the lever arms to the connections. The failure velocity equation takes drag, lift and overturning moment about the location of failure, and solves for velocity.

The failure flow rate values are again plotted against the angle of attack. Figure 9 displays the velocities that will cause the block to fail at point A. The trend shows a similarity between the upright and inverted 400 orientations, in that they do not diverge significantly away from each other throughout the increment in angles of attack. The trend is due to the moment lever used in the failure velocity in Equation (6). The H_{MP} term, or the moment lever in Equation (6), is larger for the inverted 400 series, meaning that the overall velocity decreases as the moment is larger. The upright 400 series moment is smaller yet the failure velocity is larger, which causes the failure velocity to become closer together. Although the failure velocity at 0 degrees angle of attack is 5% higher than the upright orientation, this justifies the inverted orientations instability in current flow. Lastly, the failure flow rate at point A shows that when an ACM is deployed, it is imperative that it is positioned such that it is able to withstand current forces at the 30 degree angle, as this is the position at which it will fail first. The 30 degree angle of attack position experiences the greatest amount of force that will cause it to fail due to uplift of the most frontal block.

Failure at point A assumes that the ACM is connected by some degree of articulation, either by steel rods, wire, or rope; such that the connection is relatively rigid. This means that a block adjacent to another block at the leading edge has additional effects on the mass and stability of that at the front. However, this study does not take into account these effects.

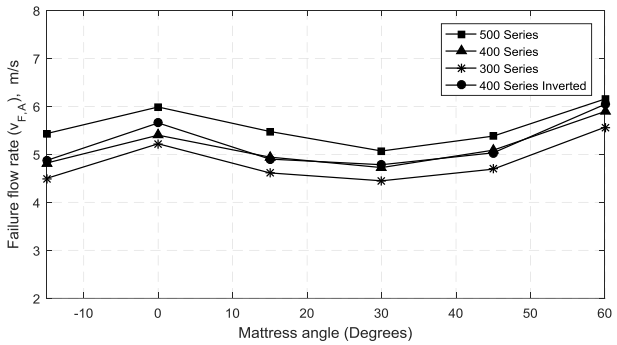

Figure 9: Failure flow rate for location A, illustrating the convergent nature of the inverted and upright 400 series comparison

Analysis of the failure flow rate at location B is also a way of quantifying the stability of the inverted 400 series ACM. Location B is located where the bottom of the ACM meets the datum, and so summation of moments are taken at this point and consequently no vertical moment lever arms are present, which is similar to the condition of failure flow rate at A. Having only horizontal moment arms and constant downward moment levers (between the load cell and the datum), the converging nature of failure at point A does not exist. Hence, an appropriate comparison was obtained, as the difference in inverted 400 and upright 400 is consistent, due to the nature of the block geometry.

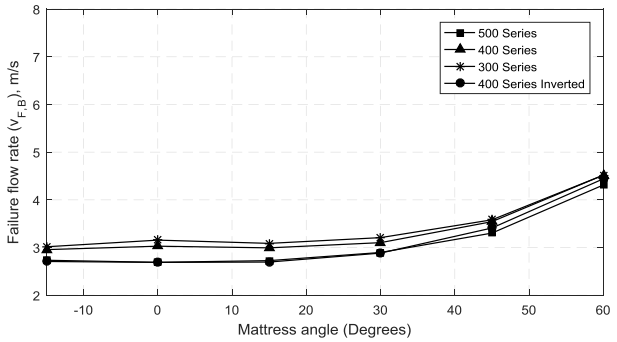

Figure 10: Failure flow rate for location B, displaying the small contrast in failure velocity of a maximum 0.3 m/s between the inverted and upright 400 series

An exponential trend is apparent in Figure 10, as the further the angle is away from the flow, the greater the force is required to cause the block to fail. More force is required at higher angles as the corner block physically blocks the centre face block. For that reason, the load cell is not exposed to large amounts of flow, and subsequent high failure velocities are present at 45 and 60 degrees. This plot is significant, as the inverted 400 series will fail at point B, 0.3 m/s before the upright position at the 0 degrees angle of attack. Notably, the failure velocity at point B stays relatively constant throughout the increase in angle of attack. This is a critical factor in offshore

applications when an ACM fails at position B. Failure at point B can occur if the joining articulation between blocks has failed, or is damaged. The phenomenon of relatively constant failure flow rate means that in scenarios where a block experiences flow angles over a 45 degree spread (0 to 45 degrees angle of attack) the block should experience similar forces about the failure location B. In addition, it is further confirmation that the vertical shift upwards in COG reduces the 400 series' stability. The shift in COG of 15mm upwards has not affected the overall stability of the inverted 400 series as much as initially predicted, according to the failure velocity at point B.

4.5 LIMITATIONS

Sources of uncertainty in this experiment may have originated from a range of experimental methods. Firstly, possible creep from the load cell can occur when it experiences load for an extended period of time. This is common for the load cell used in this experiment and it is possible that it has affected the results. The fluid profile at the CWC is another possible source of uncertainty, as the velocity the experimental set up experiences may not be the same as the input velocity. This issue can be overcome by regular flow profile checks throughout experimentation. This eventuates into uncertain hydrodynamic coefficients, as the values are calculated at incorrect velocities.

Sample uncertainties in this paper were analysed and an uncertainty confidence interval of 97 % was determined. The average range of this uncertainty was determined to be 0.011, which was a maximum of 7%, and a minimum of 2% of the data produced.

Lastly as the density of concrete assumed for this paper is 2400 kg/m^3, the failure velocity predicted is the worst case scenario. Thus, if the density is assumed to be higher (which can be up to 5000 kg/m^3 in industry applications) than this, the subsequent failure velocity will significantly increase, as the total force required to overturn the block and cause failure increases.

5. CONCLUSIONS

An experimental articulated concrete mattress set up in the AMC CWC has been successfully performed to determine stability effects of a 400 series Subcon block with a reduced centre of gravity. Reduction of the centre of gravity was achieved by inverting the ACM, and analysed by comparison of the hydrodynamic coefficients of drag, lift and overturning moment. A failure velocity in two locations was used to determine the overall effects of all combined forces, including submerged mass. It was anticipated that the inverted 400 series would show significantly less stability, due to the change in centre of gravity upon inversion. Upon inspection of computer animated geometry of the 400 series, the overall decrease in centre of gravity measured from the bottom of the block was 15 mm once the geometry was inverted, which was significantly less than first anticipated.

Analysis of the drag, lift and overturning moment coefficients concluded that the difference in lift coefficient is a maximum of 0.1, at 0 degrees angle of attack. This is consistent throughout the change in angle. Higher lift coefficient of the inverted 400 series was predictable due to the larger 250 mm section of the block at the bottom on the body. This instigated greater lifting forces acting on the bottom region and also translates into the coefficient of overturning that this lift force creates. The overturning coefficient is also 0.08 greater at 0 degrees angle of attack and is seen to decrease throughout the increase of angle of attack, as the mattress body and load cell block experiences less force, since it is less of a bluff body.

It is clear that the inverted 400 series displays lower stability than that of the upright orientation, as the inverted 400 series experiences considerably higher lift forces at all angles of attack, as well as slightly higher drag at 0 degrees angle of attack. In addition, the subsequent predicted failure velocity of the inverted 400 series is greatest at 0 degrees angle of attack and is 0.3 m/s higher compared to its correct orientation. The analysis shown in this paper illustrates that the use of the inverted 400 series has a reduced capability over the upright 400 series ACM block. If installation of the 400 series is to occur in industry, it would be eminent to the client that the blocks for the ACM should not be in the inverted position, if the failure velocity in this paper is to be considered in design calculation.

6. ACKNOWLEDGEMENTS

The author would like to extend his acknowledgements to the following people for their contributions to this experimental investigation. The supervisor Mr Josh Weber, the Co supervisor Mr Rory McLaren, A/Prof Jonathan Binns, Dr. Christopher Chin, Murphy McColl, Alex Taylor and Simon Little.

7. REFERENCES

1. ABT, S, LEECH, J, THORNTON, C & LIPSCOMB, C 2001, '*Articulated Concrete Block Stability Testing*', Journal of the American Water Resources Association, vol. 1.
2. AMTI Force and Motion 2009, *MC3-SSUDW Underwater force sensor*, AMTI Force and Motion, viewed 3rd August 2016, <http://amti.biz/select%20product%20PDFs/Force%20sensors/MC3-SSUDW.pdf>.
3. Australian Maritime College 2016, *Circulating Water Channel Information*, Australian

Maritime College, viewed 9th March 2016, <https://www.amc.edu.au/maritime-engineering/circulating-water-channel>.

4. FIGLIOLA, RS & BEASLEY, D 2015, *Theory and design for mechanical measurements*, John Wiley & Sons.
5. FRANCIS, J 2013, '*Experimental Study of Hydrodynamic Forces Acting on a Concrete Mattress in Current*', Australian Maritime College.
6. GODBOLD, J, SACKMANN, N & CHENG, L 2014, '*Stability Design for Concrete Mattresses*', in The Twenty-fourth International Ocean and Polar Engineering Conference.
7. GRIGGS, R 2014, '*3D CFD Investigation of hydrodynamic forces on subsea articulated concrete mattresses*', Edith Cowan University.
8. LAGASSE, PF 2007, *Countermeasures to protect bridge piers from scour*, vol. 593, Transportation Research Board.
9. MCLAREN, R 2015, '*Investigation of Hydrodynamic Forces on Articulated Concrete Block Mattresses in Fluid Flow from Various Horizontal Directions*', Australian Maritime College.
10. MELVILLE, B 2006, '*Bridge abutment scour: estimation and protection*', Australian Journal of Water Resources, vol. 10, no. 1, pp. 81-92.
11. VERITAS, DN 1988, *On-Bottom Stability Design of Submarine Pipelines*, Veritas, Det Norske.
12. VERITAS, DN 2007, *On-bottom stability design of submarine pipelines*, Veritas, Det Norske.
13. VERITAS, DN 2010, *Environmental conditions and environmental loads*, Veritas, Det Norske.
14. YOUNG, DM & TESTIK, FY 2009, '*Onshore scour characteristics around submerged vertical and semicircular breakwaters*', Coastal Engineering, vol. 56, no. 8, pp. 868-875.

DISCUSSION

SLIDING MODE BASED PREDICTIVE CONTROLLER OF A SPHEROIDAL UNDERWATER VEHICLE

M P R Prasad and **A Swarup**, National Institute of Technology, Kurukshetra, India

(Vol 159, Part A2, 2017 – IJME 418)

COMMENTS

Prof. P Venugopal Senior Assistant Professor, SENSE, VIT University Vellore, TN State, India

The following key points are made after reading this research paper:

1) The approach taken in the paper looks interesting and innovative;
2) The problem and solution are well motivated;
3) The design of proposed hybrid controller (Sliding Mode & Model Predictive Controller) is a new and robust technique. Both qualitative and quantitative analysis and stability analysis are discussed in this paper; and
4) The proposed flowchart for MPC looks interesting. MPC tuning is given in a standard and systematic way.

The results and discussions are highly impressive. Overall it is a new idea of controlling underwater vehicle.

Prof. D John Pradeep, Assistant Professor, SENSE, VIT University, Vellore, TN State, India

I consider that the combination of sliding mode control and predictive control is a new concept in the field of control systems and therefore to be welcomed. Stability analysis is very important for underwater vehicles and Sliding Mode Control is the best technique for stability analysis.

The proposed flow chart is interesting and the time domain analysis shows the robustness of the vehicle.

Prediction is essential for vehicle path trajectory tracking control. The controller is showing satisfactory results compared with conventional control techniques like PD, LQR. The proposed controller can also be extended to helicopter control.

AUTHOR'S RESPONSE

The comments made by **Prof. Venugopal** and **Prof. Pradeep** are positive and motivating further in my research. Once again thanks for the entire editorial team of IJME.

The Transactions of The Royal Institution of Naval Architects – Part A

International Journal of Maritime Engineering

GUIDANCE NOTES FOR AUTHORS

All papers, technical notes and discussions should be submitted in electronic form, normally in MSWord format. Authors wishing to submit in other formats should first contact RINA Headquarters. Submissions should be forwarded on PC compatible disks or CD-ROM, containing the full text, including inserted figures. Submissions less than 5Mb may be forwarded by email or online.

Authors are responsible for obtaining security clearance as required. If they so wish, authors may add a disclaimer stating that the opinions expressed are solely those of the author.

In submitting papers or technical notes for publication, authors implicitly assign copyright to the Royal Institution of Naval Architects if the paper or technical note is published. Where copyright is held elsewhere, authors must present evidence of approval to re-publish.

When submitting contributions for publication, authors must state if the paper or technical note has been published before and where, or whether it is being considered for publication by some other publisher

Papers: Papers should not normally exceed 6000 words (with up to 10 illustrations). Longer papers where the content justifies the extra length may be published at the Editor's discretion. The required format of papers submitted for publication may be obtained from the RINA website or from RINA Headquarters

Technical Notes: Technical notes should not normally exceed 1500 words (and up to 5 illustrations). The required format of technical notes submitted for publication may be obtained from the RINA website or from RINA Headquarters

Discussion: Discussion of published papers, or comment on published discussion, should not normally exceed 500 words (with up to 2 illustrations).

All submissions for publication should be forwarded to:

The Editor (IJME)
The Royal Institution of Naval Architects
8-9 Northumberland Street
London WC2N 5DA, UK
Tel: +44 (0)20 7235 4622 Fax: +44 (0)20 7259 5912
Email: ijme@rina.org.uk Online: www.rina.org.uk

THE ROYAL INSTITUTION OF NAVAL ARCHITECTS

The Royal Institution of Naval Architects is an internationally renowned professional institution and learned society, whose members are involved at all levels in the design, construction and repair of ships, boats and maritime structures, in over 80 countries. RINA is widely represented in the marine industry, universities and colleges, and maritime organisations worldwide.

Membership is open to those who are professionally qualified in naval architecture or a related subject, or who are involved or interested in the maritime industry. RINA members enjoy a wide range of benefits and services, including advice on education, training and professional development. The RINA also publishes a range of technical journals, books and papers, and organises an extensive programme of international conferences and training courses covering all aspects of naval architecture and maritime technology, available to members free or at reduced rates

The Transactions of The Royal Institution of Naval Architects

Vol 159 Part A3 2017 ISSN 1471-8751

International Journal of Maritime Engineering

CONTENTS

PAPERS

TECHNICAL NOTES

There are no Technical Notes published in this issue of IJME

DISCUSSION